Synthesis, Characterisation and Pharmacological Evaluation of Silicon-Containing Aminoquinoline Organometallic Complexes as Antiplasmodial, Antitumor and Antimycobacterial Agents

Yiqun Tony Li

UNIVERSITY OF CAPE TOWN

2013

UNIVERSITY OF CAPE TOWN
IYUNIVESITHI YASEKAPA • UNIVERSITEIT VAN KAAPSTAD

Synthesis, Characterisation and Pharmacological Evaluation of Silicon-Containing Aminoquinoline Organometallic Complexes as Antiplasmodial, Antitumor and Antimycobacterial Agents

---

Dissertation presented for the degree of Master Of Science in the Department of Chemistry

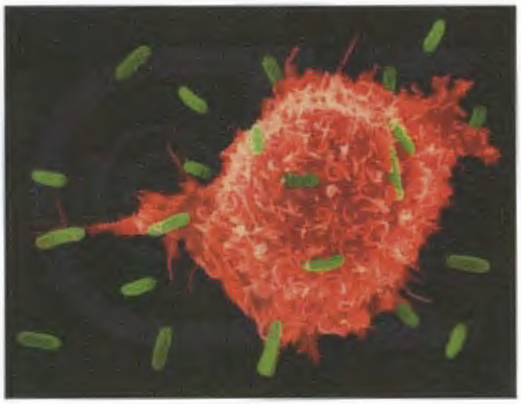

By

Yiqun Tony Li

Supervisors: Dr Gregory Smith

Co-supervisor: Professor Kelly Chibale

Department of Chemistry

University of Cape Town

Rondebosch, 7701

August 2013

PLAGIARISM DECLARATION

I declare that "**Synthesis, Characterisation and Pharmacological Evaluation of Silicon-Containing Aminoquinoline Organometallic Complexes as Antiplasmodial, Antitumor and Antimycobacterial Agents**" is my own work and to the best of my knowledge, has never been reported or submitted for any degree or examination in any university. I have not plagiarised it from any source. I know that plagiarism is a serious form of academic dishonesty. I have referenced all ideas borrowed from others, all sources of information used are cited, acknowledged and completely referenced at the end of each chapter.

I grant the University of Cape Town free licence to reproduce this dissertation in whole or in part for the purpose of research.

SIGNATURE: Signed by candidate

Yiqun Tony Li

DATE: _____

Acknowledgements

I would like to express my sincere and heartfelt gratitude towards the following people, without whom this dissertation would not have been possible:

My supervisors, Dr Greg Smith and Professor Kelly Chibale, for their expert guidance and encouragement throughout the entire project, and for their invaluable advice and knowledge that contributed greatly to this project.

The analytical staff at the University of Cape Town: Mr Pete Roberts for NMR spectra, and Dr Hong Su for single crystal X-ray structure determinations.

The mass spectrometry staff at the University of Stellenbosch, for mass spectra.

Professor Pete Smith of the Department of Medicine (Division of Pharmacology) at the University of Cape Town, for performing the *in vitro* antiplasmodial studies and contributions.

Hajira Guzgay and Denver T. Hendricks at the Division of Medical Biochemistry, Department of Clinical and Laboratory Sciences, University of Cape Town, for performing the *in vitro* antitumour studies and contributions.

Krupa Naran, Valerie Mizrahi and Digby F. Warner at the Division of Medical Microbiology, Department of Clinical Laboratory Sciences, and the Institute of Infectious Disease and Molecular Medicine, University of Cape Town, for performing the *in vitro* antimycobacterial studies and contributions.

My colleagues in the Organometallic Research group for their significant assistance over the course of this project.

For funding, I thank the Natinal Research Foundation, Professor Kelly Chibale, Dr Gregory Smith, and UCT.

Abstract

The medical success of platinum-based compounds such as cisplatin and its analogues laid the foundation for the synthesis and application of new transition metal complexes in the field of medicine. With the discovery of additional transition metal-based compounds such as ferroquine, KP1019 and NAMI-A, as therapeutic agents for the treatment of different diseases, the field of novel pharmacological transition metal agents continues to evolve. The constant increase in drug resistance and various undesirable side effects of current available therapies has led to the search for new strategies. Identifying novel drug candidates through utilising different metals of biological relevance is one such approach, and the main purpose of this study.

New mono- and heteronuclear silicon-containing ruthenium and rhodium metal complexes based on two ligand classes, have been synthesised and characterised utilising a range of analytical and spectroscopic techniques, confirming the structural integrity. The first class of compounds was constructed from a chloroquine derivative, and was synthesised via a general Schiff-base condensation reaction. Two silicon-containing aminoquinoline ligands **2.1** and **2.2** were derived from chloroquine, modified in the lateral side chain with organosilicon moieties. Compounds **2.1** and **2.2** were further reacted with dinuclear half-sandwich transition metal precursors $[Ru(Ar)(\mu\text{-}Cl)Cl]_2$ (Ar = η^6-p-^{i}PrC$_6$H$_4$Me; η^6-C$_6$H$_6$; η^6-C$_6$H$_5$OCH$_2$CH$_2$OH), $[Rh(COD)(\mu\text{-}Cl)]_2$, and $[RhCp^*(\mu\text{-}Cl)Cl]_2$, to yield a series of neutral mononuclear Ru(II), Rh(I/III) silicon-aminoquinoline metal complexes **2.8-2.17**. Ligands **2.1** and **2.2**, act as monodentate donors that selectively coordinate to the transition metals via the quinoline nitrogen of the aminoquinoline scaffold. Furthermore, the molecular structures of compounds **2.2** and **2.16** were elucidated by single-crystal X-ray diffraction analysis.

A second class of compounds based on the ferroquine scaffold was synthesised from ferroquine, again incorporating a organosilicon motif in the lateral side chain. Compound **3.6** was further reacted with the afore-mentioned Ru and Rh dinuclear half-sandwich transition metal precursors to yield a series of neutral heteronuclear Ru(II) and Rh(I/III) silicon-containing ferrocenyl aminoquinoline metal complexes **3.7-3.11** isolated in moderate yields. Compound **3.6** coordinates to the metal in a similar manner to ligands **2.1** and **2.2** (via the quinoline nitrogen), and all the complexes **3.7-3.11** were fully characterised confirming the structural integrity. Furthermore, the molecular structure of compound **3.6** was elucidated by

single-crystal X-ray diffraction analysis, showing the ferrocene and organosilicon motifs incorporated into the lateral side chain of the quinoline scaffold.

The *in vitro* pharmacological activities of the synthesised compounds were established against chloroquine-sensitive (NF54) and chloroquine-resistant (Dd2) strains of the malarial parasite, *Plasmodium falciparum*, and against the pathogenic bacterium, *Mycobacterium tuberculosis* $H_{37}R_v$, as well as an oesophageal (WHCO1) cancer cell line. All compounds were found to exhibit moderate to high antiplasmodial activities against the NF54 and Dd2 *P. falciparum* strains, with IC_{50} values in the nanomolar range for the ferroquine-derivatised series. The heterometallic series shows superior biological activity, suggesting that different metals may interact with multiple biological targets, providing chemical diversity, thus improving the physicochemical properties. The IC_{50} values of compounds **3.7-3.11** are comparable to ferroquine, and in selective cases, better than the current clinical antiplasmodial agent chloroquine. Furthermore, the more lipophilic ferroquine-derivatised series, displayed better inhibition of β-haematin through superior accumulation in the food vacuole of the parasite, and therefore better at killing the malaria parasite.

All compounds exhibited weak to moderate antitumour activities. The studies also showed that the ruthenium metal complexes generally display better activity in comparison with the rhodium complexes, and the compounds containing a 3-carbon chain spacer generally show better activity in comparison to those containing a 1-carbon spacer. The presence of the metal moiety did not significantly enhance the biological activities in comparison with the organic ligands.

In general, all compounds exhibited weak to moderate antimycobacterial activities against *M. tuberculosis* $H_{37}R_v$ strain. Overall, the turbidimetric solubility assay data suggests that these newly synthesised silicon-containing chloroquine and ferroquine derivatives are relatively good drug candidates for *in vitro* pharmacological testing. All compounds showed moderate solubility in the aqueous PBS buffer.

List of Abbreviations

δ	chemical shift
ACT	artemisinin-based combined therapy
COSY	correlation spectroscopy
Cp*	1,2,3,4,5-pentamethylcyclopentadienyl
CQ	chloroquine
CQR	chloroquine-resistant strain
CQS	chloroquine-sensitive strain
d	doublet (in NMR Spectroscopy)
DMF	dimethylformamide
Decomp.	decomposition
DMSO	dimethylsulfoxide
EA	elemental analysis
equiv.	equivalents
EI-MS	electron impact mass spectrometry
ESI-MS	electrospray ionization mass spectrometry
FQ	ferroquine
Hz	hertz
IC	inhibitory concentration
IR	infrared
J	coupling constant
m	multiplet (in NMR)
M.p.	melting point
m/z	mass/charge ratio
nM	nanomolar

NMR	Nuclear magnetic resonance
NOESY	Nuclear Overhauser Effect Spectroscopy
NP-40	Nonidet P40
PBS	Phosphate buffered saline
ppm	parts per million (in NMR Spectroscopy)
RI	resistance index
rt.	room temperature
s	singlet (in NMR Spectroscopy)
t	triplet (in NMR Spectroscopy)

Publications

Journal Article:

- Li, Y.; de Kock, C.; Smith, P. J.; Guzgay, H.; Hendricks, D. T.; Naran, K.; Mizrahi, V.; Warner, D. F.; Chibale, K.; Smith, G. S. *Organometallics*, **2013**, *32*, 141−150.

Conference Contributions:

- Poster Presentation: Y. Li, K. Chibale, G. S. Smith, Synthesis, Characterisation and Pharmacological Evaluation of Silicon-Containing Aminoquinoline Organometallic Complexes, at SACI 2013 Conference, Durban.
- Poster Presentation: Y. Li, K. Chibale, G. S. Smith, Synthesis, Characterisation and Pharmacological Evaluation of Silicon-Containing Aminoquinoline Organometallic Complexes, at H3-D, 2012 Symposium, Cape Town.
- Oral Presentation: Y. Li, K. Chibale, G. S. Smith, Synthesis, Characterisation and Pharmacological Evaluation of Silicon-Containing Aminoquinoline Organometallic Complexes, at UCT 2012 Symposium, Cape Town. (3^{rd} place)

Table of Contents

Chapter 1: INTRODUCTION

1.1. Epidemiology

There are currently several problematic diseases prevailing in the field of medical science, such as HIV-Aids[1], tuberculosis (TB)[2], and the shigella virus.[3-5] Two of the leading killers are malaria and cancer.[6,7] On a global scale, cancer combined with malaria is responsible for nearly 9 million deaths worldwide.[8] Presently there are several effective drugs made commercially available for the treatment of cancer and malaria, for example cisplatin, carboplatin, chloroquine and mefloquine.[6-9] However, despite the considerable amount of effort undertaken and invested in anticancer and antimalarial research, cancer and malaria continue to remain a major problem worldwide.[8-11] The widespread resistance to existing drug is one of the major setbacks in controlling malaria and cancer. Presently, as a result of a chloroquine-resistant strain appearing, chloroquine is losing its effectiveness for controlling malaria.[9-11]

1.2. Impact of Malaria

Malaria has been acknowledged as one of the most devastating and problematic diseases affecting mankind today.[9-11] It is an infectious disease that is widely spread by mosquitoes in the tropical and subtropical regions of the world.[11] It is endemic to over 108 countries (Figure 1.1), including much of Sub-Saharan Africa, Asia and a large part of South America.[12,13] These regions are generally warm, contain high humidity, which provides mosquiteos with the optimum environment they need to breed.[12-15]

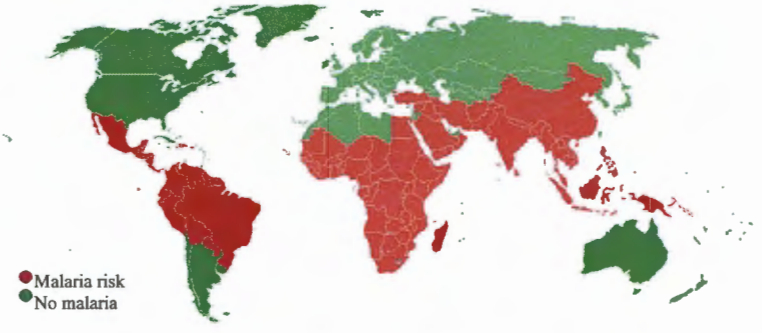

Figure 1.1: Countries where malaria is endemic.[15]

Malaria is predominantly problematic in developing countries, the widespread incidence creates undesirable conditions such as unmonitored disease growth, underprivileged management and treatments, which all affects communities poorly.[12-16] Worldwide, roughly 90% of all malaria-related deaths occur in Sub-Saharan Africa, and the majority are among

young children under the age of five.[14,16] According to the 2010 World Health Organisation (WHO) Malaria Report, it is estimated that approximately 250 million clinical cases of malaria occur annually, resulting in nearly one million deaths worldwide.[8] Despite the considerable amount of antimalarial studies, many commercial drugs such as chloroquine have been rendered powerless due to the challenges of new strains, as well as resistant strains continuously emerging.[17-19] New and innovative studies are still necessary to improve the reliability of current antimalarial research.

1.3. Malaria and the development of antimalarial drugs

1.3.1. Malaria strains and life cycle

Scientists have identified five different strains of *Plasmodium* that infect humans.[17] *P. knowlesi* was an ape strain, which has now been found to affect humans too.[17] *P. falciparum* is considered to be the most deadly form of the parasite, and it is responsible for the majority of all malaria cases.[17,18] The remaining *P. vivax*, *ovale*, and *malariae* strains generally cause milder diseases which are rarely fatal.[18] The causative agent of malaria is a parasite of the genus *Plasmodium*, this parasite is transmitted by an infected female Anopheles mosquito, which is extremely infectious to humans and pathogenic when attacking the host red blood cells.[19] A mosquito becomes infected with the parasite after it ingests blood from an infected intermediate host (Figure 1.2).[19] Once ingested, the parasite is taken up in the blood, and further differentiates into gametes, which are then fused within the mosquito's gut.[19-22] Next an ookinete will produce an oocyst, which ruptures releasing sporozoites that migrate to the mosquito's salivary glands, where they infect new hosts.[19-22]

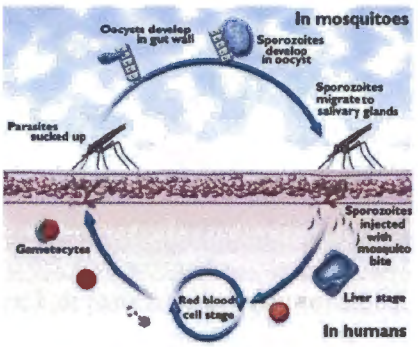

Figure 1.2: Life cycle of the malaria parasite.[20]

1.3.2. Discovery of antimalarial drugs

The very first antimalarial agent originated during the early 1600s in Peru. The Countess of Chinchon was cured of malaria when treated with the powdered bark of the *Cinchona* tree.[23] Subsequently, in the early 17th century, *Cinchona* bark was distributed as treatment for

fever throughout Europe.[23,24] Finally in 1820, two French scientists, Caventou and Pelletier, successfully isolated the active ingredient, quinine, from the *Cinchona* tree bark, and today quinine is regarded as one of the most effective antimalarial agents.[23-26] Quinine (Figure 1.3) is an alkaloid that acts as a blood schizonticide and a weak anti-gametocide against both *P. vivax* and *malariae* strains.[27-29]

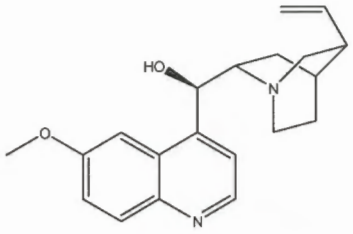

Figure 1.3: Antimalarial drug quinine.[25]

In pharmacology, drugs are commonly small organic molecules which activate or inhibit the functions of biomolecules such as enzymes, which are mostly proteins in the human body.[29,30] This results in a therapeutic benefit to the patient.[30] Historically the most widely distributed and frequently used antimalarial drug was chloroquine (CQ).[30,31] Chloroquine (Figure 1.4) was first discovered around the early 1930s, it was considered almost an ideal drug for malaria treatment due its high efficacy, safety, and low costs.[31,32] However, due to the widespread resistance, CQ and other quinoline-based drugs are showing reduced efficacy, creating a major setback in controlling malaria.[31-35]

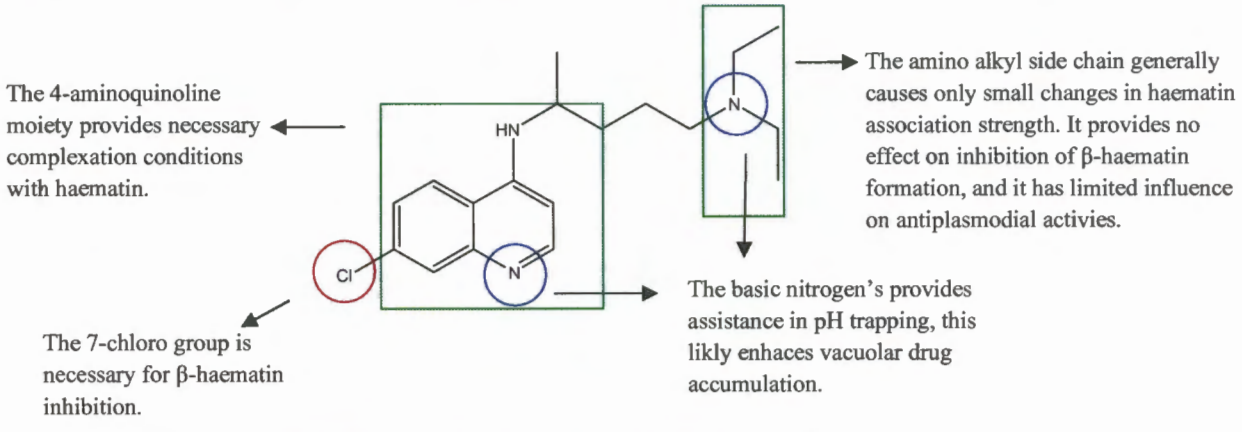

Figure 1.4: Structure-activity relationships.[31]

It has been well established that in order for a quinoline-based drug to display good antimalarial activity, it must firstly possess the ability to form a strong complex with haematin.[31,32] Secondly, it must have the ability to inhibit hemozoin formation; lastly, it must have the ability to accumulate towards therapeutic concentrations in the *Plasmodium*

digestive vacuole.[31,32] In addition, quinolines are an important class of heterocyclic compounds which contains a wide range of pharmacological activities, including antiviral[34], anticancer[35], antibacterial[36], antifungal[37], antiobesity[38], and anti-inflammatory properties.[39]

Numerous research groups have conducted structure-activity relationship investigations with a special focus on CQ derivatives.[31,40,41] It was concluded that the structural requirements, namely the three properties outlined above, are particularly important, and in some cases essential in light of the widespread resistance towards antimalarial drugs.[31,40,41]

1.3.3. Chloroquine's mechanism of action

The food vacuole is a lysosome-like organelle in which the breakdown of haemoglobin, and the detoxification of haem occur.[41] Chloroquine (Figure 1.4) is a 4-aminoquinoline compound, which, due to its alkaline nature, acts by reaching high concentrations in the food vacuole of the malaria parasite.[41-44] There are three possible mechanisms for the selective accumulation of CQ in the food vacuole.[41-45] Firstly, the protonation and ion trapping of the CQ due to the low pH of the food vacuole; secondly, the active uptake of CQ by the parasite's transporter system; and lastly, the binding of CQ to a specific receptor in the food vacuole.[42-44] As a result of the malaria parasite ingesting the host's haemoglobin, large quantities of haem are produced in the food vacuole of the parasite (Figure 1.5).[42-45] The parasite detoxifies haem in the food vacuole by a bio-crystallization process, in which the haem is sequestered into large insoluble crystals "hemozoin".[44,45] Chloroquine can bind haem and thus prevent the formation of the haemozoin crystal, thus killing the parasite.[45]

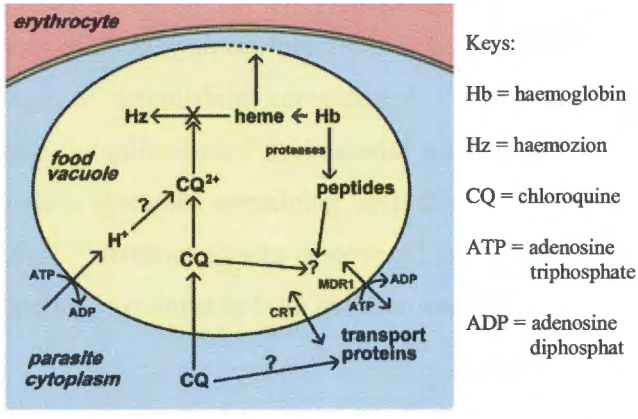

Figure 1.5: Uptake and digestion of haemoglobin in *Plasmodium*.[44,45]

1.3.4. Other organic-based antimalarial agents

In addition to CQ, over the decades, numerous organic antimalarial drugs were successfully developed and made commercially available.[46-48] For example amodiaquine (Figure 1.6) is a 4-aminoquinoline compound very similar to CQ.[47-49] Amodiaquine is a

histamine *N*-methyltransferase inhibitor, used as an antimalarial and anti-inflammatory agent.[47-49]

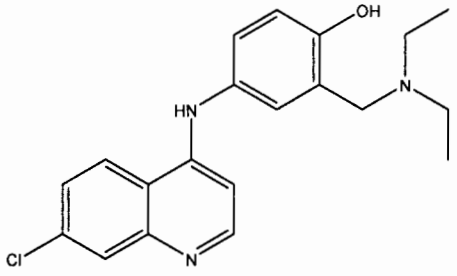

Figure 1.6: Structure of Amodiaquine.[47]

Another example is mefloquine (Figure 1.7), discovered around the late 1970s, it was widely used until the early 1980s, before mefloquine resistant strains emerged.[49,50] Today mefloquine is still used for the prevention of malaria in most areas, apart from those where the malaria parasites may have developed resistance to multiple drugs.[49,50]

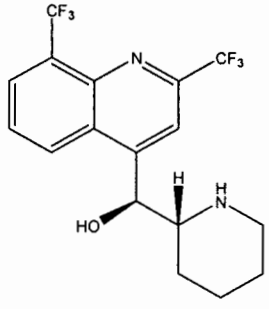

Figure 1.7: Structure of Mefloquine.[50]

In addition to pharmaceutically developed compounds, organic drug molecules which originate in nature are also an important source of novel therapeutic and diagnostic agents.[51] During the last decade, treatment of *P. falciparum* infections in many endemic countries has been transformed by the usage of artemisinin combination therapy (ACT).[52] Previous conventional quinoline- and non-quinoline-based antimalarial medicines have now largely been replaced by new combination therapies containing derivatives of the Chinese natural product artemisinin (Figure 1.8).[51-53] Artesunate was discovered around the early 1970s, and it has been established to be superior to quinine in both children and adults.[52]

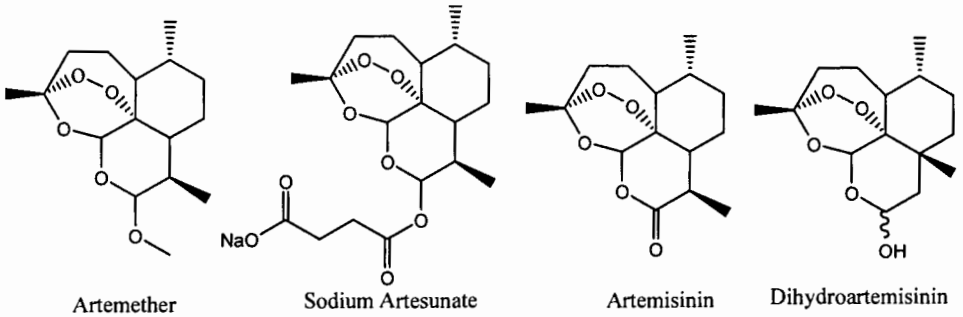

Artemether Sodium Artesunate Artemisinin Dihydroartemisinin

Figure 1.8: Structures of Artemisinin derivatives used for malaria treatments.[52]

However, with the wide distribution of the malaria parasite around the world, resistant strains against several antimalarial drugs have emerged and continue to emerge.[52-54] These include the CQ-resistant W2 (Indonesia) strain, and the Dd2 (South East Asia) strain.[54] In an attempt to combat the increasing resistance of *P. falciparum* to CQ and many other commercially available drugs, an alternative method of drug design, incorporating transition metal arenes into existing organic molecules, is being developed as the next stage in drug design strategies.[53-56]

1.3.5. Metal-based antimalarial agents

The medical accomplishments of several metal-based drugs has established ground work for research into the synthesis of new transition metal complexes with interesting and occasionally, multi-functional biological properties. It has been documented that numerous metal containing compounds provide a great variety of different and peculiar chemistries.[56-58] For example, the reactivity of a metal centre toward a target bio-molecule can be "fine-tuned" through appropriate choice of ligands.[56-58] As a result of emerging drug resistant *Plasmodium* strains, the continuous necessity to develop new antimalarial drugs has steered the field of bio-inorganic chemistry towards transition metal-based complexes.[56-58]

Medicinal inorganic chemistry is a discipline of growing importance.[56] The rich diversity of metal coordination chemistry provides many opportunities for designing new pharmaceuticals.[58] Transition metals (Figure 1.9) such as platinum, gold, ruthenium, rhodium, and iridium offer additional diversity in terms of synthetic chemistry, creating a new class of compounds to study, and acquire greater knowledge.[58-60]

One drug design strategy for new chemotherapy against tropical diseases such as malaria, is the use of organic compounds with known therapeutic value through coordination to a transition metal.[58-60] This modification could be vital within a biological system and afford some unique characteristics, and distinct physical properties. Due to the new molecular

structure, d-orbitals on the transition metal, binding capabilities and reactivity could potentially all be improved.[56-60]

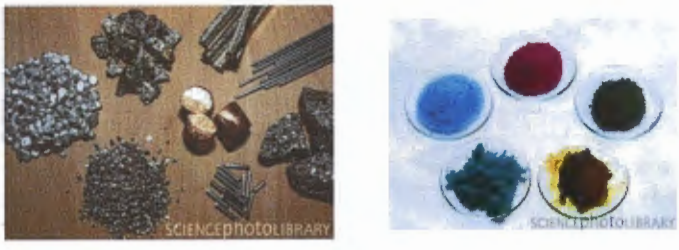

Figure 1.9: Examples of transition metals.[61]

It has been validated that in many circumstances the presence of a metal ion can systematically increase the biological activity of the drug molecule, which also contributes greatly towards its stability.[56,58,60] In this regard, a number of transition metals such as ruthenium, rhodium, gold and chromium have demonstrated excellent coordination chemistry towards CQ and other aminoquinoline moieties.[62-65] Several transition metal complexes of CQ have been synthesised and evaluated for antiplasmodial activity with varying degrees of success;[62-66] and in some cases the incorporation of a metal onto an organometallic moiety has resulted in higher activity against both CQ-sensitive and CQ-resistant strains of the malaria parasite.[62-66] Thus, this concept of modifying existing compounds with known or potential biological activity, through the incorporation of a transition metal into their molecular structure, have greatly accelerated drug developments.[64-67]

1.4. Examples of metal-based antimalarial agents

1.4.1. Iron-based complexes, Ferroquine

Iron is the most common element by mass on earth, establishing much of the earth's outer and inner core.[68] Iron exists in a range of oxidation states, the most common being +2 and +3.[68,69] Furthermore, iron-proteins exist in nearly all living organisms, including haem proteins, haemoglobin, and myoglobin, the utmost vital proteins found in humans. Thus, iron is considered a necessary element in almost all living organisms.[67-69] Therefore, it is no surprise that Fe has found its way into medicinal chemistry, and several drug development programs.[69-71] Many multinuclear complexes incorporating ferrocenyl moieties and platinum group metals have already shown promising results,[71] as seen in the ruthenium-arene CQ derivatives reported by Biot and Sánchez-Delgado.[51,67]

The most notable example is the drug candidate ferroquine (FQ, Figure 1.10), discovered around the mid-1990s, FQ is essentially a CQ analogue containing a ferrocene unit integrated into the side chain.[72-74] Furthermore, ferroquine retains all the essential parts of the CQ-

template mentioned in section 1.3.2., and the additional ferrocene unit enhances the biological potency against CQ-resistant parasitic strains.[72-74]

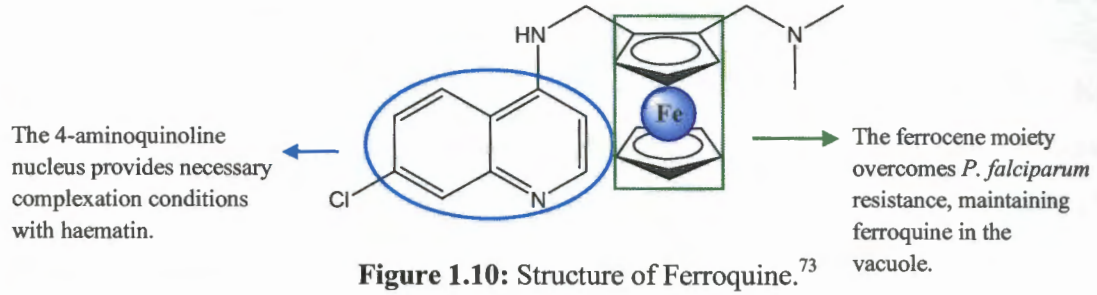

Figure 1.10: Structure of Ferroquine.[73]

New structures aimed at better drug development programs drawing inspiration from ferroquine are emerging (Figure 1.11).[75-77] Complexes **1.1-1.4** illustrate examples of modifications in the lateral side chain of CQ. Ferrocene has offered many interesting opportunities for modelling new complexes; its relatively small and rigid sandwich structure allows effective penetration across cellular membranes, and excellent lipophilic properties.[75-78] Additionally, ferrocene is relatively stable in aqueous and aerobic media, as a direct result of these characteristics, ferrocene analogues are a very attractive choice for drug designs purposes.[76]

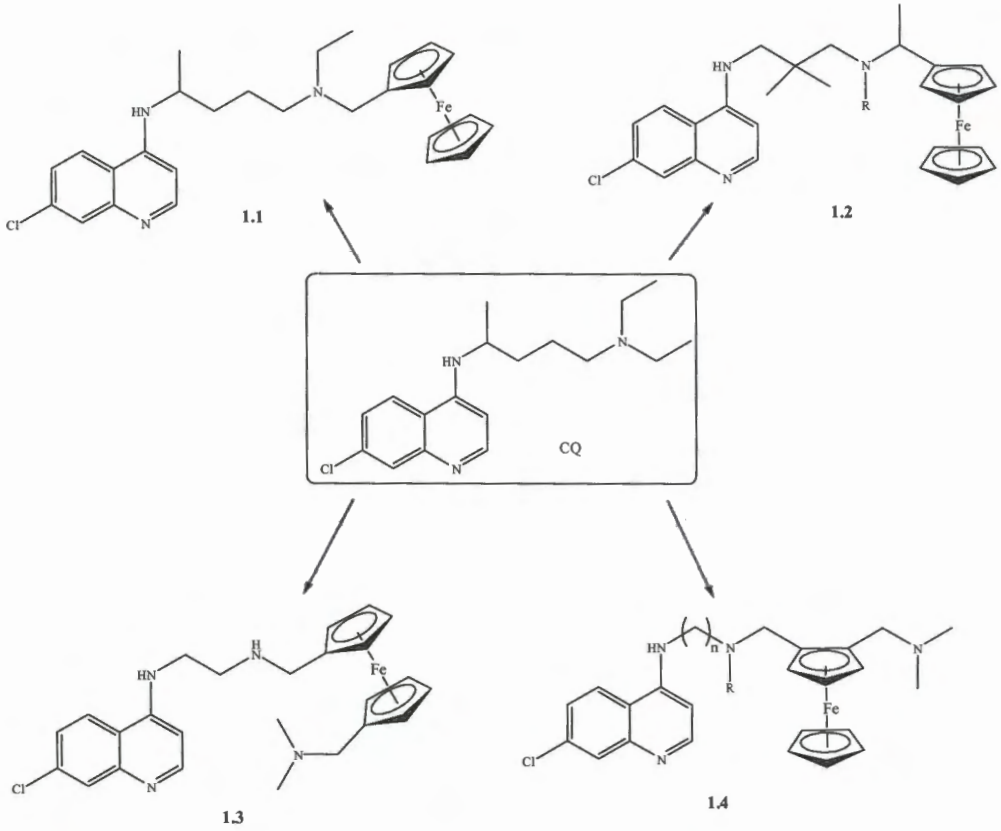

Figure 1.11: Examples of lateral side chain modifications of CQ complexes.[76]

1.4.2. Ruthenium-arene half-sandwiched complexes

The concept of using ruthenium-arene compounds, as potential anticancer agents for cytotoxicity enhancement by the coordination of metals; was introduced by Tocher in the early 1990s.[77] Thereafter, several research groups have demonstrated this concept by co-ordinating ruthenium-containing fragments to CQ.[78,79] This has resulted in enhanced activity against CQ-resistant parasites.[78,79] The extra ruthenium metal counterpart appears to greatly increase the drug's potency.[78,79] Examples of ruthenium-based drugs containing CQ (Figure 1.12) are emerging as promising alternatives for the treatment of malaria.[77-79]

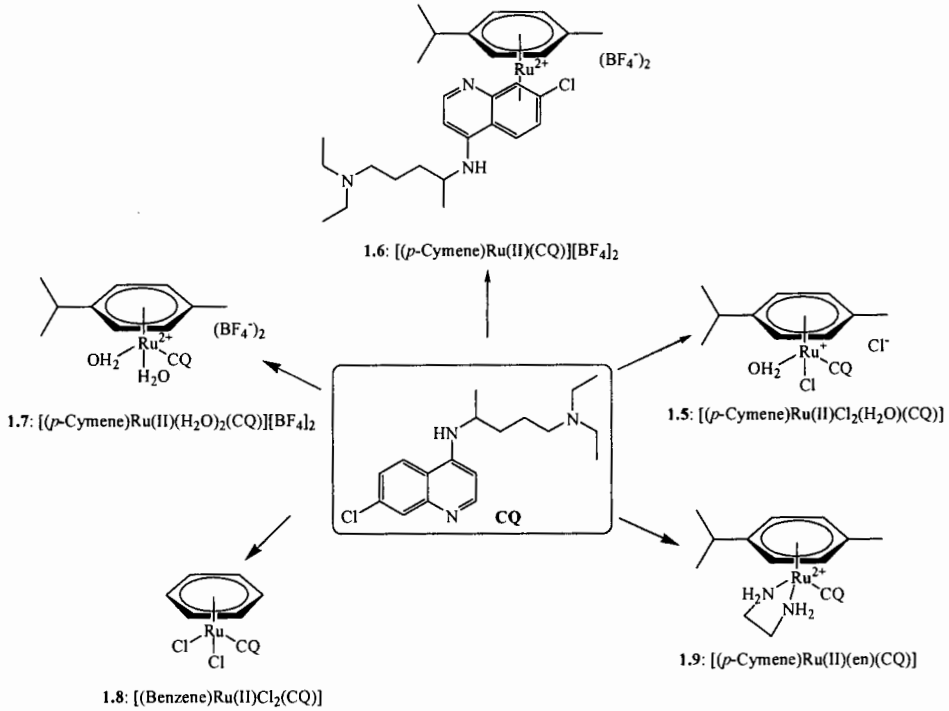

Figure 1.12: Examples of ruthenium-CQ complexes.[76]

Ruthenium is generally versatile, and encompasses a variety of oxidation states namely Ru(II-IV), Ru(II) being more biologically active.[78-80] These oxidation states are easily accessible under physiological conditions.[80] Furthermore, ruthenium is subjugated by rich synthetic chemistry; NMR studies have indicated that CQ binds to the ruthenium through the unsubstituted quinoline nitrogen, which is an excellent donor site.[78-81] In addition, the compounds **1.5-1.9** (Figure 1.12) all display *in vitro* activity against four CQ-susceptible strains (FcB1, 3D7, PFB, F32) and three CQR strains (W2, Dd2, K1) of *P. falciparum*.[80,81] The biological potency of all these complexes was better than that of CQ diphosphate.[78-81] In summary the combination of Ru(II) with CQ in a single molecule is a very promising

apparel to potential antiplasmodial agents. Thus, ruthenium is a particularly attractive choice for developing new metallo-pharmaceuticals.[79-81]

1.4.3. Rhodium complexes

Rhodium was first discovered in the early 1800s and approximately eighty percent of global rhodium production is consumed in catalysis.[82,83] Despite its previous lack of use in drug advances, recently there has been an increasing interest in the use of rhodium towards novel drug development.[82-84] Reactions involving $[RhCl(COD)]_2$ with CQ under mild conditions have led to the formation of RhCl(COD)(CQ) (Figure 1.13).[85] Rhodium coordinates to the quinoline nitrogen atom forming a 16-electron aqua-planar Rh(I) complex.[85] Subsequently, the *in vitro* antiplasmodial studies of the rhodium-CQ complex provided IC_{50} values in the range of 61-81 nM, which is in a similar range to that of CQ diphosphate against the malaria parasites.[85]

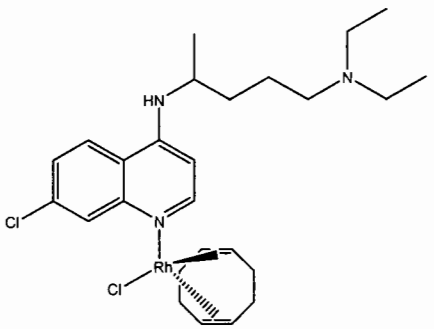

Figure 1.13: Rh-CQ complex.[85]

In summary, the progress in antimalarial drug discovery research are developing rather slow, although numerous investigations/studies around transition metal complexes are under way, many problems still arise with these studies. As mentioned above, there is a strong demand to develop new therapeutic agents.

1.5. Silicon chemistry

1.5.1 Motivation

Under this umbrella of bio-organometallic chemistry, the field continuous to grow through combination of organometallic complexes with organic compounds of known therapeutic values.[91-93] In this regard, several research groups including the work done by Biot, Sánchez-Delgado and Navarro, have also introduced various organometallic fragments in the basic amine side chain in an attempt to enhance the antimalarial activity.[76-80]

The basis for our study is based on a series of recent publications including the work done by Tacke, all illustrating that bio-organosilicon chemistry can provide a novel and

powerful source of chemical diversity in medicinal drug design.[94-96] There are several examples of silicon-containing drugs in the literature.[94-96] Polydimethylsiloxanes (I, Figure 1.14) are well known for their unusual rheological properties.[96] The structure of cyclohexyl(phenyl)(3-piperidin-1-yl)propyl) silanol(II, Figure 1.14) contains some interesting silicon chiral centers and sila-derived phthalocyanine provides some promising results in photodynamic cancer therapy.[96] In addition, many silicon-containing drugs such as silperisone, Tac101, BNP 1350, have already entered human clinical trials.[96]

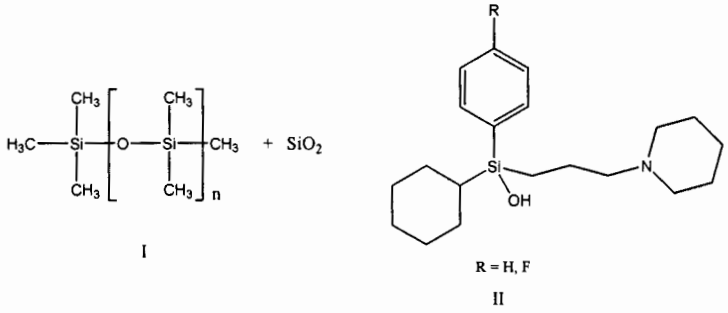

Figure 1.14: Biologically active organosilicon compounds.[96]

This strategy of incorporating organosilicon moieties has been used to augment biological activity, and reduce toxicity in a bid to enhance the therapeutic value of existing drugs.[96-98] Many organosilicon compounds remain chemically stable under physiological conditions.[97-99] Their ease of synthesis from a number of commercially available precursors facilitates chemical modification of existing drugs.[96] In addition, silicon analogues are generally more lipophilic, which can result in a remarkable increase in the distribution of a molecule.[96-98] Their selective uptake by tumors could also result in a greater drug loading in tumorous cells.[98]

1.5.2. Current work

Silicon is a tetravalent metalloid that is widely distributed in nature. It is the second most abundant element found in the earth's crust, and mostly distributed in dust, sand, planetoids and various forms of Si dioxide.[98,99] In addition, Si is also commonly found in biological systems exemplified by structural elements in organisms such as sponges and horsetails.[100-102] Silicon is involved in the formation of connective tissues and is considered an essential element for mammals, though only tiny traces of it are required.[101]

Silicon has displayed many chemical properties similar to its neighbouring carbon atom.[100] However, unlike carbon, Si lacks the ability to form chemical bonds with diverse types of atoms. This limits chemical versatility, which is necessary for metabolism.[99,100]

But the concept of sila-substitution, which is a carbon silicon switch, has been successfully utilised in the development of several new silicon-based drugs.[102]

1.5.3. Advantages of silicon

One of the most widely known features of Si chemistry is the lipophilic nature mentioned above.[96,97]An increase in lipophilicity of a compound, gives several physiological benefits, including an increase in bio-availability, better tissue and cell penetration.[96-100] Carbon and silicon are both group 14 elements, and are similar in that they form four covalent bonds with many other elements.[100] However, the striking differences: silicon (1.17 Å) has a larger covalent radius compared to carbon (0.77 Å), which results in the formation of longer bonds thus, increased size of the sila-analogue, and superior conformational flexibility.[101] An increased lipophilicity is observed for most silicon compounds compared with their corresponding carbon analogues.[100-103]

Silicon (1.74, Allred-Rochow scale) is correspondingly less electronegative than carbon (2.50), which implies different polarizations.[96,97] Furthermore, another advantage of Si, is the versatility in its coordination numbers;[96,97] Unlike carbon, Si can increase its oxidation state to 5 or 6, to form relatively stable penta- and hexacoordinate Si compounds.[96,97] Coordination numbers +2 (sp hybridization) and +3 (sp^2 hybridization) are disfavoured over +4 (sp^3 hybridization), and as a direct result, Si readily forms tetracoordinate species.[97-99]

The characteristics of Si mediate many interesting pharmacological and medicinal properties. The enhanced lipophilicity may improve pharmacokinetics, in some cases the presence of a strong OH acidity group on SiOH, may serve to enhance receptor binding.[96,100-103] The manifestation of Si may also alter bonding conformations and modify charge distributions which will result in a new class of protease inhibitors.[100-103]

In summary, the introduction of metals and silicon into the field of bio-organometallic chemistry has unlocked many possibilities. However, there is still a great deal of concern regarding the role of the inorganic elements. The following section will take a closer look at cancer, in a similar manner to the coverage on malaria.

1.6. Cancer and anticancer drugs

1.6.1. Record of cancer

Evidence for cancer existed throughout documented history, with the earliest evidence of cancer found amongst fossilized bone tumours, and even human mummies in ancient Egypt.[104] During the 18th century, there were three important observations that supported the underlying principal and launched the field of cancer epidemiology.[105,106] Firstly, during the early 17th century, Bernardino Ramazzini, an Italian doctor characterised the fundamental absence of cervical cancer, and the relatively high incidence of breast cancer.[107] Subsequently, around the late 1700s, Percival Pott of the Saint Bartholomew's Hospital in London recognised occupational cancer.[108] This in turn initiated many studies that identified occupational carcinogenic exposures.[108] The result brought about public health measures to reduce cancer risks.[108] Lastly, around 1620 Thomas Venner of London, who was one of the first to warn about tobacco dangers, navigated towards the empirical observations that associate tobacco with cancer.[109] The conclusion brought about the published epidemiologic research in the early 1960s;[109] which had a profound impact on the world, and the tobacco industry, as it revealed that smoking causes lung cancer.[109]

1.6.2. Cell cycle

The cell cycle machinery controls all cell proliferation, and cancer is a disease that deregulates cell proliferation, by causing uncontrolled division of abnormal cells.[110] There are multiple genetic fluctuations that will need to occur in the evolution process of normal cells into cancer cells, which are facilitated in cancer cells by the loss of fidelity in replication, repairs, and segregation of the genome.[110,111] Fundamentally, all cancer permits is the existence of too many cells. For example, a single adult stem cell or progenitor cell in a tissue can suffer a mutation during the cell cycle (Figure 1.15).[110-112] This will give that cell a slight growth advantage over other dividing cells.[110-113] As the cell matures into a clone, a number of its descendants will suffer another transformation during the processing cell-cycle.[110,113] This further deregulates the cell cycle of that cell and its descendants.[110,113] As the rate of mitosis in the clone increases, the chances of further DNA damage increases.[113] Eventually, so many mutations occur resulting in the growth of the clone becoming completely unregulated, causing full-blown cancer.[110-114]

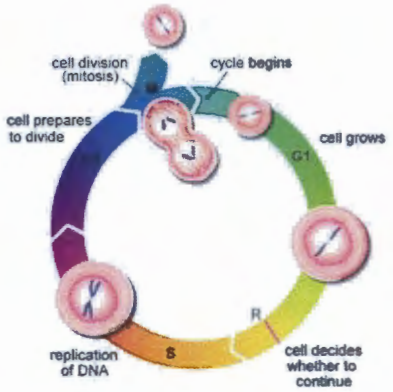

Figure 1.15: Cell cycle.[114]

1.6.3. Organic chemotherapeutic drugs

Many of the commercially available anticancer drugs today have a distinct mechanism of action, which varies depending on their effects on different types of normal and cancer cells.[113] However, it has been demonstrated that there are very few bio-chemical differences between cancerous and normal cells.[113] As a consequence, the effectiveness of many anticancer drugs is limited by their toxicity to normal growing cells.[113,115]

The main objectives of most chemotherapeutic drugs are to slow and hopefully halt the growth and spread of cancer.[113-116] Chemotherapeutic drugs in general can be divided into three main categories based on their mechanism of action (Figure 1.16). Firstly, direct damage to the DNA of the affected cancer cells.[116] Secondly, inhibition of the synthesis of newly formed DNA strands, to stop the cell from replicating, thus preventing tumours from growing; and lastly, the inhibition of mitosis, which will prevent splitting of the original cell into two new cells, stopping cell division and replication of the cancer.[115-117]

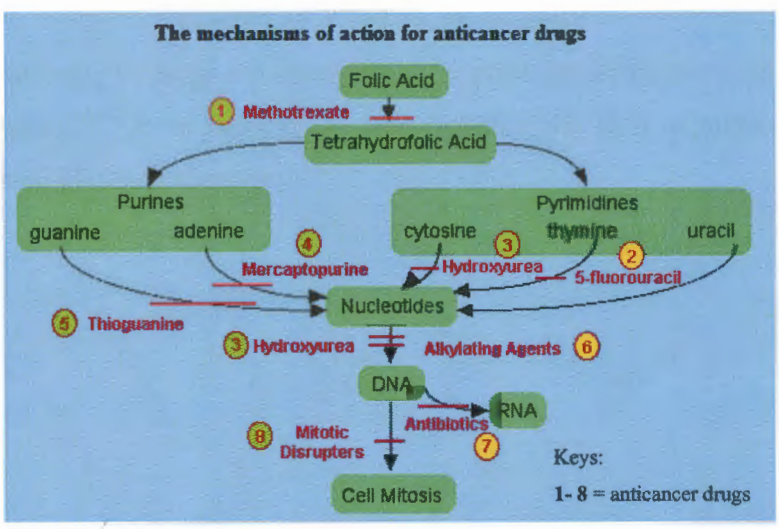

Figure 1.16: Mechanisms of action for anticancer drugs.[116]

The general approach of all chemotherapy is to decrease cell division of the cancer cells.[119] Unfortunately, this results in many side effects, which can be observed in bodily systems that naturally have rapid turnover of cells, including skin, hair, gastrointestinal, and bone marrow.[119,120] Consequently, some of the healthy normal cells are also being damaged by chemotherapy.[120,121] Furthermore, the cancerous cells, which are initially suppressed by a specific drug may develop resistance towards that drug.[120,121] As a result of this, many cancer chemotherapy treatments invoke several drugs in combination for various lengths of time for better and more effective treatment.[120,121]

1.6.4. Platinum-based drugs

While many drugs are organic, metals in the periodic table offer additional diversity in chemistry, and a selection of different applications (Section 1.3.5.). The field of metal-based therapeutic drugs originated with the encounter of cisplatin in 1965, the very first Pt-based antitumor drug in the world.[122] Today cisplatin is one of the leading agents used clinically against cancer, and there are over three thousand Pt-derived drugs which have been synthesised and tested against cancer, all sparked by the discovery of cisplatin.[122] A few examples of cisplatin analogues include oxaliplatin, carboplatin, and nedaplatin (Figure 1.17).[122,123] It is estimated that over 50% of all cancer patients are treated with platinum-based drugs, and the annual trade of these drugs exceeds over two billion dollars.[123]

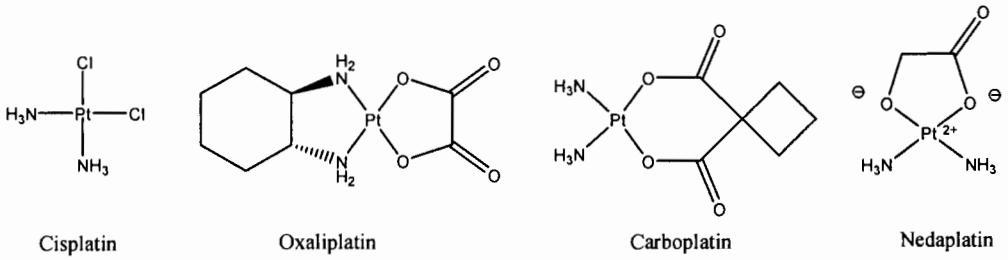

Figure 1.17: Cisplatin analogues.[123]

While cisplatin and Pt drugs are among the most effective anticancer drugs, their toxicity is a major drawback.[124] As a direct consequence of this, the field of metal-based drugs is developing beyond platinum chemistry.[123-125]

1.6.5. Ruthenium-based drugs

Since the late 1990's, numerous advances have being made in the field of ruthenium antitumor complexes.[126] The field of antitumoural and antimetastatic ruthenium-arene complexes was pioneered by Dyson, Sadler and Sánchez-Delgado.[126,127] Initially, the prototype Ru(II)-arene complexes evaluated for anticancer properties in 2001 were RAPTA-C, from Dyson's laboratory, the hexafluorophosphate salt from Sadler's laboratory (Figure 1.18),[127] and the interactions of π-arene-Ru(II)-chloroquine complexes with human serum albumin (HSA) done by Sánchez-Delgado's group.[127(e)]

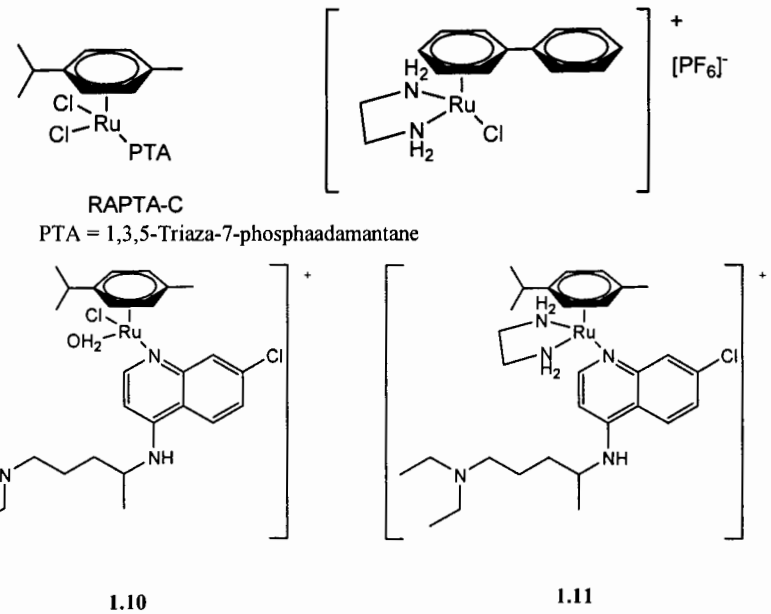

Figure 1.18: Ru(II)-arene-CQ complexes.[127]

Among the most outstanding accomplishments in ruthenium-based anticancer research, NAMI-A (Figure 1.19) synthesised in 1999 by Allessio *et al.* has been in clinical trials for many years.[128,129] NAMI-A has been shown to be relatively non-toxic, and is effective against metastases, which is a secondary cancerous growth formed by transmission of cancerous cells by primary growth located elsewhere in the body.[128-130] Another highlight is Hind[trans-$RuCl_4(ind)_2$] or KP1019 (Figure 1.19), which was developed by Keppler and co-workers.[129-131] This potential anticancer agent is also in clinical trials, and has also attracted much attention.[129-131]

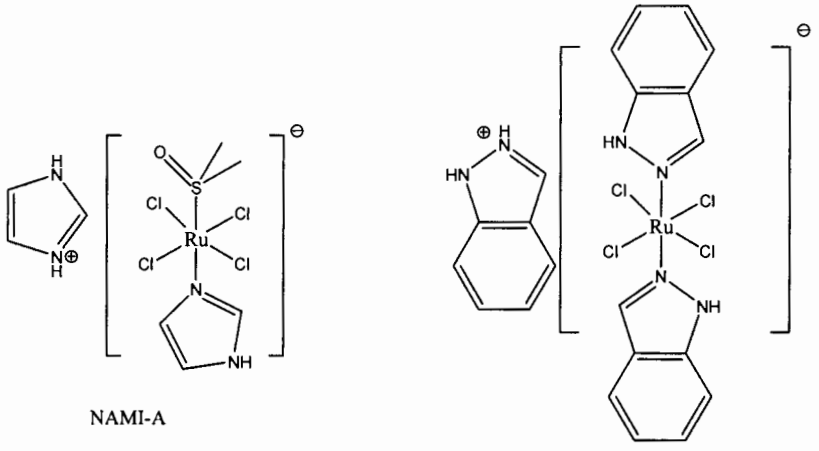

Figure 1.19: Structures of NAMI-A (left) and KP1019 (right).[129-131]

1.6.6. Rhodium complexes

Rhodium is a platinum group metal and many rhodium complexes have demonstrated anti-tumour activity against several tumour cell lines.[132,133] However, their toxicity effects limit their use.[132,133] Recent studies suggest that the anti-tumour diRh(II) carboxylates may bind in a similar manner to cisplatin.[132,133] Generally speaking, most anti-tumour Rh(I) compounds with *in vivo* activity are neutral, and usually consist of a square planar geometry (Figure 1.20).[133,134]

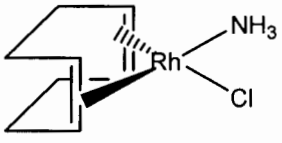

Figure 1.20: A Rh(I) cyclo-octadiene derivative.[133,134]

However, many Rh(I) compounds are not air stable and have several toxic side effects.[132,133] Furthermore, most Rh(I) complexes are usually not active against a wide enough range of cancer cell lines.[133] Regardless, this field of incorporating rhodium metals onto other molecular structures is beginning to unfold, and this research is demonstrating potential.[134]

1.7. Conclusion

Over the years, numerous metal-CQ complexes have been successfully synthesised, characterised and evaluated for their biological properties. Most of them have shown relatively good therapeutic values. In addition, the versatile CQ-based ligands due to their ability to bond to several different types metals such as ruthenium and rhodium, which has led to a growing interest in biological applications. Essentially this chapter establishes a foundation for some understanding towards the problems beset the treatment of different diseases today, in particular malaria and cancer.

1.8. Research Questions

To the best of our knowledge, there are no reports on the use of silicon-containing aminoquinoline transition metal complexes as chemotherapeutic agents in the field of bio-organometallic antimalarial research. Thus in this research project, the strategy is to synthesise, characterise and pharmacologically evaluate a series of new silicon-containing aminoqinoline ligands and their transition metal complexes by incorporating different ruthenium and rhodium arenes.

1.9. Specific objectives

- The synthesis and characterisation of $[Ru(II)(\eta^6\text{-}C_6H_6)Cl_2]_2$, $[Ru(\eta^6\text{-}p\text{-}Pr^iC_6H_4Me)(\mu\text{-}Cl)Cl]_2$, $[Ru(II)(\eta^6\text{-}C_6H_5OCH_2CH_2OH)(\mu\text{-}Cl)Cl]_2$, $[Rh(I)Cl(COD)]_2$ and $[Rh(III)Cl_2(Cp^*)]_2$ metal dimers.

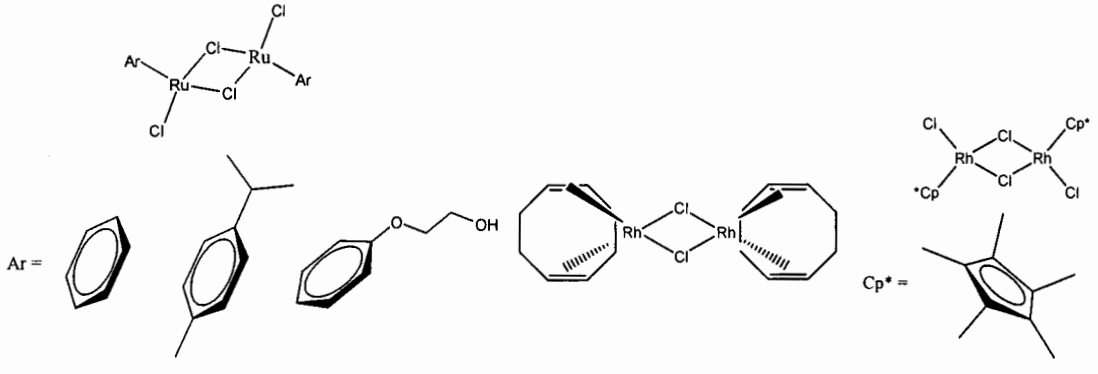

- The synthesis and characterisation of silicon-containing CQ-derived aminoquinoline ligands.

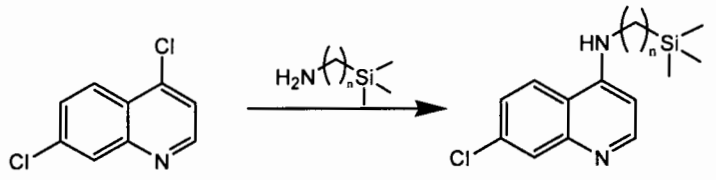

- The synthesis and characterisation of mononuclear Ru(II), Rh(I) and Rh(III) silicon-containing aminoquinoline transition metal complexes.

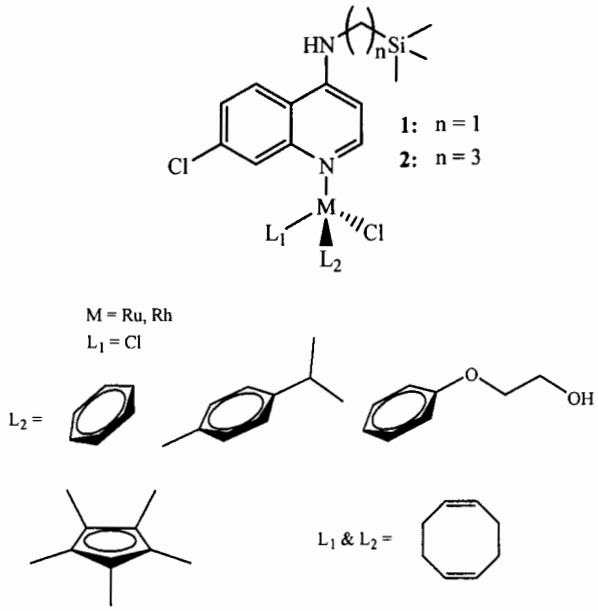

- Characterisation of the various target compounds using ^{1}H, ^{13}C NMR as well as 2-D NMRs, namely HSQC and COSY; IR spectroscopy, Electrospray Ionisation (ESI) or electron impact (EI) mass spectrometry, single crystal X-ray diffraction analysis, and melting point analysis.
- *In vitro* pharmacological evaluations to determine antiplasmodial, antitumour and antimycobacterial activities.
- Turbidimetric solubility and β-hematin inhibition studies.

1.10. References

1. *Source* <http://www.who.int/hiv/en/>, (Accessed March 2012).
2. D. E. Goldberg, A. F. G. Slater, A. Cerami, G. B. Henderson, *Proc. Natl. Acad. Sci.* 1990, **87**, 2931.
3. P. Cravo, R. Culleton, A. Afonso, I. D. Ferreira, do Rosário, V. E. *Anti-Infect. Agents Med. Chem.* 2006, **5**, 63.
4. Salas, P. F.; Herrmann, C.; Orvig, C. *Chem. Rev.* **2013**, *113*, 3450.
5. *Source* <http://www.who.int/topics/shigella/en/>, (Accessed March 2012).
6. (a) R. G. A. Feachem, A. A. Phillips, J. Hwang, C. Cotter, B. Wielgosz, B. M. Greenwood, O. Sabot, M. H. Rodriguez, R. R. Abeyasinghe, T. A. Ghebreyesus, R. W. Snow, *Lancet*. 2010, **376**, 1566. (b) J. N. Burrows, K. Chibale, T. N.C. Wells, *Curr. Top. Med. Chem.* 2011, **11**, 1226. (c) S. I. Hay, C. A. Guerra, A. J. Tatem, A. M. Noor, R. W. Snow, *Lancet Infect. Dis.* 2004, **4**, 327.
7. A. Jemal, F. Bray, M. M. Center, J. Ferlay, E. Ward, D. Forman, *CA CANCER J CLIN.* 2011, **61**, 69.
8. (a) *Source* <http://www.who.int/cancer/en/index.html>, (Accessed 18 Jan. 2012). (b) World Malarial Report (2010), *Source* <http://www.who.int/malaria/world_malaria_report_2010/worldmalariareport2010.pdf>, (Accessed 27 Feb. 2012).
9. (a) K. R. Dronamraju, P. Arese, Malarial: *Genetic and Evolutionary Aspects* (Emerging Infectious Diseases of the 21st Century); Springer: New York, 2010, 81. (b) R. B. de Oliveira, E. M. de Souza-Fagundes, R. P. P. Soares, A. A. Andrade, A. U. Krettli, C. L. Zani, *Eur. J. Med. Chem.* 2008, **43**, 1983. (c) P. L. Trigg, A. V. Kondrachine, In Malaria. Parasite Biology, pathogenesis and protection; I. W. Sherman, Ed., ASM Press: Washington, DC, 1998, 11.
10. (a) R. N. Price, E. Tjiltra, C. A. Guerra, S. Yeung, N. J. White, N. M. Anstey, Vivax malaria: neglected and not benign. *Am. J. Trop. Med. Hyg.* 2007, **77 (Suppl. 6)**, 79. (b) S. B. Sirima, S. Cousens, P. Druilhe, *N. Engl. J. Med.* 2011, **365**, 1062.
11. (a) I. Y. Gluzman, S. E. Francis, A. Oksman, C. E. Smith, K. L. Duffin, D. E. Goldberg, *J. Clin. Invest.* 1994, **93**, 1602. (b) C. Biot, W. Castro, C. Y. Bottéd, M. Navarro, *Dalton Trans.* 2012, **41**, 6335.
12. (a) Murray, C. J. L.; Rosenfeld, L. C.; Lim, S. S.; Andrews, K. G.; Foreman, K. J.; Haring, D.; Fullman, N.; Naghavi, M.; Lozano, R.; Lopez, A. D. *Lancet.* **2012**, *379*,

413. (b) K. K. Eggleson, K. L. Duffin, D. E Goldberg, *J. Biol. Chem.* 1999, **274**, 3241.

13. I. W. Sherman, *Malaria: Parasite biology, pathogenesis and protection*, American Society for Microbiology, Washington, 1998, chap. 10.
14. World's scientific and social network for malaria professionals <http://www.malariaworld.org/blog/we-thought-we-were-down-655000-deaths-2010-right>, (Accessed 31 Jan. 2012).
15. *Source* <http://ftp.bhfglobal.com/malaria-took-more-lives-than-estimated-3022012>, (Accessed 31 Jan. 2012).
16. (a) N. Chavain, H. Vezin, D. Dive, N. Touati, J. F. Paul, E. Buisine, C. Biot, *Mol. Pharm.* 2008, **5**, 710. (b) F. Bienvenu, S. Jirawatnotai, J. E. Elias, C. A. Meyer, K. Mizeracka, A. Marson, et al., *Nature*. 2010, **463**, 374.
17. (a) F. Bellot, F. Coslédan, L. Vendier, J. Brocard, B. Meunier, A. Robert, *J. Med. Chem.* 2010, **53**, 4103. (b) *Sources* <www.malariasite.com/malaria/Malarial Parasite.htm>, *(*Accessed 26 Jan. 2012).
18. (a) L. H. Bannister, J. M. Hopkins, R. E. Fowler, S. Krishna, G. H. Mitchell, *Parasitol. Today.* 2000, **16**, 427. (b) *Sources* <www.dpd.cdc.gov/dpdx/HTML/PDF_Files/.../chap_26.pdf>, (Accessed 18 Jan. 2012).
19. "Malaria." *MicrobiologyBytes.* Ed. Dr Alan Cann. *Sources* <http://www.microbiologybytes.com/introduction/Malaria.html>, (Revised 8 Apr. 2009), (Accessed 18 Jan. 2012).
20. *Sources* <http://clarosci.com/wp-content/uploads/2011/04/Malaria_red295x300.jpg>, (Accessed 8 Feb. 2012).
21. K. Haldar, T. Akompong, R. Banerjee, D. E. Goldberg, In Antimalarial Chemotherapy: Mechanisms of Action, Resistance, and New Directions in Drug Discovery; Rosenthal, *P. J., Ed.; Humana Press*: New York, 2001; p 23.
22. (a) Z. J. Guo, P. J. Sadler, *Adv. Inorg. Chem.*, 2000, **49**, 183. (b) P. J. Dyson, G. Sava. *Dalton Trans*. 2006, **5**, 1929.
23. (a) M. J. Hannon, *Pure Appl. Chem.* 2007, **79**, 2243. (b) D. B. Jacoby, R. M. Youngson, Encyclopedia of family health. 3rd ed., Marshall Cavendish, 2004. (c) M. J. Schiewer, M. A. Augello, K. E. Knudsen, *M.J. Schiewer et al. Cell. Biol.* 2011, **31 (22)**, 4513.

24. (a) K. J. Arrow, C. B. Panosian, H. Gelband, eds, *Saving Lives, Buying Time: The Economics of Malaria Drugs in an Age of Resistance*, The National Academies Press, Washington D. C., 2004. (b) M. Foley, L. Tilley, *Pharmacol. Ther.* 1998, **79**, 55.

25. (a) D.B. Agus, C. Cordon-Cardo, W. Fox, M. Drobnjak, A. Koff, D.W. Golde, et al., *J. Natl. Cancer Inst.* 1999, **91**, 1869. (b) J. Achan, A. O. Talisuna, A. Erhart, A. Yeka, J. K. Tibenderana, F. N. Baliraine, *et al.* Quinine, an old anti-malarial drug in a modern world: role in the treatment of malaria. *Malaria J.* 2011, **10**, 144.

26. (a) A. Kiszweski, A. Mellinger, A. Spielman, P. Malaney, S. Ehrlich Sachs, J. Sachs, *Am. J. Trop. Med. Hyg.* 2004, **70**, 486. (b) K. Yearick, K. Ekoue-Kovi, D. P. Iwaniuk, J. K. Natarajan, J. Alumasa, A. C. de Dios, P. D. Roepe, C. Wolf, *J. Med. Chem.* 2008, **51**, 1995.

27. (a) R. G. Ridley, *Nature*. 2002, **415**, 686. (b) D. De, F. M. Krogstad, L. D. Byers, D. J. Krogstad, *J. Med. Chem.* 1998, **41**, 4918.

28. (a) I. M. Hastings, P. G. Bray, S. A. Ward, *Science*. 2002, **45**, 2001. (b) P. Chellan, N. Shunmoogam-Gounden, D. T. Hendricks, J. Gut, P. J. Rosenthal, C. Lategan, P. J. Smith, K. Chibale, G. S. Smith, *Eur. J. Inorg. Chem.* 2010, **22**, 3520.

29. (a) L. Glans, A. Ehnbom, C. de Kock, A. Martinez, J. Estrade, P. J. Smith, M. Haukka, R. A. Sanchez-Delgado, E. Nordlander, *Dalton Trans.* 2012, **41(9)**, 2764. (b) T. Storr, K. H. Thompson, C. Orvig, *Chem. Soc. Rev.* 2006, **35**, 534.

30. (a) I. M. Hastings, P. G. Bray, S. A. Ward, *Science*. 2002, **45**, 2001. (b) L. M. B. Ursos, P. D. Roepe, *Med. Res. Rev.* 2002, **22**, 465.

31. T. J. Egan, R. Hunter, C. H. Kaschula, H. M. Marques, A. Misplon, J. Walden, *J. Med. Chem.* 2000, **43**, 283.

32. (a) J.E. Hyde, *an insight. FEBS Journal*. 2007, **274**, 4688. (b) E. R. T. Tiekink, *Gold Bull.* 2003, **36**, 117.

33. L. Martinez-Gamboa, H-P. Brezinschek, G. R. Burmester and T. Dörner, *Autoimmun. Rev.* 2006, **5**, 437.

34. M. Font, A. Monge, I. Ruiz, B. Heras, *Drug Des. Discovery*. 1997, **14**, 259.

35. T. Nakamura, M. Oka, K. Aizawa, H. Soda, M. Fukuda, K. Terashi, K. Ikeda, Y. Mizuta, Y. Noguchi, Y. Kimura, T. Tsuruo, S. Kohno, Biochem. *Biophys. Res. Commun.* 1999, **255**, 618.

36. D. Kaminsky, R. J. Meltzer, *J. Med. Chem.* 1968, **11**, 160.

37. R. Musiol, J. Jampilek, V. Buchta, L. Silva, H. Niedbala, B. Podeszwa, A. Palka, K. Majerz-Maniecka, B. Oleksyn, J. Polanski, *Bioorg. Med. Chem.* 2006, **14**, 3592. (f)

38. N. C. Warshakoon, J. Sheville, R. T. Bhatt, W. Ji, J. L. Mendez-Andino, K. M. Meyers, N. Kim, J. A. Wos, C. Mitchell, J. L. Paris, B. B. Pinney, O. Reizes, X. E. Hu, *Bioorg. Med. Chem. Lett.* 2006, **16**, 5207.

39. A. E. Sloboda, D. Powell, J. F. Poletto, W. C. Pickett, J. J. Gibbons, D. H. Bell, A. L. Oronsky, S. S. Kerwar, *J. Rheumatol.* 1991, **18**, 855.

40. (a) R. A. Sánchez-Delgado, A. Anzellotti, L. Suárez, *Med. Chem.* 2004, **4**, 23. (b) M. Navarro, *Coord. Chem. Rev.* 2009, **253**, 1619.

41. (a) R. W. Snow, J-F. Trape, K. Marsh, *Trends Parasitol.* 2001, **17**, 593. (b) M. A. Jakupec, M. Galanski, V. B. Arion, C. G. Hartinger, B. K. Keppler, *Dalton Trans.* 2008, **21**, 183.

42. (a) M. J. Clarke, *Coord. Chem. Rev.* 2003, **236**, 209. (b) M. Navarro, S. Pekerar, H. Pérez. *Polyhedron.* 2007, **6**, 2420.

43. K. A. de Villiers, T. J. Egan, *Molecules*, 2009, **14**, 2868.

44. (a) T. J. Egan, H. M. Marques, *Coord. Chem. Rev.* 1999, **190-192**, 493. (b) C. R. Chong, D. J. Sullivan, *Biochem. Pharmacol.* 2003, **66**, 2201.

45. P. J. Rosenthal, Ed., *Antimalarial Chemotherapy: mechanism of action, resistance and new directions in drug discovery*, Humana Press, New Jersey, 2001.

46. C. R. Chong and D. J. Sullivan, *Biochem. Pharmacol.* 2003, **66**, 2201.

47. (a) D. C. Warhurst, J. C. Craig, I. S. Adagu, D. J. Meyer, S.Y. Lee, *Malaria J.* 2003, *2* **(26)**, 1. (b) *Source* < http://www.drugbank.ca/>, (Accessed 30 Jan. 2012).

48. (a) M. J. Clarke, *Coord. Chem. Rev.* 2003, **236**, 209. (b) S. R. Hawley, P.G. Bray, P. M. O'Neill, B. K. Park, S. A. Ward, *Biochem. Pharmacol.* 1996, **52 (5)**, 723.

49. A. Llinas, R. C. Glen, J. M. Goodman, *J. Chem. Inf. Model.* 2008, **48** (7), 1289.

50. J. Wiesner, D. Henschker, D. B. Hutchinson, E. Beck, H. Jomaa, *Antimicrob. Agents Chemother.* 2002, **46** (**9**), 2889.

51. (a) C. Biot, G. Glorian, L. A. Maciejewski, J. S. Brocard. *J. Med. Chem.* 1997, **40**, 3715. (b) D. Dive, C. Biot, *J. Med. Chem.* 2008, **3**, 383.

52. (a) R.K. Haynes, B. Fugmann, J. Stetter, K. Rieckmann, H. -D. Heilmann, H. -W. Chan, M.-K. Cheung, W.-L. Lam, H.-N. Wong, S.L. Croft, L. Vivas, L. Rattray, L. Stewart, W. Peters, B. L. Robinson, M. D. Edstein, B. Kotecka, D. E. Kyle, B. Beckermann, M. Gerisch, M. Radtke, G. Schmuck, W. Steinke, U. Wollborn, K.

Schmeer, A. Romer, *Angewandte Chemie, Inl Ed.* 2006, **45 (13)**, 2082. (b) A. Brossi, B. Venugopalan, G. L. Dominguez, H. J. C. Yeh, J. L. Flippen-Anderson, P. Buchs, X. D. Luo, W. Milhous, W. Peters, *J. Med. Chem.* 1988, **31 (3)**, 645.

53. P. Beagley, M. A. Blackie, K. Chibale, C. Clarkson, J. R. Moss, P. J. Smith, *Chem. Soc. Dalton Trans.* 2002, **15**, 4426.

54. (a) F. A. Beckforda, G. Leblanca, J. Thessinga, *Inorg. Chem. Commun.* 2009, **12**, 1094. (b) A. A. El-Asmy, O. A. El-Gammal, H. S. Saleh, *Spectrochimica Acta Part A: Mol. Biomol. Spec.* 2008, **71**, 39.

55. (a) A. G. Quiroga, J. M. Perez, E. I. Montero, C. Alonso, C. Navarro-Ranninger, *J. Inorg. Biochem.* 1999, **75**, 293. (b) M. A. Jakupec, M. Galanski, V. B. Arion, C. G. Hartinger, B. K. Keppler, *Dalton Trans.* 2008, **21**, 183.

56. (a) N. Wash, H. B. Singh, A. Gajanana, A. N. Raichowdhary, *Inorg. Chim. Acta.* 1987, **135**, 133. (b) S. R. Hawley, P. G. Bray, P. M. O'Neill, B. K. Park, S. A. Ward, *Biochem. Pharmacol.* 1996, **52**, 723.

57. (a) Z. Guo, P. J. Sadler, *Angew. Chem., Int. Ed.* 1999, **38**, 1512. (b) N. Chavain, C. Biot, *Curr. Med. Chem.* 2010, **17 (25)**, 2729. (c) L. Ronconi, P. J. Sadler, *Coord. Chem. Rev.* 2007, **251**, 1633.

58. (a) G. Gasser, N. Metzler-Nolte, *Curr. Opin. Chem. Biol.* 2012, **16**, 84. (b) M. Patra, G. Gasser, *Chem. BioChem.* 2012, **13**, 1232. (c) M. A. Jakupec, M. Galanski, V. B. Arion, C. G. Hartinger, B. K. Keppler, *Dalton Trans.* 2008, 183. (d) G. Jaouen, Ed. Bioorganometallics; Biomolecules, Labeling, Medicine; Wiley-VCH: Weinheim, 2006. (e) P. J. Dyson, G. Sava, *Dalton Trans.* 2011, **40**, 9069.

59. (a) M. G. Voronkov, G. I. Zelchan, E. Lukevitz, *Silizium und Leben* (Ed.: K. Ruhlmann), Akademie, Berlin, 1975. (b) B. S. Sekhon, N. Bimal, *J Pharm Educ Res*, 2012, **3 (2)**, 52.

60. (a) A. F. A. Peacock, P. J. Sadler, *Chem. Asian J.* 2008, **3 (11)**, 1890. (b) G. Süss-Fink, *Dalton Trans.* 2010, **39** (7), 1673. (c) G. Gasser, I. Ott, N. Metzler-Nolte, *J. Med. Chem.* 2011, **54**, 3. (d) R. A. Sánchez-Delgado, M. Navarro, H. Pérez, J. A. Urbina, *J. Chem. Med.* 1996, **39**, 1095.

61. (a) *Sources* <http://www.sciencephoto.com/media/1798/enlarge>, (Accessed 1 March, 2012). (b) *Sources* <http://accol.tumblr.com/post/6538246516/chemistry-transition-metal-salts>, (Accessed 2 March, 2012).

62. G. Lümmen, H. Sperling, H. Luboldt, T. Otto, H. Rübben, *Cancer Chemother. Pharmacol.* 1998, **42**, 415.

63. E. Prats, F. Aisa, M. D. Abós, L. Villavieja, F. García-López, M. J. Asenjo, P. Razola, J. Banzo, *J. Nucl. Med.* 1999, **40**, 296.

64. P. Baiocco, G. Colotti, S. Franceschini and A. Ilari, *J. Med. Chem.* 2009, **52**, 2603.

65. (a) L. Glans, D. Taylor, C. de Kock, P. J. Smith, M. Haukka, J. R. Moss, E. Nordlander. *J. Inorg. Biochem.* 2011, **105**, 985. (b) L. Trynda-Lemiesz, B. K. Keppler, H. Kozlowski, *J. Inorg. Biochem.* 1999, **73**, 123.

66. (a) L. Trynda-Lemiesz, A. Karaczyn, B. K. Keppler, H. Kozlowski, *J. Inorg. Biochem.* 2000, **78**, 341. (b) L. Trynda-Lemiesz, H. Kozlowski, B. K. Keppler, *J. Inorg. Biochem.* 1999, **77**, 141. (c) T. Ikeue, M. Handa, A. Chamberlin, A. Ghosh, O. Ongayi, M. G. Vicente, A. Ikezaki, M. Nakamura, *Inorg. Chem.* 2011, **50**, 3567.

67. (a) S. K. Rajapakse, A. Martínez, B. Naoulou, A. Jarzecki, L. Suárez, C. Deregnaucourt, V. Sinou, J. Schrével, E. Musi, G. Ambrosini, G. K. Schwartz, R. A. Sánchez-Delgado, *Inorg. Chem.* 2009, **2**, 1122. (b) B. Therrien, *Eur. J. inorg. Chem.* 2009, **4**, 2445. (c) M. Fujia, H. Oka, K. Ogura, *Tetrahedron Lett,* 1995, **1**, 5247.

68. G. Jaouen (Ed.). Bioorganometallics: Biomolecules, Labelling, Medicine, Wiley-VCH, Weinheim 2005.

69. (a) D. R. Van Staveren, N. Metzler-Nolte, *Chem. Rev.* 2004, **104**, 5931. (b) A. Vessieres, S. Top, W. Beck, E.Hillard, G. Jaouen. *Dalton Trans.* 2006, **529**.

70. (a) G. Gasser, N. Metzler-Nolte, *Curr. Opin. Chem. Biol.* 2012, **12**, 1. (b) M. M. Harding, G. Mokdsi. *Curr. Med. Chem.* 2000, **7**, 1289.

71. (a) G. Gasser, I. Ott, N. Metzler-Nolte, *J. Med. Chem.* 2011, **54**, 3. (b) E. R. T. Tiekink, *Gold Bull.* 2003, **36**, 117. (c) P. J. Sadler, H. Li, H. Sun, *Coord. Chem. Rev.* 1999, **185**, 689.

72. (a) M. Patra, G. Gasser, N. Metzler-Nolte, *Dalton Transc*, 2012, **41**, 6350. (b) M. Woodward, C. Morrison, K. McColl, *J. Clin. Epidemiol.* 2000, **53**, 175.

73. (a) W. Daher, L. Pelinski, S. Klieber, F. Sadoun, V. Meunier, M. Bourrie, C. Biot, F. Ois Guillou, G. Fabre, J. Brocard, L. Fraisse, J. P. Maffrand, J. Khalife, D. Dive, *Malarial J.* 2005, **352**, 1565. (b) C. Atteke, J. M. Ndong, A. Aubouy, L. A. Maciejewski, J. S. Brocard, J. Lebibi, P. J. Deloron, *Antimicrob. Chemother.* 2005, **51**, 1021.

74. (a) A. N. Nesmeyanov, L. G. Bogomolova, V. Viltcheskaya, N. Palitsyne, I. Andrianova, O. Belozerova, U.S. Patent 119356, 1971. (b) N. Yang, H. Sun, *Coord. Chem. Rev.* 2007, **251**, 2354. (c) L. Glans, D. Taylor, C. de Kock, P. J. Smith, M. Haukka, J. R. Moss, E. Nordlander, *J. Inorg. Biochem.* 2011, **105**, 985.

75. (a) K. Mustfa, I. Landau, A. G. Chabaud, J. M. Chavatte, J. Chandenier, T. H. Duong, D. Richard-Lenoble, *Sante*, 2011, **21**, 133. (b) Clinical trials (2012) <http://clinicalttrials.gov/ct2/show/NCT00988507>, (Accessed 26 Feb, 2012).

76. (a) C. Biot, W. Castro, C. Y. Botte, M. Navarro, *Dalton Trans.*, 2012, **41**, 6335. (b) R. A. Sánchez-Delgado, M. Navarro, H. Pérez, J. A. Urbina, *J. Med. Chem.* 1996, **39**, 1095.

77. (a) L. D. Dale, J. H. Tocher, T. M. Dyson, D. I. Edwards, D. A. Tocher, *Anti-Cancer Drug Design.* 1992, **7 (1)**, 3. (b) C. S. Allardyce, P. J. Dyson, *Platium Metals Rev.* 2001, **45 (2)**, 62.

78. (a) M. Navarro, W. Castro, C. Biot, *Organometallics.* 2012, **31**, 5717. (b) D. Gambino, L. Otero, *Inorg. Chim. Acta.* 2012, **393**, 103.

79. (a) A. Martinez, J. Suárez, T. Shand, R. S. Magliozzo, R. A. Sánchez-Delgado, *J. Inorg Biochem*, 2011, **105 (1)**, 39. (b) A. Martnez, C. S. Rajapakse, *J. Biol Inorg Chem.* 2008, **13 (5)**, 703.

80. (a) C. G. Hartinger, S. Zoebas-Selfried, M. A. Jakupee, B. Kynast, H. Zorbas, B. K. Keppler, *J. Inorg. Biochem.* 2006, **100**, 891. (b) P. Minodier, P. Parola, *Travel Med. Infect. Dis.*, 2007, **5**, 150. (c) P. Desjeux, *Comp. Immunol. Microbiol. Infect. Dis.* 2004, **27**, 305.

81. (a) Y. K. Yan, M. Melchart, A. Habtemariam, P. J. Sadler, *Chem. Commun.* 2005, **4764**. (b) L. Thunus, R. Lejeune, *Coord. Chem. Rev.* 1999, **184**, 125. (c) S. J. Goldsmith, S. Vallabhajosula, *Semin. Nucl. Med.* 2009, **39**, 2.

82. (a) N. Katsaros, A. Anagnostopoulou, *Crit Rev Oncol Hematol.* 2002, **42**, 297. (b) V. Brabec, O. Novakova, V. Bursova, C. Hofr, M. Vojtiskova, H. Chen, P. J. Sadler, V. Brabec. *Chem. Biol.* 2005, **12**, 121.

83. (a) M. Navarro, F. Vásquez, R. A. Sánchez-Delgado, H. Pérez, V. Sinou, J. Schrével, *J. Med. Chem.* 2004, **47**, 5204. (b) R. A. Howard, A. P. Kimball, J. L. Bear, *Cancer Rev.* 1979, **39**, 2568.

84. (a) N. Katsaros, A. Anagnostopoulou, *Crit. Rev. Oncol Hematol.* 2002, **42**, 297. (b) G. A. Hulett, H. W. Berger, *J. Am. Chem. Soc.* 1904, **26 (11)**, 1512.

85. (a) A. Roberto, Sánchez-Delgado, M. Navarro, H. Perez, A. J. Urbina, *J. Med. Chem.* 1996, **39**, 1095. (b) T. Giraldi, G. Zassinovich, G. Mestroni, *Chem. Biol.Interact.* 1974, **9**, 389.

86. (a) W. Bains, R. Tacke, *Curr. Opin. Drug Discovery Dev.* 2003, **6**, 526. (b) J. O. Daiss, C. Burschka, J. S. Mills, J. G. Montana, G. A. Showell, I. Fleming, C. Gaudon, D. Ivanova, H. Gronemeyer, R. Tacke, *Organometallics.* 2005, **24**, 3192.

87. (a) M. Merget, K. Günther, M. Bernd, E. Günther, R. J. Tacke, *Organomet. Chem.* 2001, **628**, 183. (b) R. Tacke, M. Merget, R. Bertermann, M. Bernd, T. Beckers, T. Reissmann, *Organometallics.* 2000, **19**, 3486.

88. (a) B. Arkles, CHEMTECH 1983, 13, 542. (b) R. Tacke, D. Reichel, M. Kropfhans, P. G. Jones, E. Mutschler, J. Gross, X. Hou, M. Waelbroeck, G. Lambrecht, *Organometallics.* 1995, **14**, 251.

89. (a) G. Lambrecht, R. Feifel, U. Moser, M. Wagner-Röder, C. Strohmann, H. Zilch, R. Tacke, M. Waelbroeck, J. Christophe, H. Boddeke, E. Mutschler, *Eur. J. Pharmacol.* 1989, **168 (1)**, 71. (b) M. E. Kenney, N. L. Oleinich, B. D. Rihter, Y. S. Li, Phthalocyanine Photosensitiziers for Photodynamic Therapy and Methods for Their Synthesis and Use. U.S. Patent 5484778, 1996. (c) Y. S. Li, M. E. Kenney, Novel Methods of Synthesis of Phthalocyanine Compounds. U.S. Patent 5763602, 1998.

90. (a) J. S. Mills, G. A. Showell, *Expert Opin. Investig. Drugs* 2004, **13**, 1149. (b) P. Englebienne, A. Van Hoonacker, C. V. Herst, *Drug Des. Rev.*-Online 2005, **2**, 467.

91. (a) S. Farkas, *CNS Drug Rev.* 2006, **12**, 218. (b) T. Mitchell, G. A. Showell, *Curr Opin Drug Discovery Dev.* 2001, **4(3)**, 314. (c) N. Chavain, C. Biot, *Curr. Med. Chem.* 2010, **17 (25)**, 2729.

92. (a) L. Ronconi, P. J. Sadler, *Coord. Chem. Rev.* 2007, **251**, 1633. (b) G. Sava, A. Bergamo, *Int. J. Oncol.* 2000, **17**, 353.

93. (a) J. M. Rademaker-Lakhai, D. Van den Bongard, D. Pluim, J. H. Beijnen, J. H. Schellens, *Clin. Caner Res.* 2004, **10**, 3717. (b) B. Rosenberg, T. G. Spiro (Ed.), Nucleic Acid-Metal Ion Interactions, Wiley, New York, 1980.

94. (a) T. Ikeue, M. Handa, A. Chamberlin, A. Ghosh, O. Ongayi, M. G. Vicente, A. Ikezaki, M. Nakamura, *Inorg. Chem.* 2011, **50**, 3567. (b) W. P. Walters, M. A. Murcko, *Adv Drug Deliv Rev.* 2002, **54(3)**, 255. (c) W. Bains, R. Tacke, *Curr Opin Drug Discovery Dev.* 2003, **6(4)**, 526.

95. (a) R. Tacke, Angew Chem Int Ed., 1999, **38(20)**, 3015. (b) *Silicon and Siliceous Structures in Biological Systems* (Eds.: T. L. Simpson, B. E. Volcani), Springer, New York, 1981.

96. (a) Silicon Biochemistry (Eds.: D. Evered, M. O'Connor), Wiley, Chichester, 1986. (b) G. Lambrecht, R. Feifel, U. Moser, M. Wagner-Röder, C. Strohmann, H. Zilch, R. Tacke, M. Waelbroeck, J. Christophe, H. Boddeke, F. Mutschler, *E. Eur. J. Pharmacol.* 1989, **168 (1)**, 71.

97. (a) M. E. Kenney, N. L. Oleinich, B. D. Rihter, Y. S. Li, Phthalocyanine Photosensitiziers for Photodynamic Therapy and Methods for Their Synthesis and Use. U.S. Patent 5484778, 1996. (b) Y. S. Li, M. E. Kenney, Novel Methods of Synthesis of Phthalocyanine Compounds. U.S. Patent 5763602, 1998.

98. (a) J. S. Mills, G. A. Showell, *Expert Opin. Investig. Drugs.* 2004, **13**, 1149. (b) P. Englebienne, A. Van Hoonacker, C. V. Herst, *Drug Design Rev.* 2005, **2**, 467. (c) W. Bains, R. Tacke, *Curr. Opin. Drug Discovery Dev.* 2003, **6**, 526.

99. (a) G. A. Showell, J. S. Mills, *Drug Discovery Today.* 2003, **8**, 551. (b) J. O. Daiss, C. Burschka, J. S. Mills, J. G. Montana, G. A. Showell, J. B. H. Warneck, R. Tacke, *Organometallics.* 2006, **25**, 1188.

100. (a) R. Tacke, M. Merget, R. Bertermann, M. Bernd, T. Beckers, T. Reissmann, *Organometallics.* 2000, **19**, 3486. (b) M, Merget. K, Gunther, M. Bernd, E. Gunther, R. Tacke, *J. Organomet. Chem.* 2001, **628**, 183.

101. (a) R. Tacke, T. Kornek, T. Heinrich, C. Burschka, M. Penka, M. Pulm, C. Mutschler, G. Lambrecht, *J. Organomet. Chem.* 2001, **640**, 140. (b) R. Tacke, V. I. Handmann, K. Kreutzmann, C. Keim, E. Mutschler, G. Lambrecht, *Organometallics.* 2002, **21**, 3727.

102. (a) R. Tacke, H. Linoh in The Chemistry of Organic Silicon Compounds, Part 2 (Eds.: S. patai, Z. Rappoport), Wiley, Chichester, 1989, 1143. (b) R. Tacke, S. A. Wagner in The Chemistry of Organic Silicon Compounds, Part 3, Vol. 2 (Eds.: Z. Rappoport, Y. Apeloig), Wiley, Chichester, 1998, 2363.

103. R. Tacke, T. Heinrich, R. Bertermann, C. Burschka, A. Hamacher, M. U. Kassack, *Organometallics.* 2004, **23**, 4468.

104. (a) *Source* <http://www.cancer.org/Cancer/CancerBasics>, (Revised 5 Sep. 2011), (Accessed 18 Jan. 2012). (b) R. Gagliardi, G. Sava, S. Pacor, G. Mestroni, E. Alessio,

Clin. Exp. Metastasis. 1994, **12**, 93. (c) M. Magnarin, A. Bergamo, M. E. Carotenuto, S. Zorzet, G. Sava, *Anticancer Res.* 2000, **20**, 2939.

105. (a) B. K. Keppler, M. Henn, U. M. Juhl, M. R. Berger, R. Niebl, F. E. Wagner, *Prog. Clin. Biochem. Med.* 1989, **10**, 41. (b) E. D. Kreuser, B. K. Keppler, W. E. Berdel, A. Piest, E. Thiel, *Semin. Oncol.* 1992, **19**, 73.
106. (a) M. Fujita, H. Oka, K. Ogura, *Tetrahedron Lett.* 1995, **36**, 5247. (b) K. Kumar, P. Singh, L. Kremer, Y. Guérardel, C. Biot, V. Kumar, *Dalton Trans.* 2012, **41 (19)**, 5778. (c) T. J. Egan, *Mol. Biochem. Parasitol.* 2008, **157**, 127.
107. (a) R. W. Snow, C. A. Guerra, A. M. Noor, H. Y. Myint, S. I. Hay, *Nature.* 2005, **434**, 214. (b) J. M. Pisciotta, D. Sullivan, *Parasitol. Int.* 2008, **57**, 89. (c) E. Hempelmann, T. J. Egan, *Trends Parasitol.* 2002, **18**, 11.
108. (a) J.E. Hyde, *an insight. FEBS Journal.* 2007, **274**, 4688. (b) M. J. Schiewer, M. A. Augello, K. E. Knudsen, *M.J. Schiewer et al. / Molecular and Cellular Endocrinology.* in press. (c) D.B. Agus, C. Cordon-Cardo, W. Fox, M. Drobnjak, A. Koff, D.W. Golde, et al., *J. Natl. Cancer Inst.* 1999, **91**, 1869.
109. (a) F. Bienvenu, S. Jirawatnotai, J. E. Elias, C. A. Meyer, K. Mizeracka, A. Marson, et al., *Nature.* 2010, **463**, 374. (b) C. D. Chen, D. S. Welsbie, C. Tran, S. H. Baek, R. Chen, R. Vessella, et al., *Nat. Med.* 2004, **10**, 33.
110. (a) Y. Chen, C. L. Sawyers, H. I. Scher, *Curr. Opin. Pharmacol.* 2008, **8**, 440. (b) L. Cheng, R. V. Lloyd, A. L. Weaver, T. M. Pisansky, J. C. Cheville, D. M. Ramnani, et al., *Clin. Cancer Res.* 2000, **6**, 1896.
111. (a) E. P. Gelmann, *J. Clin. Oncol.* 2002, **20**, 3001. (b) JD. Kemp, T. Cardillo, BC. Stewart, E. Kehrberg, G. Weiner, B. Hedlund, PW. Naumann, *Cancer Res.* 1995, **55**, 3817.
112. (a) DL. Becton, P. Bryles, *Cancer Res.* 1988, **48**, 7189. (b) L. R. Kelland, Metal Compounds in Cancer Therapy, S. P. Fricker (ed.), Chapman and Hall, London, 1994.
113. (a) S. Ivancsits, A. Pilger, E. Diem, HW. Rudiger, *Mutat Res.* 2002, **26**, 25. (b) JP. Fawcett, SJ. Farquhar, T. Thou, BI. Shand, *Pharmacol Toxicol.* 1997, **80**, 202. (c) D. P. Iwaniuk, E. D. Whetmore, N. Rosa, K. Ekoue-Kovi, J. Alumasa, A. C. de Dios, P. D. Roepe, C. Wolf, *Bioorg. Med. Chem.* 2009, **17 (18)**, 6560.
114. *Sources* <http://www.hivaidscd4.com/contentUploadFiles/contentImage/ 438px-Symptoms_of_cancer_metastasis_svg.png>, (Accessed 18 Jan. 2012).

115. (a) J. E. Garcia, A. Puentes, M. E. Patarroyo, *Clin. Microb. Rev.* 2006, **19**, 686. (b) P. G. Bray, M. Mungthin, R. G. Ridley, S. A. Ward, *Mol. Pharmacol.* 1998, **54**, 170.

116. (a) N. Farrell, T. T. B. Ha, J. –P. Souchard, F. L. Wimmer, S. Cros, N. P. Jphnson., *J. Med. Chem.* 1989, **32**, 2240. (b) E. I. Montero, S. Diaz, A. M. Gonzalez-Vadillo, J. M. Perez, C. Alonso, C. Navarro-Ranninger, *J. Med. Chem.* 1999, **42**, 4264.

117. (a) M. M. Harding, G. Mokdsi, *Curr. Med. Chem.* 2000, **7**, 1289. (b) S. Jahan, UA. Ashfaq, M. Qasim, S. Khaliq, MJ. Saleem, N. Afzal, *Infectious Agents and Cancer.* 2012, 7, 2.

118. (a) E. Wong, C. M. Giandomenico, *Chem. Rev.* 1999, **99**, 2451 and references therein Curret status of platinum-based antitumor drugs. (b) *Sources* <http://www.elmhurst.edu/~chm/vchembook/655cancer.html>, (Accessed 28 Jan. 2012).

119. (a) H. Riaz, T. Riaz, SA. Hussain, *Infectious Agents and Cancer.* 2012, 7, 1. (b) P. M. Takahara, A. C. Rosenzweig, C. A. Frederick, S. J. Lippard, *Nature*. 1995, **377**, 649.

120. (a) U. M. Ohndorf, M. A. Rould, Q. He, C. O. Pabo, S. J. Lippard, *Nature*. 1999, **399**, 708. (b) P. Eale, I Judson, A. O'Donnell, Br. *J. Cancer.* 2003, **88**, 1128.

121. (a) B. Rosenberg, *Cisplatin, Chemistry and Biochemistry of a Leading Anticancer Drug*, B. Lippert (Ed.), Wiley-VCH, Weinheim, 1999. (b) G. Jaouen, S. Top, A. Vessiéres, G. Leclercq, J. Quivy, L. Jin, A. Croisy, C. R. Acad, *Sci., Ser. IIc: Chim.* 2000, **3**, 89.

122. (a) M. A. Bennett, A. K. Smith, *J. Chem. Soc., Dalton Trans.* 1975, **2**, 233. (b) J. Reedijk, Chem. Commun. 1996, 7, 801.

123. (a) M. U. Raja, E. Sindhuja, R. Ramesh, *Inorg. Chem. Commun.* 2010, **13**, 1321. (b) M. Fujita, H. Oka, K. Ogura, *Tetrahedron Lett.* 1995, **36**, 5247. (c) T. Ikeue, M. Handa, A. Chamberlin, A. Ghosh, O. Ongayi, M. G. Vicente, A. Ikezaki, M. Nakamura, *Inorg. Chem.* 2011, **50**, 3567.

124. (a) P. J. Dyson, G. Sava, *Dalton Trans.* 2006, 1929. (b) L. Cerasino, M. J. Hannon, E. Sletten, *Inorg Chem.* 2007, **46**, 6245. (c) F. Wang, RL. Elliott, JF. Head, *Anticancer Res.*, 1999, **19**, 445. (d) G. Jaouen, S. Top, A. Vessiéres, G. Leclercq, M. J. McGlinchey, *Curr. Med. Chem.* 2004, **11**, 2505.

125. (a) S. Top, J. Tang, A. Vessiéres, D. Carrez, C. Provot, G. Jaouen, *Chem. Commun.* 1996, 955. (b) S. Top, A. Vessiéres, G. Leclercq, J. Quivy, J. Tang, J. Vaissermann, M. Huche, G. Jaouen, *Chem.–Eur. J.* 2003, **9**, 5223. (c) J. D. Kemp, T. Cardillo, B. C.

Stewart, E. Kehrberg, G. Weiner, B. Hedlund, P. W. Naumann, *Cancer Res.* 1995, **55**, 3817. (b) E. Badia, J. Oliva, P. Balaguer, V. Cavailles, *Curr. Med. Chem.* 2007, **11**, 950.

126. (a) M. P. Goetz, J. M. Rae, V. J. Suman, S. L. Safgren, M. M. Ames, D, W. Visscher, C. Reynolds, F. J. Couch, W. L. Lingle, D. A. Flockhart, Z. Desta, E. A. Perez, J. N. Ingle, *Journal of Clinical Oncology.* 2005, **23 (36)**, 9312. (b) H. Gronemeyer, J. A. Gustafsson, V. Laudet, *Nat. Rev. Drug Discovery.* 2004, **3**, 950. (c) A. K. Shiau, D. Barstad, P. M. Loria, L. Cheng, P. J. Kushner, D. A. Agard, G. L. Greene, *Cell.* 1998, **95(7)**, 927. (d) V. C. Jordan, *J. Med. Chem.* 2003, **46**, 883.

127. (a) H. Depenbrock, S. Schmelcher, R. Peter, B. K. Keppler, G. Weirich, T. Block, J. Rastetter, A. R. Hanauske, *Eur. J. Cancer.* 1997, **33**, 2404. (b) C. S. Allardyce, P. J. Dyson, D. J. Ellis, S. L. Heath, *Chem. Commun.* 2001, **15**, 1396. (c) C. S. Allardyce, P. J. Dyson, D. J. Ellis, P. A. Salter, R. Scopelliti, *J. Organomet. Chem.* 2003, **668**, 35. (d) Z. Guo, P. J. Sadler, *Angew. Chem., Int. Ed. Engl.* 1999, **38**, 1512.

128. (a) Z. Desta, B. A. Ward, N. V. Soukhova, D. A. Flockhart, *The American Society for Pharmacology and Experimental Therapeutics.* 2004, **310 (3)**, 1062. (b) A. Roberto, S.Delgado, M. Navarro, H. Pe´rez, J. A. Urbina, *J. Med. Chem.* 1996, **39**, 1095. (c) G. H. Beaven, S. H. Chen, A. d'Albis, W.B. Gratzer, *Eur. J. Inorg. Biochem.* 1974, **41**, 539. (d) H. Sun, H. Li, P. J. Sadler, *Chem. Rev.* 1999, **99**, 2817.

129. (a) J. M. Rademaker-Lakhai, D. Van den Bongard, D. Pluim, J. H. Beijnen, J. H. Schellens, *Clin. Caner Res.* 2004, **10**, 3717. (b) B. Rosenberg, T. G. Spiro (Ed.), Nucleic Acid-Metal Ion Interactions, Wiley, New York, 1980. (c) P. V. Scaria, J. C. Craig, R. H. Shafer, *Biopolymer.* 1993, **33**, 887. (d) T. Peters Jr., *Clin. Chem.* 1997, **23(1)**, 5.

130. (a) E. D. Kreuser, B. K. Keppler, W. E. Berdel, A. Piest, E. Thiel, *Semin. Oncol.* 1992, **19**, 73. (b) Z. Hrkal, M. Kociczek, Z. Vodrazka, B. Meloun, L. Moravek, *Int. J. Biochem.* 1978, **9**, 349. (c) A. Martinez, J. Suarez, T. Shand, R. S. Magliozzo, R. A. Sanchez-Delgado, *J. Inorg. Biochem.* 2011, **105**, 39. (d) G. Sava, A. Bergamo, *Int. J. Oncol.* 2000, **17**, 353.

131. (a) B. K. Keppler, M. Henn, U. M. Juhl, M. R. Berger, R. Niebl, F. E. Wagner, *Prog. Clin. Biochem. Med.* 1989, **10**, 41. (b) R. Gagliardi, G. Sava, S. Pacor, G. Mestroni, E. Alessio, *Clin. Exp. Metastasis.* 1994, **12**, 93. (c) M. Magnarin, A. Bergamo, M. E.

Carotenuto, S. Zorzet, G. Sava, *Anticancer Res.* 2000, **20**, 2939. (d) P. F. Salas, C. Herrmann, C. Orvig, *Chem. Rev.* 2013, **113 (5)**, 3450.

132. N. Farrell, B. R. James, R. Ugo (Eds.), Transition Metal Complexes as Drugs and Chemotherapeutic Agents, in Catalysis by Metal Complexes, Kluwer, Dordrecht, 1989.

133. (a) N. Katsaros, A. Anagnostopoulou, *Crit. Rev. Oncol. Hematol.* 2002, **42**, 297. (b) R. A. Howard, A. P. Kimball, J. L. Bear, *Cancer Res.* 1979, **39**, 2568. (c) R. A. Howard, T. G. Spring, J. L. Bear, *Cancer Res.* 1976, **36**, 4402.

134. (a) T. Giraldi, G. Sava, G. Bertoli, G. Mestroni, *Chem. Biol. Interact.* 1974, **9**, 389. (b) R. Chibber, I. J. Stratford, P. O'Neill, P. W. Sheldon, I. Ahmed, B. Lee, *Int. J. Radiat. Biol. Relat. Stud. Phys. Chem. Med.* 1985, **48**, 513.

Chapter 2:
SYNTHESIS AND CHARACTERISATION OF SILICON-CONTAINING AMINOQUINOLINE LIGANDS AND THEIR METAL COMPLEXES

2.1. Introduction

The success of several therapeutics such as cisplatin, ferroquine and NAMI-A, has established research into the synthesis of new transition metal complexes with interesting multi-functional biological properties.[1-3] Under this umbrella, bio-organometallic chemistry has emerged as an important field for developing new metallochemotherapeutics (Chapter 1).[4-11] New strategies of incorporating different moieties into the side chain of chloroquine has demonstrated some promising results.[12-16] Thus, we were interested in investigating the effects of introducing a silicon moiety into the lateral side chain of chloroquine.

As mentioned in Section 1.5, several recent publications were published on bio-organosilicon chemistry, which provide a novel and powerful source of chemical diversity in medicinal drug design.[17-19] In addition to the examples given in Section 1.5, there are many other examples of silicon-containing compounds in the literature with interesting properties.[20-22] The use of organosilicon chemistry in drug design has been reviewed previously by Tacke and Linoh,[23] Tagne Kuate, *et al.*,[24a] Showell and Mills,[25a] Chenthamarakshan and Ajayaghosh,[26c] Pooni and Showell,[27a] Gately and West.[28a] Recently, there has being a growing interest in silicon chemistry, as this is stimulated by their potential applications in numerous biological systems,[27-29] and medicine.[30-32]

Figure 2.1 illustrates examples of novel carbon/silicon switch compounds, which display increased biological potency.[24a-c] The literature suggests that one proposed reason for enhanced biological potency is that the carbinol serves as a hydrogen bond donor within the pharmacophore, and in some cases silanol is a much better hydrogen bond donor than the corresponding carbinol.[24b-26] Much of this work was published by Tacke.[24a-h]

In addition, some studies suggest that the replacement of the quaternary R_3COH carbon atom of haloperidol by a silicon atom significantly altered its metabolic fate.[24] For the haloperidol, the pyridinium metabolite is formed via dehydration and oxidation of the piperidine ring to the pyridinium ion.[24] However, for the sila-haloperidol case, the analogous sila-pyridinium ion was not formed, and new metabolic pathways originating from opening of the piperidine ring were observed.[24-26]

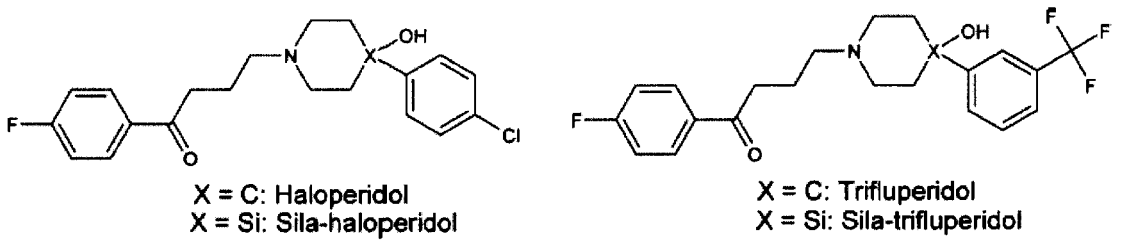

Figure 2.1: Sila-substituted compounds.[24a]

With regard to combating resistance, new strategies in drug design of utilising several transition metal complexes of chloroquine have been synthesised and evaluated for antiplasmodial activity with varying degrees of success (Section 1.4).[33-35] In some instances, transition metals such as ruthenium and rhodium seem to provide additional stability to the drug and a better means of delivery to their desired targets.[34-36] Thus in this chapter, the synthesis and characterisation of new silicon analogues of CQ, and their mononuclear Ru and Rh transition metal complexes is described. Furthermore, several aspects of compound characterisation such as ^{1}H, ^{13}C, and 2D-NMR spectroscopy, COSY, NOESY, and HSQC are discussed.

2.2. Synthesis of silicon-containing aminoquinoline ligands (2.1 and 2.2)

Two silicon-containing aminoquinoline ligands **2.1** and **2.2** were prepared via a nucleophilic substitution reaction of 4,7-dichloroquinoline with the appropriate amine-terminated silane as depicted in Scheme 2.1. Two silane precursors, aminomethyltrimethylsilane and 3-aminopropyltrimethylsilane, were used. The rationale was to compare the effect of the alkyl spacer (n = 1, 3) between the terminal trimethylsilane and the secondary amine group, both on the modified lateral side chain. In addition, with regard to the increasing alkyl chain length, the question arises, what effect will this have on the biological and physical properties?

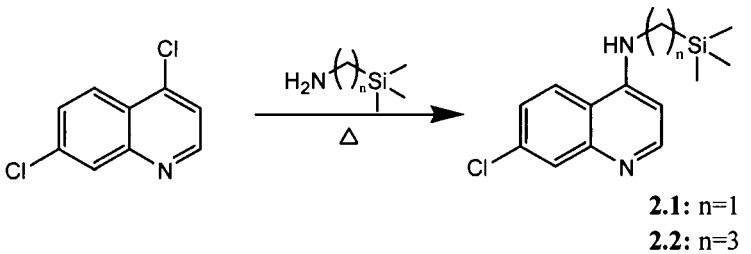

Scheme 2.1: Synthetic route to silicon-containing aminoquinoline ligands **2.1** and **2.2**.

Physical properties

Both of the silicon-containing aminoquinoline ligands **2.1** and **2.2** were isolated in moderate yields ranging between 63-79 %. They exhibit melting point temperatures ranging between 125-129 and 165-168 °C respectively (Table 2.1). Compounds **2.1** and **2.2** are insoluble in water, hexane and petroleum ether. They are slightly soluble in alcoholic solvents such as MeOH, EtOH, and selected organic solvents such as diethyl ether, toluene and ethyl acetate with slight heating. Furthermore, both compounds display good solubility in acetone, DCM and DMSO.

Table 2.1: Physical appearance, yields and melting points for compounds **2.1** and **2.2**.

Compound number	n	Yield (%)	Physical Appearance	M.p. (°C)
2.1	1	79.2	white solid 	125 - 129
2.2	3	63.4	white solid 	165 - 168

2.2.1. Spectroscopic and analytical characterisation

All compounds were characterised using ^{1}H, ^{13}C NMR, and infrared spectroscopy. The assignment of peaks was supported by using 2D-NMR spectroscopy. Furthermore, elemental analysis, mass spectrometry, and single-crystal X-ray analysis confirmed the integrity of the synthesised ligands.

^{1}H NMR spectroscopy

The ^{1}H NMR spectra of compounds **2.1** and **2.2** display distinctive peaks associated with the proposed structure. The trimethylsilane protons are observed at 0.1 ppm as a singlet, integrating for nine protons which confirm the presence of the three methyl groups. In addition, the silicon atom causes a strong shielding effect, which results in the methyl protons being detected close to 0 ppm. Likewise, as a direct result of the electronic and shielding effect of the silicon atom, the CH_2 protons appear relatively upfield. Three signals for the aliphatic chain in compound **2.2** are observed as multiplets in the range of 0.54-0.70 ppm, 1.64-1.82 ppm, and 3.32-3.37 ppm respectively, all integrating for two protons each. The ^{1}H NMR spectrum of compound **2.2** is presented in Figure 2.2 as an example.

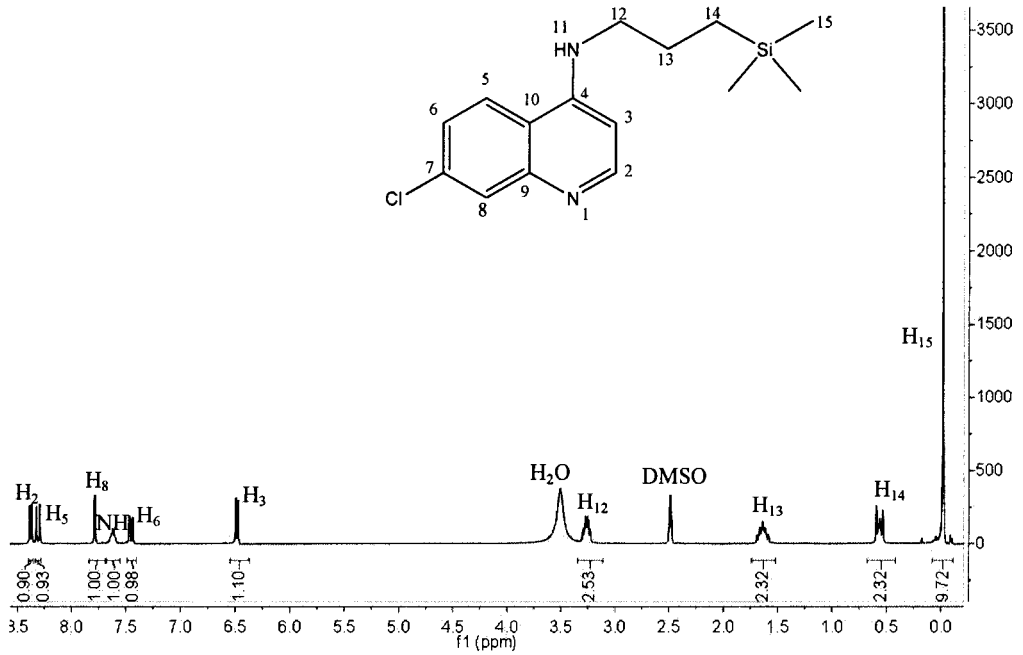

Figure 2.2: ^{1}H NMR spectrum of compound **2.2** recorded in DMSO-d_6.

Compound **2.1**, containing only one carbon spacer, displays one peak as a singlet at 2.02 ppm. Furthermore, for both compounds, the quinoline protons appear in the aromatic region of 6.50-8.50 ppm. The chemical shifts of the quinoline motif appear in the same region as for similar compounds reported in the literature.[37] Lastly, the amine proton NH, being adjacent to the aromatic ring appears relatively deshielded as a broad singlet. This is observed at around 7.1 and 7.6 ppm for compound **2.1** and **2.2** respectively. In addition, a 2D-NMR experiment, namely Correlation Spectroscopy (COSY), which is a two-dimensional homonuclear technique, was used to ascertain proton-proton couplings (Figure 2.3).

On inspection of the COSY spectrum for compound **2.2**, it is observed that the most deshielded proton (H_2) detected as a doublet, couples to its adjacent proton (H_3) at around 6.5 ppm. H_2 has a coupling constant of 5.68 Hz, very similar to other quinoline-based compounds reported in literature.[37] Likewise, H_6 appears around 7.4 ppm as a doublet of a doublet; it couples to its adjacent proton H_5 and through-space coupling to H_8. H_6 has two coupling constant values of 2.23 and 8.99 Hz, which correspond to literature coupling constant values.[37] The three CH_2 groups are observed as multiplets, at around 0.8, 1.8, and 3.1 ppm respectively. Lastly, the most shielded protons, methyl groups on the silicon atom couples to itself at around 0.1 ppm as a singlet.

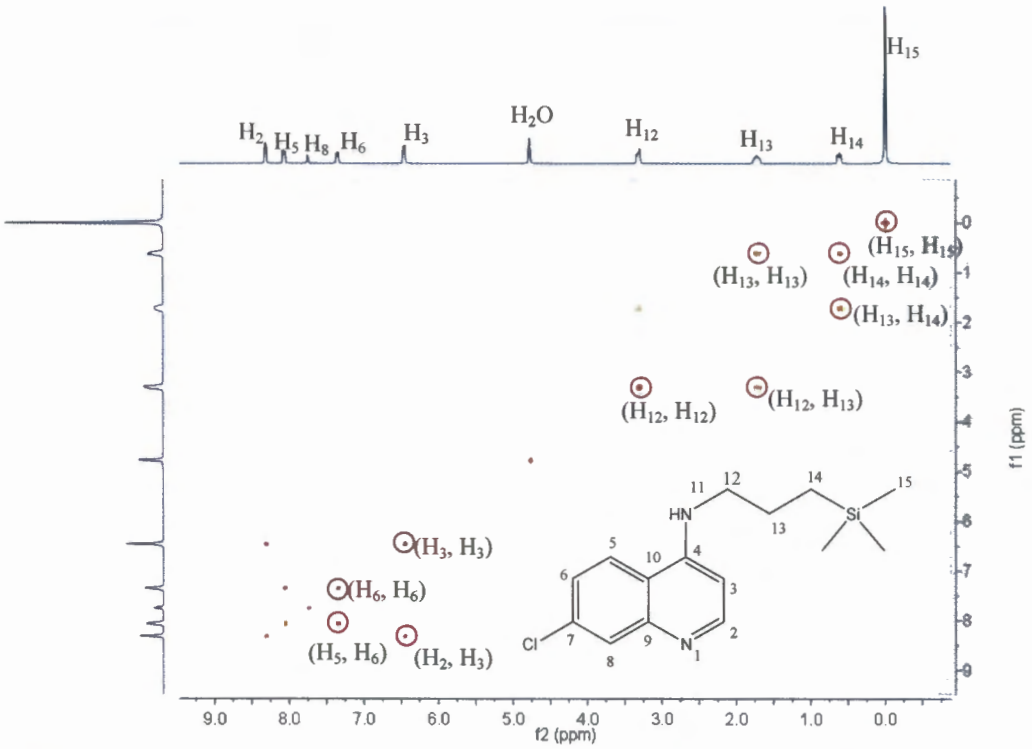

Figure 2.3: COSY 2D-NMR spectrum of compound **2.2** recorded in DMSO-d_6.

The Nuclear Overhauser Effect spectroscopy (NOESY), which illustrates cross relaxation between nuclear spins, was used to establish the cross peak coupling resonances from nuclei that are spatially close. This provided further validation of the proton assignments (Figure 2.4). On inspection of the NOESY spectrum for compound **2.2**, it is observed that H_8 couples to H_6 across the chloro-group on the quinoline moiety at around 7.5 ppm. Also, proton H_{14} couples to proton H_{12} at around 0.6 ppm through a CH_2 group in the lateral side chain.

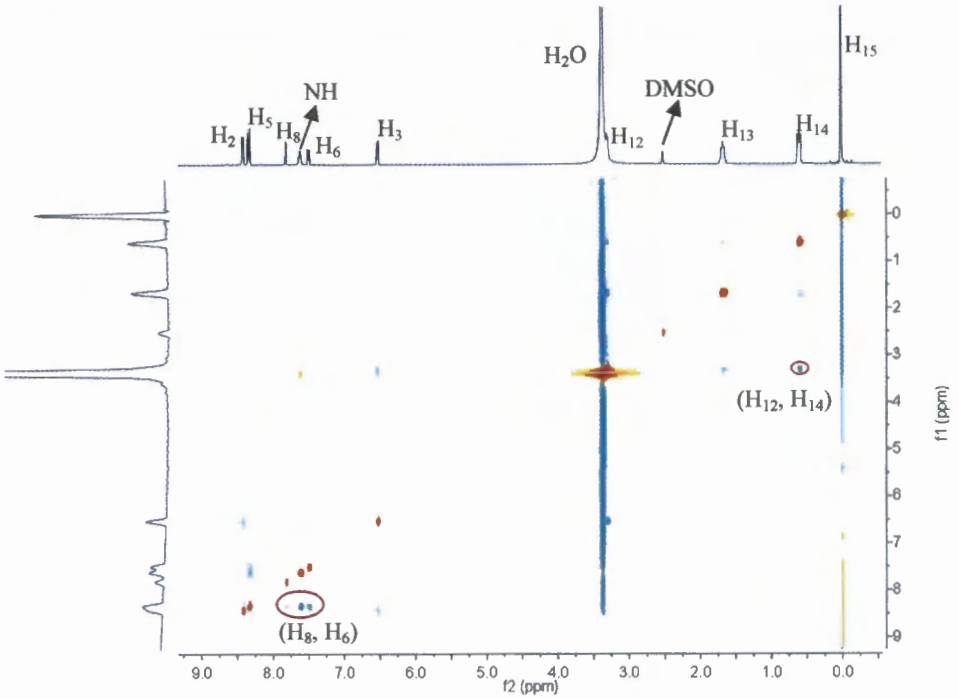

Figure 2.4: NOESY 2D-NMR spectrum of compound **2.2** recorded in DMSO-d_6.

^{13}C NMR spectroscopy

The ^{13}C NMR spectra of compounds **2.1** and **2.2** displays nine singlets corresponding to the quinoline aromatic carbon atoms between 98.6-151.9 ppm. Due to electronic and shielding effect of the silicon atom, a singlet is observed at -3.1 ppm integrating for the three terminal methyl group carbon atoms. Likewise, the single $\underline{C}H_2$ spacer was detected around 32.4 ppm for compound **2.1**, and for compound **2.2** similar resonances were observed associated with the trimethylsilane ($Si\underline{C}H_3$), and the aromatic carbon signals remain comparable to compound **2.1**. In addition, due to electronic effects, the three $\underline{C}H_2$ groups were detected relatively upfield at around 13.5, 22.6, and 45.9 ppm respectively for compound **2.2**. Furthermore, additional 2D-NMR experiments such as Heteronuclear Spin-Quantum Coupling Spectroscopy (HSQC) were carried out to illustrate proton couplings to other nuclei, namely ^{13}C, and thus, offering further validation for the carbon assignments. Figure 2.5 shows HSQC 2D-NMR spectrum of compound **2.2** as an example.

On examination of the HSQC spectrum for compound **2.2**, it is observed that the most deshielded proton, H_2, couples to the most deshielded carbon, C_2, at around 150 ppm. The remaining protons on the quinoline moiety, namely H_3, H_5, H_6, and H_8, couple to carbon atoms in the region 95-125 ppm; with H_3 coupling to C_3 being the most shielded at around 95 ppm. The three CH_2 groups correspond to three carbon atoms at around 18, 22, and 53 ppm respectively. Lastly, the most shielded protons (H_{15}) on the methyl groups attached to

the silicon atom couple to one carbon atom at around 1 ppm. The three carbon atoms (C_{15}) of the methyl group are equivalent, being in the same chemical environment; thus, one peak is observed in the ^{13}C NMR and the HSQC spectrum.

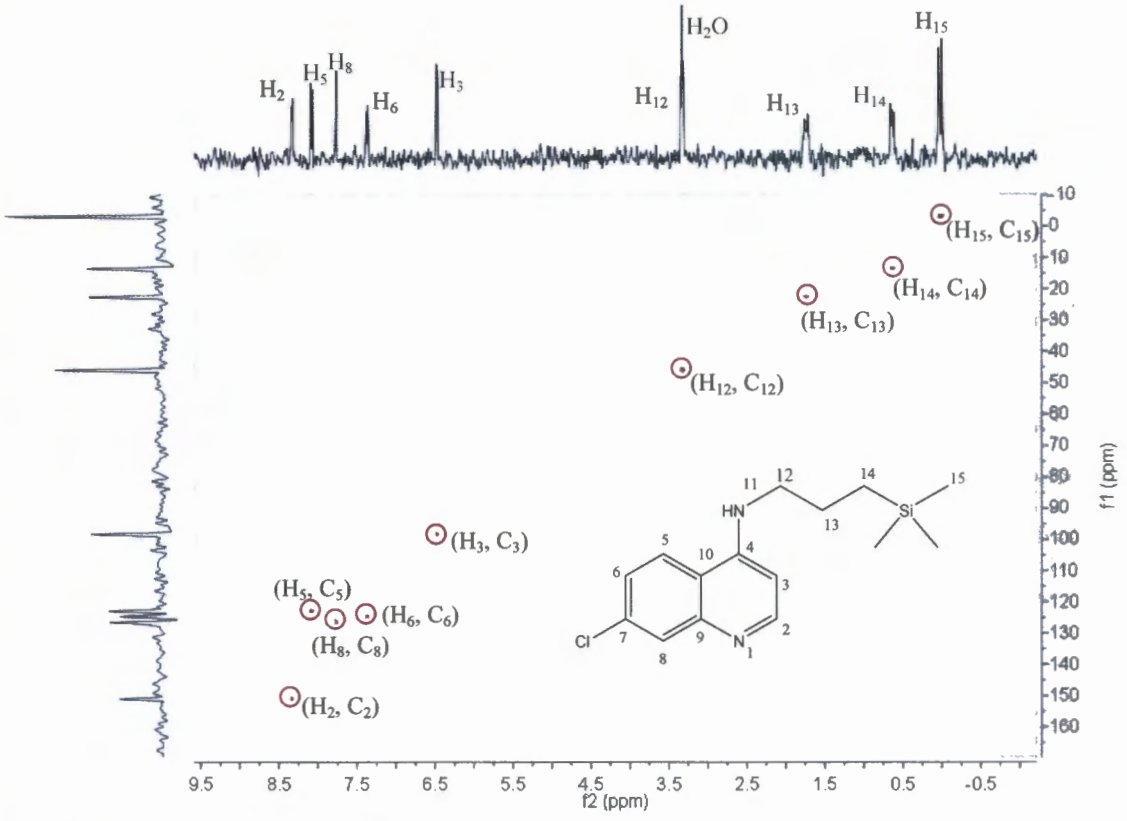

Figure 2.5: HSQC 2D-NMR spectrum of compound **2.2** recorded in DMSO-d_6.

Infrared spectroscopy

All IR spectra were recorded using KBr pellets. The quinoline carbon-nitrogen (C=N) absorption bands were observed at relatively similar frequencies for both compounds **2.1** and **2.2** as a strong sharp band at around 1615 cm^{-1}. This corresponds to analogous compounds with similar carbon-nitrogen (C=N) bond vibrations reported in literature, typically in the range of 1580-1650 cm^{-1}.[37]

Furthermore, due to the strong electron withdrawing properties of the silicon atom, taking more electron density away from the rest of the molecule, the secondary amine absorption bands for both compounds **2.1** and **2.2** were observed at 3246 and 3340 cm^{-1} respectively, which is at a slightly lower frequency compared to analogous compounds found in reported literature. A typical amine bond vibration is generally found in the range of 3300-3500 cm^{-1},[37] and as a direct result of the electron withdrawing effect of the quinoline motif, the secondary amine absorption bands for both compounds **2.1** and **2.2** were observed in the range of 3248-3438 cm^{-1}. Lastly, both compounds **2.1** and **2.2** displays a strong sharp band at

1578 cm^{-1}, and this was assigned to the C=C present in the quinoline scaffold, which agrees with similar quinoline-type compounds found in reported literature.[37]

Elemental analysis

The elemental analysis of both compounds **2.1** and **2.2** attested to the chemical composition for the proposed structures. The percentages of carbon, hydrogen, and nitrogen were found to strongly correlate with the calculated values, all within an error range of 0.4 %.

Electron impact mass spectrometry

Mass spectrometry was a tool used to further confirm molecular fragments/masses of each compound. The isotopic distribution of the parent ion was compared to calculated values, and both compounds **2.1** and **2.2** were analysed using low resolution EI^+-MS. A base peak at 292.09 in the EI^+-MS for **2.1** corresponds to the molecular ion, and an additional peak observed at 291.02 corresponds to the molecular ion of **2.1** with the loss of one hydrogen atom. Similarly, a base peak at 264.07 in the EI^+-MS for **2.2** corresponds to the molecular ion, while an additional peak observed at 249.05 corresponds to the molecular ion **2.2** with the loss of one methyl group.

Molecular structure of compound 2.2

Single crystals of compound **2.2** were obtained by exposing a DMSO solution of **2.2** to air. Table 2.2 lists the crystal data for compound **2.2**, whilst Table 2.3 lists selected bond angles and lengths. Compound **2.2** (Figure 2.6) crystallises in a *P*bca space group, with an orthorhombic system.

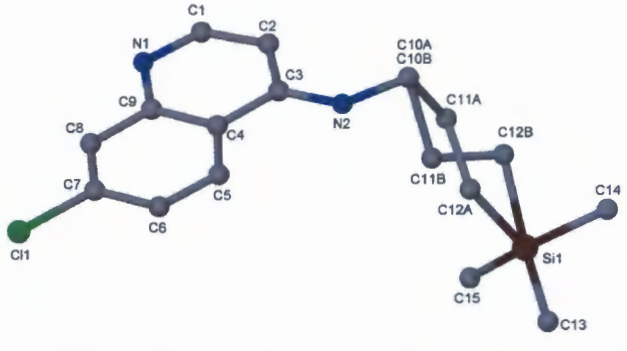

Figure 2.6: Molecular structure of **2.2** showing the atomic numbering scheme.

For compound **2.2**, the hydrogen atom on N_2 was located around different electron density maps and refined independently with simple bond length constraint [d (N-H) = 0.97(1) Å]. The carbon atoms C_{11} and C_{12} were disordered over two places: C_{11A} and C_{12A} versus C_{11B} and C_{12B}, with refined site occupancy factors of 0.777(7) and 0.223(7) respectively. This is the result of the free rotation around the propyl chain, which

can be seen in the dissimilar bonding angles around N_2-C_{10}-C_{11}-C_{12}-Si_1. C_{10A} and C_{10B} are in fact one atom and they were made for the purpose of refinements. The structure was refined to R factor of 0.0500.

Table 2.2: Crystal data for compound **2.2**.

	2.2
Chemical formula	$C_{15}H_{21}ClN_2Si$
Formula weight	292.88
Crystal system	Orthorhombic
Space group	*P*bca (No. 61)
Crystal color and shape	Clear white crystalline
Crystal size	0.07 x 0.11 x 0.13
a / Å	12.3956 (12)
b / Å	13.0995 (13)
c / Å	19.6103 (18)
α / °	90.000
β / °	90.000
γ / °	90.000
V /Å^3	3184.3 (5)
Z	8
T / K	173(2)
D_c / g·cm^{-3}	1.222
μ / mm^{-1}	0.305
Scan range / °	$2.1 < \theta < 26.4$
Unique reflections	3260
Reflections used [$I > 2\sigma(I)$]	2183
R_{int}	0.048
R indices (all data)	R_1 0.0500, wR_2 0.1243, S 1.03
Goodness-of-fit	1.028
Min, Max $\Delta\rho$/e Å^{-3}	-0.63, 0.57
Radiation [Å]	0.71073

For compound **2.2**, the carbon-carbon bond length around the quinoline component is approximately equivalent; delocalisation of the π-electrons contributes to the planar geometry. The bond lengths observed between the silicon and the carbon atoms C_{13}, C_{14}, and C_{15} appear to be longer in comparison with other atoms in the rest of the molecule (Table 2.3). A search in the literature suggests that this could be due to the relatively larger size and additional electron density around the silicon atom compared to carbon and nitrogen atoms.[24,26]

The quinoline nitrogen-carbon (N=C) bond length on the quinoline component, and the nitrogen-carbon bond length around the secondary amine, both appear to be very similar, this is due to the delocalisation of electrons in the aromatic ring. As mentioned above, there is free rotation around the propyl chain, resulting in similar bond length around the carbon

atoms (C_{10}, C_{11} and C_{12}); but no constancy is observed in the bonding angles for C_{10}, C_{11} and C_{12}. The geometry around the silicon atom appears to be close to tetrahedral. The silicon is surrounded by four carbon atoms, creating four faces with bonding angles very close to 109.5°, which provides minimum distortion around the central silicon atom. This geometry around the silicon appears similar compared to other silicon-containing compounds in the literature.[24,38] The apparent elongation of the bonds is not chemically significant as it results only from the imprecise location of the atoms in the disordered group. In short, the bond distances are inaccurate due to imprecise atom locations and thermal motion.

Table 2.3: Selected Bond Lengths (Å) and Angles (°) for compound **2.2.**

Inter atomic distances (Å)	
Atoms	**2.2**
Si1-C13	1.851 (4)
Si1-C14	1.844 (4)
Si1-C15	1.856 (3)
Si1-C12A	1.919 (4)
Si1-C12B	1.861 (12)
N1-C1	1.321 (3)
N1-C9	1.364 (3)
N2-C10A	1.455 (3)
N2-C10B	1.455 (3)
Angles (°)	
C13-Si1-C14	108.1 (17)
C13-Si1-C15	111.1 (15)
C14-Si1-C15	110.1 (15)
C1-N1-C9	115.8 (19)
N2-C3-C2	123.2 (2)
Cl1-C7-C8	120.2 (19)
C3-C4-C5	123.7 (2)

2.3. Synthesis of dimeric Ru and Rh precursors

Metal dimers **2.3-2.7** (Table 2.4) are all known transition metal complexes, and were prepared according to literature methods.[39-43] All metal dimers were obtained in relatively high yields in the range of 73-82%. Partial characterisation was conducted, and the ^{1}H NMR spectrum was used to confirm the acquired products against reported literature. All five metal dimers **2.3-2.7** displayed poor solubility in most organic solvents. However, they appeared to

be slightly soluble in MeOH and EtOH; and with the exception of compound **2.6**, all metal dimers decomposed above 200 °C.

Table 2.4: Physical appearance, yields and melting points for the metal dimers **2.3-2.7**.

Compound number	Structures	Yield (%)	Physical Appearance	M.p. (°C)
2.3	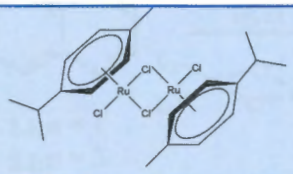	81.0	Red solid	Decomp. 251
2.4	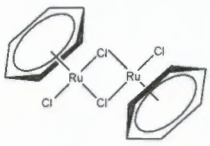	74.5	Red-oragne solid	Decomp. 310
2.5	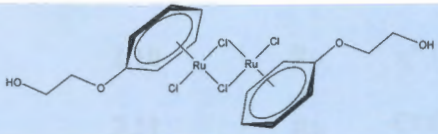	76.5	Red-orange solid	Decomp. 215
2.6	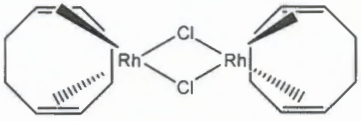	81.9	Yellow solid	251-253
2.7	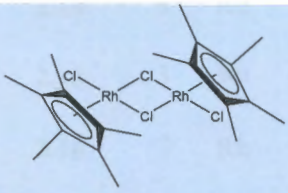	73.2	Red solid	Decomp. 340

2.4. Synthesis of Ru(II), Rh(I/III) organosilicon metal complexes (2.8-2.17)

The complexation reactions were conducted under gentle reflux conditions at 45 °C in dry DCM. Two different rhodium dimers, $[Rh(n^4\text{-}C_8H_{12})(\mu\text{-}Cl)]_2$ and $[Rh(n^5\text{-}C_{10}H_{15})(\mu\text{-}Cl)_2Cl]_2$, and three different ruthenium metal dimers, namely $[Ru(n^6\text{-}C_6H_5OCH_2CH_2OH)(\mu\text{-}Cl)Cl]_2$, $[Ru(n^6\text{-}C_6H_6)(\mu\text{-}Cl)Cl]_2$, and $[Ru(n^6\text{-}p\text{-}^iPrC_6H_4Me)(\mu\text{-}Cl)Cl]_2$, all with different ancillary ligands were used. Neutral mononuclear complexes **2.8-2.12** were obtained by reacting the precursor **2.1** with the five metal dimers **2.3-2.7**; whereas complexes **2.13-2.17** were obtained by reacting the precursor **2.2** with the different metal dimers **2.3-2.7** as depicted in Scheme 2.2.

For each mononuclear complex, the reaction results in selective coordination of the metal, to the nucleophilic nitrogen on the quinoline scaffold. As a direct result of this

metallation reaction, the two bridging chlorides linking the two metal centers in the dimer are cleaved. The complexation reactions successfully yielded a series of new neutral mononuclear ruthenium(II), rhodium(III), and square planar rhodium(I) silicon-containing aminoquinoline complexes.

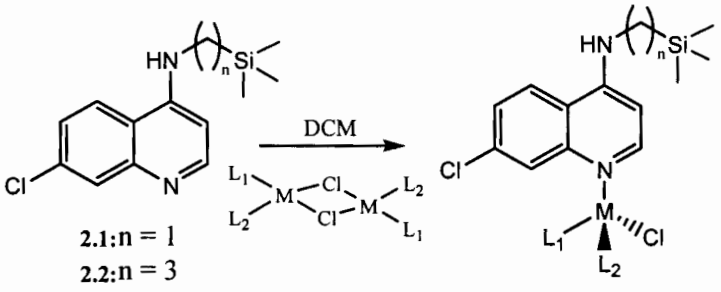

Compound	n	M	L_1	L_2
2.8	1	Ru	η^6-*p*-cymene	Cl
2.9	1	Ru	η^6-benz	Cl
2.10	1	Ru	η^6-$C_6H_5C_2H_4OH$	Cl
2.11	1	Rh	COD	-
2.12	1	Rh	Cp*	Cl
2.13	3	Ru	η^6-*p*-cymene	Cl
2.14	3	Ru	η^6-benz	Cl
2.15	3	Ru	η^6-$C_6H_5C_2H_4OH$	Cl
2.16	3	Rh	COD	-
2.17	3	Rh	Cp*	Cl

Scheme 2.2: Synthetic route to mononuclear complexes **2.8-2.17**.

Physical properties

All silicon-containing aminoquinolines metal complexes **2.8-2.17** were isolated in moderate yields ranging between 51-62%. All metal complexes exhibit relatively high melting point temperatures in the range of 170-290 °C (Table 2.5). The newly synthesised metal complexes were generally obtained as light orange or yellow solids, and are all air-stable. The metal complexes **2.8-2.17** all displayed poor solubility in most organic solvents.

However, they are slightly soluble in MeOH and EtOH, and all the metal complexes were soluble in DMSO.

Table 2.5: Physical appearance, yields and melting points of the organosilicon metal complexes **2.8-2.17**.

Compound number	Yield (%)	Physical Appearance	M.p. (°C)
2.8	60.1	Dark yellow-brown solid 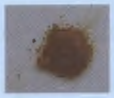	238-241
2.9	55.5	Orange solid 	261-265
2.10	53.9	Light orange solid 	222-225
2.11	61.2	Light yellow solid 	268-270
2.12	51.6	Bright orange solid 	285-289
2.13	62.1	Light yellow-orange solid 	171-172
2.14	61.8	Yellow-orange solid 	282-285
2.15	61.4	Light yellow solid 	237-240
2.16	59.4	Bright yellow solid 	270-272
2.17	53.7	Bright orange solid 	263-266

2.4.1. Spectroscopic and analytical characterisation

^{1}H NMR spectroscopy

Inspection of the ^{1}H NMR spectra data for complexes **2.8-2.17** revealed prominent characteristics supporting the proposed structures. The proton resonances of the quinoline motif appeared in the region 5.8-8.7 ppm, while protons on the terminal trimethylsilane tail appeared in the region 0.0-0.2 ppm for complexes **2.8-2.17**. These are comparable to those observed in the precursors **2.1** and **2.2**. However, due to the electronic effects of extended metal coordination, altering the chemical environment, proton signals for the quinoline motif for all complexes **2.8-2.17** are slightly shifted upfield compared to the free ligands **2.1** and **2.2**. For example, proton H_2 being adjacent to the nitrogen attached to the metal center appears around 8.3 ppm in the ligand, but is shifted to around 8.4-8.6 ppm in the metallated complexes. Similarly, proton H_3 also shifted 0.2-0.4 ppm upfield from 6.1-6.4 ppm in the ligand to around 6.4-6.6 ppm in the metallated complex.

Furthermore, in the metallated complexes, proton H_8 were observed as a doublet in most cases as a result of through-space coupling to H_6, this was evident in the NOESY 2D-NMR. However, H_8 is observed as a singlet in some instances such as in the case of complexes **2.12** and **2.17**, this is due to the sensitivity of the NMR machine. Additional peaks due to the ancillary ligands co-ordinating to the metal center are also observed. In the case of the ruthenium *p*-cymene, two doublets are observed around 5.77 and 5.81 ppm, integrating for two protons each corresponding to two C<u>H</u> groups. A multiplet observed at around 2.83 ppm, integrates for one proton corresponding to the Ar<u>CH</u>$(CH_3)_2$. Likewise, a singlet detected at around 2.09 ppm integrating for three protons correspond to the single methyl group, while a doublet at around 1.19 ppm integrating for six protons accoutered for the remaining two methyl groups joined by the CH group.

In the case of the ruthenium benzene complex, a singlet at around 5.97 ppm integrating for six protons is observed in the ^{1}H NMR spectrum of complexes **2.9** and **2.14**. Similarly, in the case of the rhodium Cp* complex, a singlet at around 1.63 ppm integrating for 15 protons confirms the presence of the pentamethylcyclopentadienyl in complexes **2.12** and **2.17**. Furthermore, additional proton signals associated with the ancillary ligands, namely the ruthenium $C_6H_5C_2H_4OH$ in complexes **2.10** and **2.15**, and rhodium COD in complexes **2.11** and **2.16**, were all evident in the ^{1}H NMR spectra. Additional COSY 2D-NMR experiments were conducted, which provided alternative validations for the proton assignments. The ^{1}H NMR spectrum of complex **2.13** is represented in Figure 2.7 as an example.

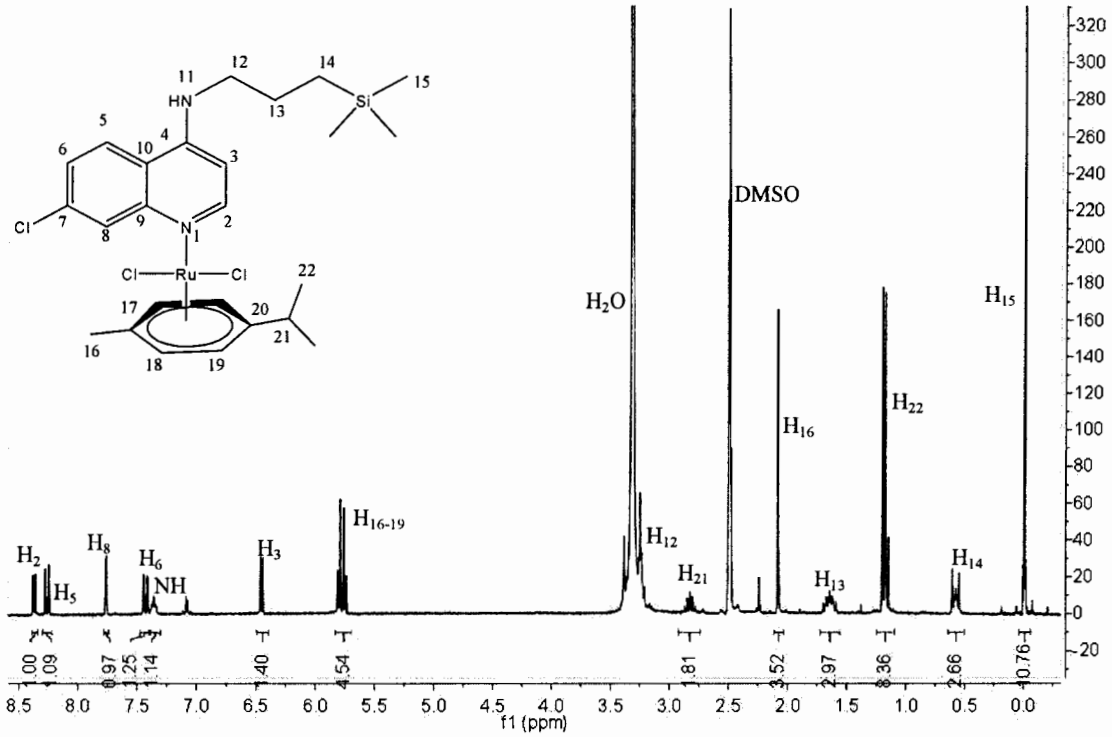

Figure 2.7: ^{1}H NMR spectrum of compound **2.13** recorded in DMSO-d_6.

On inspection of the COSY spectrum of complex **2.14** in Figure 2.8, similar coupling patterns to those of the precursor compound **2.2** are observed. The most deshielded proton, H_2 observed as a doublet, couples to its adjacent proton H_3 at around 6.4 ppm. H_6 appear around 7.5 ppm as a doublet of doublets; it couples to its adjacent proton H_5 and through space coupling to H_8. The three $C\underline{H_2}$ groups couple to each other at around 0.7, 1.5, and 3.2 ppm respectively. Lastly, the most shielded protons due to the silicon atom, the three methyl groups couple to each other at around 0.1 ppm. In addition to the aminoquinoline ligand, the extra metal moiety containing the glycol tether results in additional coupling, for example $H_{16\text{-}18}$ on the arene couples to each other appearing in the range of 5.3-5.7 ppm; and H_{19} and H_{20} on the glycol tether couple to each other at around 3.8 ppm. In summary, peaks associated with protons on the glycol tail are all evident in the COSY spectrum. Figure 2.8 illustrates a COSY 2D-NMR spectrum of complex **2.14** as a typical example for these types of mononuclear metal complexes.

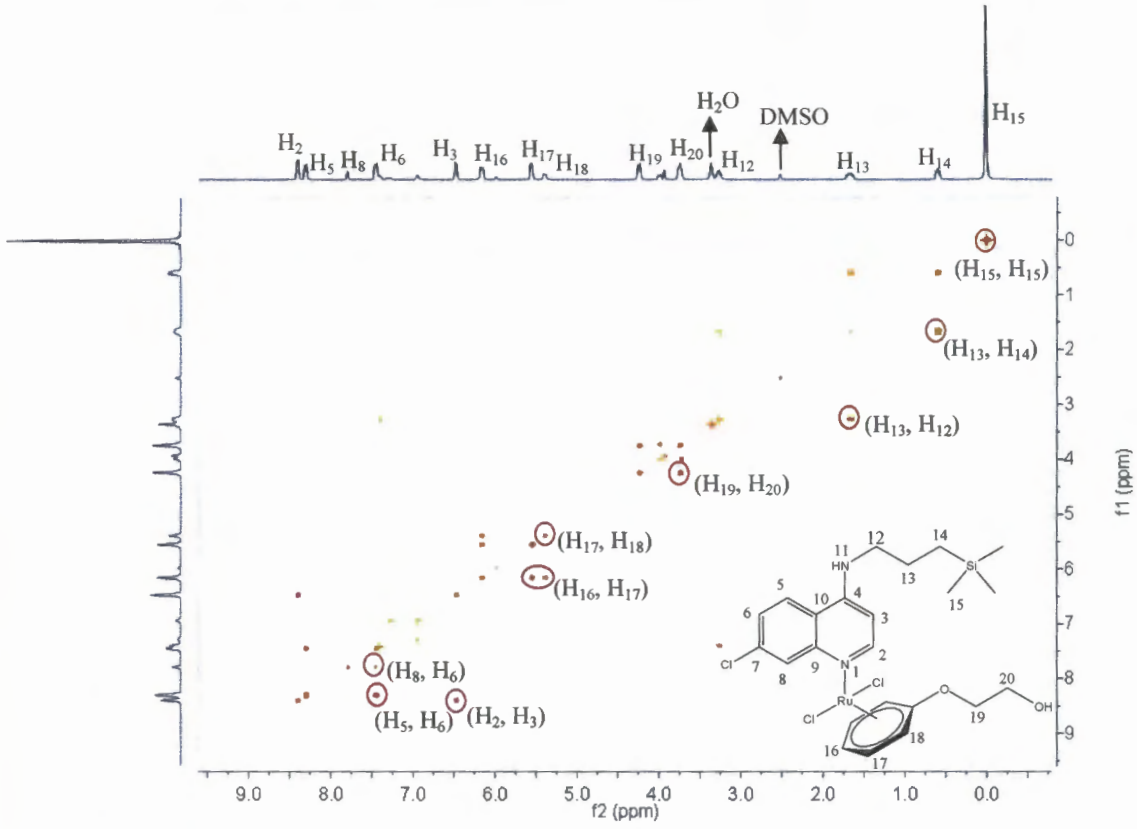

Figure 2.8: COSY 2D-NMR spectrum of compound **2.14** recorded in DMSO-d_6.

^{13}C NMR spectroscopy

Examination of the ^{13}C NMR spectra of complexes **2.8-2.17** revealed distinctive peaks associated with the proposed structure. Due to the electronic effects of the arene scaffold attached to the metal, the quinoline aromatic carbon atoms, generally observed in the range of 98-160 ppm for complexes **2.8-2.17** were all slightly shifted upfield compared with the free ligands **2.1** and **2.2** observed in the range of 97-151 ppm. The methyl group carbon atoms attached to the silicon atom is relatively shielded, thus the methyl protons fall in the range of -1.0 to -1.9 ppm. Furthermore, the carbon atom of the $\underline{C}H_2$ group is generally observed in the range of 20-50 ppm, and the number of carbon signals identified agrees with the proposed structure.

Additional peaks corresponding to the different ancillary metal ligands are also evident in the ^{13}C NMR spectrum. For example, in the case of the Rh COD complex, three additional peaks are observed in the ^{13}C NMR, in the region of 23-46 ppm corresponding to the 1,5-cycloctadiene moiety. Likewise, in the case of the Rh Cp*, two additional peaks at 9.0 and 46 ppm respectively corresponded to $\underline{C}H_3$ and $R\underline{C}CH_3$ on the pentamethyl-cyclopentadienyl ligand.

Overall, the ^{13}C NMR spectra of the metal complexes **2.8-2.17** are comparable to their respective ligand precursors **2.1** and **2.2** with addition of the ancillary arene on the metal. Furthermore, additional 2D-NMR experiments such as HSQC were carried out to provide extra validation for the carbon assignments.

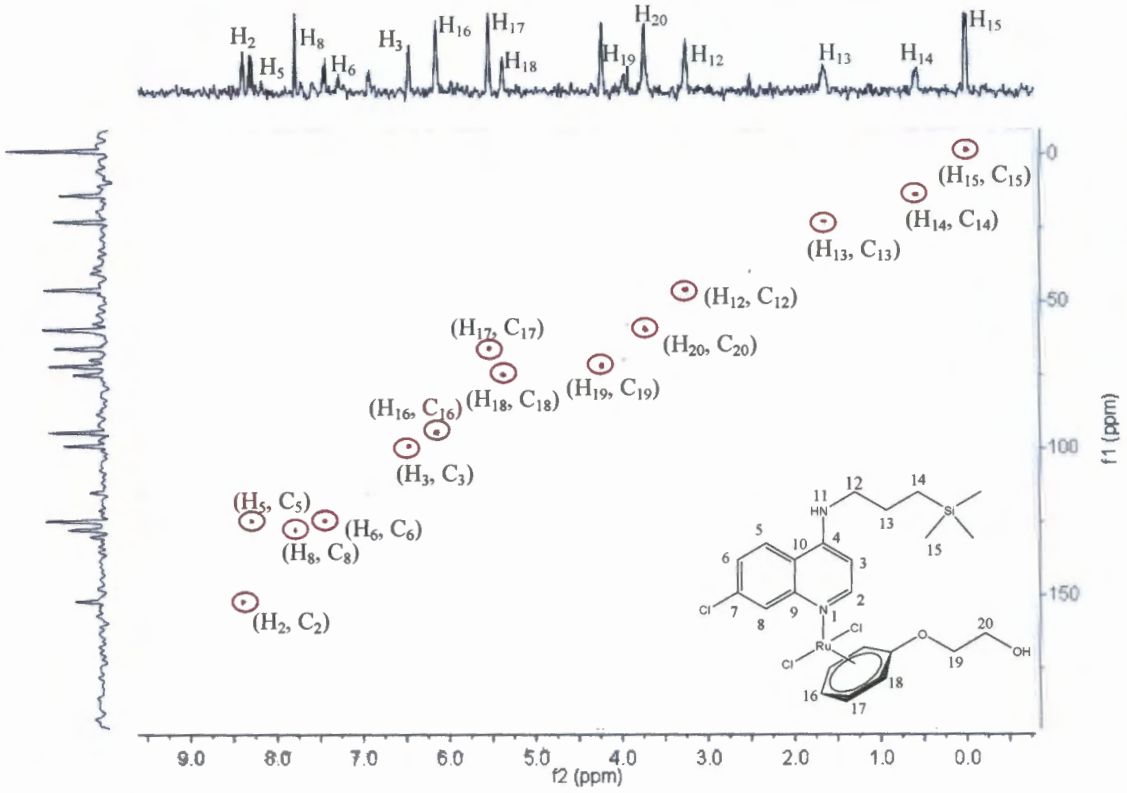

Figure 2.9: HSQC 2D-NMR spectrum of compound **2.14** recorded in DMSO-d_6.

On examination of the HSQC for complex **2.14** (Figure 2.9), it is observed that the most deshielded proton at around 151 ppm, H_2 being adjacent to the nitrogen connecting to the metal center couples to the most deshielded carbon atom C_2. The remaining protons on the quinoline moiety, couple to carbon atoms which appear in the region of 100-130 ppm, comparable to the precursor **2.2**.

Due to the auxiliary metal scaffold, the aromatic peaks in the ^{13}C NMR spectrum generally appear 1-5 ppm upfield compared to the precursor compound **2.2**. The three CH_2 groups correspond to three carbon atoms observed at around 20, 30, and 48 ppm respectively, and these appear slightly upfield by 1-3 ppm compared to the precursor **2.2**.

Lastly, the most shielded protons, the terminal methyl groups on the silicon atom couple to one carbon atom at around 1 ppm. The remaining carbon signals around 110-150 ppm appearing with no coupling correspond to carbon atoms, namely C_4, C_7, C_9 and C_{10} on the quinoline scaffold which are not attached to any hydrogen atoms. Overall, all peaks in the NMR spectra were accounted for, with 2D-NMR providing further validation and supports the assignments made.

Infrared spectroscopy

Inspection of the IR spectra for complexes **2.8-2.17** revealed similar vibrational frequencies compared to those of compounds **2.1** and **2.2**. However, one noticeable shift in the IR spectra was the characteristic strong sharp absorption band due to the C=N aromatic vibration of the quinoline scaffold from 1575 cm^{-1} in the free ligand, to a higher absorption at around 1610 cm^{-1} in the metallated complexes. This is due to a significant degree of ligand to metal π-electron donation involving the lone-pair of electrons on nitrogen atom and the vacant d-orbitals on the metal center. As a result of this, the C=C aromatic vibration also shifts from 1578 cm^{-1} in the free ligand to a higher absorption at around 1587-1591 cm^{-1} in the metallated complexes, further supporting evidence for the metal coordination to the quinoline nitrogen.

Electrospray ionisation mass spectrometry

Again mass spectrometry was a tool used to further confirm the molecular fragments/masses of each compound. Complexes **2.8-2.17** were analysed using low resolution ESI^+-MS, and all complexes exhibited peaks in the ESI^+-MS correlating to the corresponding molecular ion. Furthermore, with the exception of compounds **2.13**, **2.14**, and **2.17** observed as either $[M]^+$ or $[M+H]^+$ ion, all other metal complexes were observed as the $[M-Cl]^+$ ion (Table 2.6).

Table 2.6: ESI^+-MS for metal complexes **2.8-2.17**.

Compound number	Molecular formula	Molecular weight (g/mol)	m/z
2.8	$C_{23}H_{31}Cl_3N_2RuSi$	571.67	536.5 $[M-Cl]^+$
2.9	$C_{19}H_{24}Cl_3N_2RuSi$	516.56	479.0 $[M-Cl]^+$
2.10	$C_{21}H_{25}Cl_3N_2O_2RuSi$	573.59	538.0 $[M-Cl]^+$
2.11	$C_{21}H_{29}Cl_2N_2RhSi$	511.38	475.1 $[M-Cl]^+$
2.12	$C_{23}H_{32}Cl_3N_2RhSi$	573.87	539.1 $[M-Cl]^+$
2.13	$C_{25}H_{35}Cl_3N_2RuSi$	599.71	601.1 $[M+H]^+$
2.14	$C_{21}H_{25}Cl_3N_2RuSi$	541.59	542.8 $[M+H]^+$
2.15	$C_{23}H_{29}Cl_3N_2O_2RuSi$	601.64	566.1 $[M-Cl]^+$
2.16	$C_{23}H_{33}Cl_2N_2RhSi$	539.43	503.1 $[M-Cl]^+$
2.17	$C_{25}H_{36}Cl_3N_2RhSi$	601.93	601.1 $[M]^+$

Elemental analysis

Elemental analysis results of complexes **2.8-2.17** attested to the chemical composition for the proposed structures. The percentages of carbon, hydrogen, and nitrogen were found to correlate with the calculated values, all in with a 0.4% error range, indicating pure compounds.

Molecular structure of compound 2.16

Single crystals of complex **2.16** suitable for single-crystal X-ray diffraction were obtained by exposing a DMSO solution of the complex to air. Table 2.7 lists the crystal data for complex **2.16**, and similarly, Table 2.8 lists selected bond angles and lengths.

The molecular structure of complex **2.16** (Figure 2.10) indicates that the shape around the rhodium atom is a typical square-planar geometry. The rhodium metal center is surrounded by the aminoquinoline, a terminal chloride ligand and the cyclooctadienyl ligand.

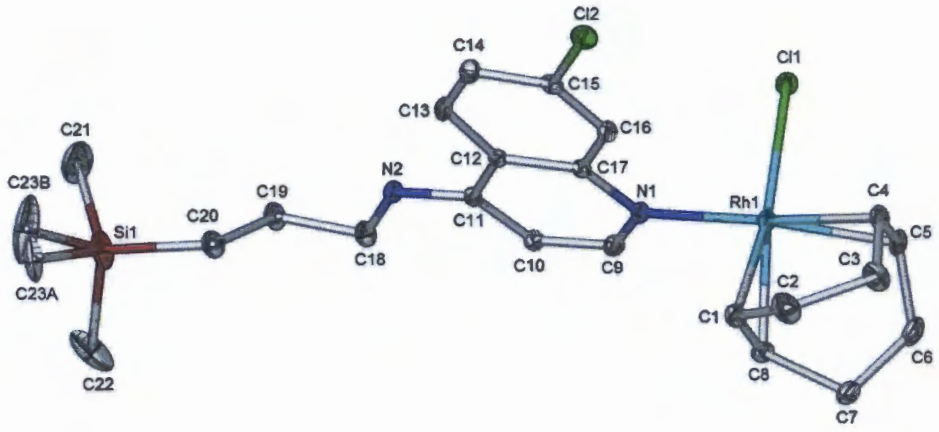

Figure 2.10: Molecular structure of complex **2.16** at 30% probability ellipsoids.

Complex **2.16** crystallises in a monoclinic crystal system. All non-hydrogen atoms were refined anisotropically. All hydrogen atoms, except H_2 on N_2, were placed in idealised positions and refined with geometrical constraints. The hydrogen atom H_2 was located in the difference electron density maps and refined with N-H distance restraint to the value of 0.88(1) Å. One methyl carbon atom C_{23} was disordered over two sites: C_{23A} and C_{23B}, each having a site occupancy factor of 0.5. Refinement was performed with temperature factor restraints. The distances C_{22A}-Si_1, C_{23B}-Si_1 and C_{22}-Si_1 were restrained to be the same as that of C_{21}-Si_1.

Table 2.7: Crystal data for complex **2.16**.

	2.16
Chemical formula	$C_{23}H_{33}Cl_2N_2SiRh$
Formula weight	539.43
Crystal system	Monoclinic
Space group	*C*2/c
Crystal color and shape	Yellow crystalline
Crystal size	0.11 x 0.18 x 0.22
a / Å	32.1880 (12)
b / Å	10.7870 (2)
c / Å	15.5010 (6)
α / °	90.00
β / °	115.3050 (10)
γ / °	90.00
V /Å^3	4865.7 (3)
Z	8
T / K	173 (2)
D_c / g·cm^{-3}	1.473
μ / mm^{-1}	0.983
Scan range / °	$2.7 < \theta < 27.5$
Unique reflections	5574
Reflections used [$I > 2\sigma(I)$]	4019
R_{int}	0.052
R indices (all data)	R_1 0.0319, wR_2 0.0754, S 1.00
Goodness-of-fit	1.003
Min, Max Δρ/e Å^{-3}	-0.50, 0.92
Radiation [Å]	0.71073

For complex **2.16**, the bond length around the quinoline core and its planar geometry is very similar when compared with the precursor **2.2**. Again the carbon-carbon bond length around the quinoline component is equivalent resulting in the planar geometry. The bond lengths between the silicon and the carbon atoms are longer in comparison with other atoms in the rest of the molecule (Table 2.8). As observed in precursor **2.2**, there is still free rotation around the propyl chain, and the geometry around the silicon atom still remains closely to tetrahedral. Atoms around the rhodium atom appear to have longer bond lengths compared with the rest of the molecule. This is due to the larger size and bonus electron density around the rhodium atom compared to other atoms.[44,45] The molecular structure also confirms that the planar aminoquinoline motif selectively coordinates to the rhodium metal center through the quinoline nitrogen in a monodentate manner. The geometric structure around the rhodium atom is comparable to analogous mononuclear Rh(I)-cyclooctadienyl complexes found in reported literature.[44,45]

Table 2.8: Selected Bond Lengths (Å) and Angles (°) for complex **2.16**.

Inter atomic distances (Å)	
Atoms	**2.16**
Rh1-N1	2.103 (18)
Rh1-C1	2.108 (2)
Rh1-C4	2.146 (3)
Rh1-C5	2.136 (2)
Rh1-C8	2.125 (2)
Si1-C21	1.861 (4)
Si1-C22	1.870 (4)
Si1-C23A	1.874 (12)
Si1-C23B	1.875 (16)
Angles (°)	
Cl1-Rh1-N1	88.84 (5)
Cl1-Rh1-C1	158.9 (8)
Cl1-Rh1-C4	93.38 (6)
Cl1-Rh1-C5	90.13 (6)
Cl1-Rh1-C8	162.6 (8)
N1-Rh1-C1	89.55 (9)
N1-Rh1-C4	162.3 (9)

2.5. Conclusion

Two aminoquinoline ligands **2.1** and **2.2** containing organosilicon moieties modified in the lateral side chain, and a corresponding series of ruthenium and rhodium silicon-containing aminoquinoline neutral mononuclear complexes **2.8-2.17,** have been successfully synthesised. Both compounds **2.1** and **2.2** act as monodentate donors that coordinate to the transition metals selectively via the quinoline nitrogen of the aminoquinoline scaffold. Furthermore, all the compounds are air-stable, and were characterised using various analytical and spectroscopic techniques. The molecular structures of compounds **2.2** and **2.16** were elucidated by single-crystal X-ray diffraction analysis further confirming their structural integrity.

2.6. Experimental

2.6.1. *General methods*

All synthetic procedures were performed under inert gas, standard Schlenk and vacuum-line techniques were employed. All reagents were purchased from either Sigma-Aldrich or ABCR Specialty Chemicals and used as received without further purification. Reaction solvents were purchased from the commercial supplier Kimix, distilled and stored over molecular sieves.

Nuclear Magnetic Resonance (NMR) Spectra were recorded on a Varian Unity XR400 MHz (^{1}H at 399.95 MHz, ^{13}C at 100.58 MHz), Varian Mercury XR300 (^{1}H at 300.006 MHz, ^{13}C at 75.46 MHz) or alternatively a Bruker Biospin GmbH (^{1}H at 400.22 MHz, ^{13}C at 100.65 MHz) spectra at ambient temperature. All chemical shifts for ^{1}H and ^{13}C NMR shifts are reported using tetramethylsilane (TMS) as the internal standard. Furthermore, NMR spectra were recorded in deuterated dimethylsufoxide (DMSO-d_6) unless otherwise stated.

Infrared absorptions (IR) were measured on a Perkin-Elmer Spectrum 100, FT-IR Spectrometer as KBr pellets. Melting points were determined using a Büchi melting point B-540 apparatus and corrected. Microanalyses for C, H, N were carried out using a Thermo Flash 1112 Series CHN-O Analyser.

Mass Spectrometry determinations were carried out on all new compounds using either electron impact (EI+) on a JEOL GC Matell instrument or alternatively, electrospray ionisation (ESI+) on a Waters API Quattro Micro instrument in the positive-ion mode.

2.6.2. Synthesis of Silicon-containing aminoquinoline ligands

2.6.2.1. Silicon-containing aminoquinoline ligand (2.1)

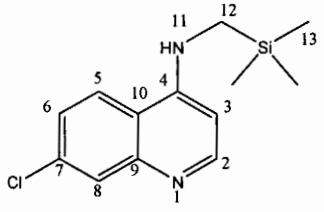

4,7-Dichloroquinoline (1.08 g, 5.10 mmol) was added to an excess of aminomethyltrimethylsilane (1.91 mL, 14.3 mmol). The light-yellow mixture was then heated slowly without stirring in an oil-bath. After an hour of heating at 80 °C, the light-yellow homogeneous solution mixture was heated further to 120 °C with stirring over a thirty minute interval. Subsequently, the light-yellow reaction mixture was then refluxed further for six hours at 120 °C. The reaction mixture was then cooled to room temperature. The resulting white solid obtained from the reaction, was then immediately washed with (5 x 10 mL) of

distilled H_2O, to neutralise any by-product formed during the duration of the reaction. The white solid was then filtered, washed with (3 x 10 mL) of distilled H_2O, and finally dried under vacuum, yielding **2.1** as a white solid.

Compound **2.1** was then recrystallised in a minimum amount of hot DCM, and washed with (3 x 5 mL) of cold DCM. The recrystallization process was preformed three times to yield the purified **2.1** as a white solid.

Yield = 1.07 g (79.2%). **M.p.** 125-129 °C. **^{1}H NMR** (300.006 MHz, DMSO-d_6): δ (ppm) = -0.37 (9H, s, H_{13}); 2.36 (2H, s, H_{12}); 6.01 (1H, d, $^3J_{HH}$ = 5.59 Hz, H_3); 6.97 (1H, d, $^3J_{HH}$ = 8.82 Hz, H_6); 7.10 (1H, s, NH); 7.31 (1H, s, H_8); 7.89 (2H, m, H_5, H_2). **^{13}C NMR** (75.46 MHz, CD_3OD): δ (ppm) = -3.1 ($\underline{C}_{13}$); 32.4 ($\underline{C}_{12}$); 98.6, 118.9, 121.2, 122.9, 123.4, 137.2, 148.6, 149.8, 151.9 (ArC). **IR** (KBr, cm^{-1}): ν(NH) 3341; ν(CH aromatic) 3030; ν(C=N) 1615; ν(C=C aromatic) 1578. **Elemental Analysis** (%): Calc. For $C_{13}H_{17}ClN_2Si.H_2O$ (282.85): C, 55.20; H, 6.06; N, 9.90; Found: C, 55.83; H, 6.51; N, 10.11. **MS** (EI$^+$, *m/z*): 264.1 $[M-H]^+$.

2.6.2.2. Silicon-containing aminoquinoline ligand (2.2)

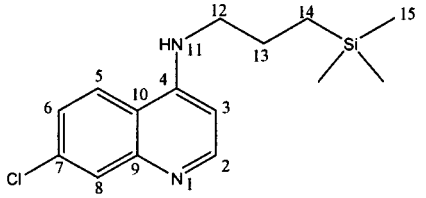

Compound **2.2** was prepared using a similar methodology to compound **2.1**. Neat 4,7-dichloroquinoline (1.01 g, 5.04 mmol) was reacted with 3-aminopropyltrimethylsilane (1.92 mL, 12.0 mmol). The reaction yielded **2.2** as a white solid.

Yield = 0.911 g (63.0%). **M.p.** 165-168 °C. **^{1}H NMR** (399.95 MHz, DMSO-d_6): δ (ppm) = -0.02 (9H, s, H_{15}); 0.56 (2H, m, H_{14}); 1.64 (2H, m, H_{13}); 3.26 (2H, m, H_{12}); 6.48 (1H, d, $^3J_{HH}$ = 5.74 Hz, H_3); 7.45 (1H, dd, $^4J_{HH}$ = 2.23 Hz, $^3J_{HH}$ = 8.99 Hz, H_6); 7.62 (1H, s, NH); 7.79 (1H, d, $^3J_{HH}$ = 2.74 Hz, H_8); 8.31 (1H, d, $^3J_{HH}$ = 9.05 Hz, H_5); 8.38 (1H, d, $^3J_{HH}$ = 5.68 Hz, H_2). **^{13}C NMR** (100.58 MHz, CD_3OD): δ (ppm) = -3.1 ($\underline{C}_{15}$); 13.5 ($\underline{C}_{14}$); 22.6 ($\underline{C}_{13}$); 45.9 ($\underline{C}_{12}$); 98.2 (C_3); 118.5 (C_{10}); 122.9 (C_5); 124.0 (C_6); 126.2 (C_8); 135.1 (C_9); 149.1 (C_4); 150.9 (C_2); 151.5 (C_7). **IR** (KBr, cm^{-1}): ν(NH) 3246; ν(CH aromatic) 3064; ν(CH aliphatic) 2952; ν(C=N) 1615; ν(C=C aromatic) 1578; ν(Si-CH_3) 1245; ν(C-Cl) 839. **Elemental Analysis** (%): Calc. For $C_{15}H_{21}ClN_2Si.(1/2)H_2O$ (301.89): C, 59.68; H, 7.01; N, 9.28; Found: C, 59.54; H, 7.09; N, 9.15. **MS** (EI$^+$, *m/z*): 292.09 $[M]^+$.

2.7. Synthesis of dimeric metal precursors

2.7.1. Synthesis of $[Ru(\eta^6\text{-}p\text{-}^iPrC_6H_4Me)(\mu\text{-}Cl)Cl]_2$ (2.3)[39]

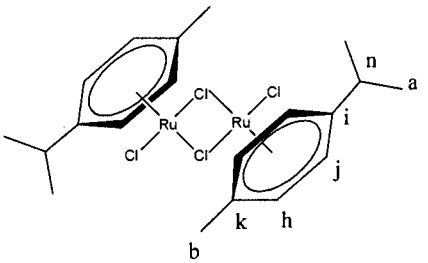

Ruthenium (III) trichloride trihydrate (2.72 g, 10.4 mmol) was dissolved in dry ethanol (50 mL). A large excess amount of α-phellandrene (10 mL, 61.0 mmol) was added dropwise to the solution. The solution mixture was then heated to 81 °C, and refluxed for 12 hours. The solution mixture was then cooled to room temperature and reduced to less than half of the initial volume.

The solution was then placed in ice for 30 minutes to aid precipitation of the product. A red-brown solid was then filtered, and dried under vacuum, yielding the Ru dimer **2.3** as a fine red-brown powder. The filtrate was collected, and reduced to less than half of its volume. The reduced filtrate was then cooled in ice to precipitate additional product. Diethyl ether (10.0 mL) was added to the filtrate to aid the precipitation process. The precipitate formed was filtered, washed with cold diethyl ether (3 x 20.0 mL), and finally dried under vacuum to yield additional **2.3**.

Complex **2.3** was further purified by dissolving in minimum amount of methanol, followed by the addition of cold diethyl ether (10.0 mL) to precipitate **2.3**. The solution was placed in ice to aid the precipitation process. The precipitated **2.3** was washed with cold diether ether (3 x 20.0 mL) and then dried under vacuum. The recrystallisation process was done twice, to yield the purified **2.3** as a fine light red-brown powder. Yield = 2.70 g (81.0%). **Lit. M.p.** 200 °C.[104] **2.3** decomposed without melting at 251 °C. **^{1}H NMR** (399.95 MHz, $CDCl_3$): δ (ppm) = 1.27 (12H, d, $^3J_{HH}$ = 6.9 Hz, H_a); 2.14 (6H, s, H_b); 2.91 (2H, m, H_n); 5.31 (4H, d, $^3J_{HH}$ = 6.1 Hz, H_j); 5.45 (4H, d, $^3J_{HH}$ = 6.0 Hz, H_h).

2.7.2. Synthesis of $[Ru(\eta^6\text{-}C_6H_6)(\mu\text{-}Cl)Cl]_2$ (2.4)[40]

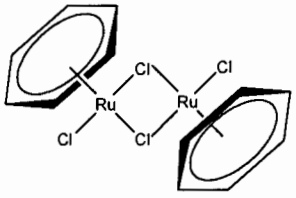

Ruthenium (III) trichloride trihydrate (1.71 g, 6.54 mmol) was dissolved in 90% aqueous ethanol (50 mL). A large excess amount of 1,3-cyclohexadiene (6.10 mL, 64.0 mmol) was added dropwise to the Ru-ethanol solution. The red-black solution mixture was heated to 45 °C with stirring, and refluxed further for five hours.

The resulting red solution mixture was then cooled to room temperature while stirring, after which the solution mixture was reduced to less than half of the initial volume. The reduced solution mixture was then placed in ice for 30 minutes, to aid the precipitation process. A light red-orange precipitate formed as a suspension. The light red-orange solid was then filtered, washed with dry ethanol (3 x 10 mL), and dried under vacuum, yielding **2.4** as a light red-orange solid. Yield = 1.21 g (74.5%). **2.4** decomposed without melting at 310 °C. **^{1}H NMR** (399.95 MHz, DMSO-d_6): δ (ppm) = 5.74 (12H, s, ArH).

2.7.3. Synthesis of $[Ru(\eta^6\text{-}C_6H_5OCH_2CH_2OH)(\mu\text{-}Cl)Cl]_2$ (2.5)[41]

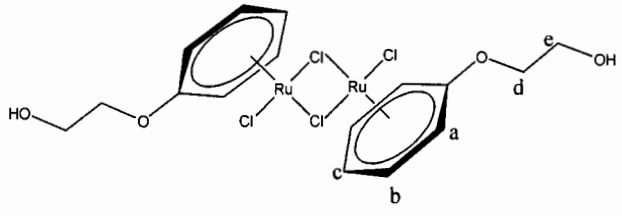

Ruthenium (III) trichloride trihydrate (1.03 g, 3.82 mmol) was reacted with a large excess amount of 1-methoxy-1,4-cyclohexadiene (4.5 mL, 38.4 mmol) in a solution of 1,2-ethanediol (15 mL). The dark-black solution mixture was then heated to 80 °C with stirring, after which it was further refluxed for five hours. The resulting red-brown solution was cooled to room temperature and left standing overnight.

An orange precipitate formed as a suspension. The orange precipitate was then filtered, and it was washed firstly with cold H_2O (3 x 5 mL), and then dry methanol (3 x 5 mL). After which the red solid was dried under vacuum, yielding **2.5** as a bright orange solid. Yield = 0.90 g (76.5%). **2.5** decomposed without melting at 215 °C. **^{1}H NMR** (399.95 MHz, DMSO-d_6): δ (ppm) = 3.73 - 3.75 (4H, m, $^3J_{HH}$ = 5.0 Hz, H_e); 4.21 - 4.22 (4H, m, $^3J_{HH}$ = 5.0 Hz, H_d); 5.38 (2H, m, $^3J_{HH}$ = 5.3 Hz, H_c); 5.53 (4H, m, $^3J_{HH}$ = 6.5 Hz, H_b); 6.14 - 6.16 (4H, m, $^4J_{HH}$ = 8.8, $^3J_{HH}$ = 3.2 Hz, H_a).

2.7.4. Synthesis of $[Rh(\eta^4\text{-}C_8H_{12})(\mu\text{-}Cl)]_2$ (2.6)[42]

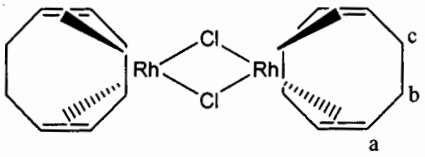

Rhodium (III) trichloride trihydrate (1.02 g, 3.82 mmol) was reacted with a large excess amount of 1,5-cycloctadiene (2.8 mL, 23.1 mmol) in a solution of 90% aqueous ethanol (50 mL). The dark-black solution mixture was then heated to 85 °C with stirring, after which it was further refluxed at 85 °C for an additional five hours. The resulting yellow solution was cooled to room temperature and left standing overnight.

A light-yellow precipitate formed as a suspension. The yellow precipitate was then filtered, and washed dry ethanol (3 x 5 mL). After which the light-yellow solid was then dried under vacuum, yielding **2.6** as a canary yellow solid. Yield = 0.871 g (81.9%). **M.p.** 215-253 °C. **^{1}H NMR** (399.95 MHz, $CDCl_3$): δ (ppm) = 1.53 - 1.80 (8H, m, $^3J_{HH}$ = 5.0 Hz, H_b); 2.45 - 2.54 (8H, m, $^3J_{HH}$ = 5.0 Hz, H_c); 4.22 (8H, s, H_a).

2.7.5. Synthesis of $[Rh(\eta^5\text{-}C_{10}H_{15})(\mu\text{-}Cl)_2Cl]_2$ (2.7)[43]

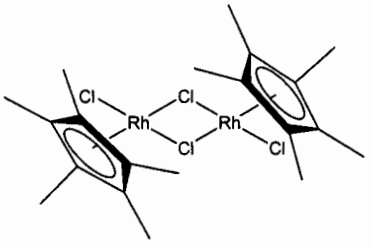

Rhodium (III) trichloride trihydrate (1.04 g, 3.89 mmol) was reacted with a large excess amount of penta-methyl-cyclopentadiene (1 mL, 6.4 mmol) in a solution of dry methanol (25 mL). The dark-black solution mixture was then heated to 105 °C with stirring, after which it was refluxed further at 105 °C for an additional 21 hours overnight. The resulting red-orange solution mixture was cooled to room temperature and left standing overnight.

The red-orange precipitate was then filtered, and washed with cold diethyl ether (3 x 10.0 mL). After which the red-orange solid was then dried under vacuum, yielding **2.7** as a red-orange solid. Yield = 0.881 g (73.2%). Complex **2.7** decomposed without melting at 340 °C. **^{1}H NMR** (399.95 MHz, $CDCl_3$): δ (ppm) = 1.61 (30H, s, CH_3).

2.8. Synthesis of neutral silicon-containing aminoquinoline Ru and Rh complexes (2.8-2.17)

Complexes **2.8-2.12** was synthesised by reacting precursor **2.1** with the appropriate Ru(II)-arene (benzene, *p*-cymene, $C_6H_5C_2H_4OH$), Rh(I) COD or Rh(III) Cp* dimers, and complexes **2.13-2.17** was synthesised by reacting precursor **2.2** with the appropriate Ru(II) or Rh(I/III) dimers. The general synthetic procedure is described below.

2.8.1. Synthesis of neutral mononuclear ruthenium complex 2.8

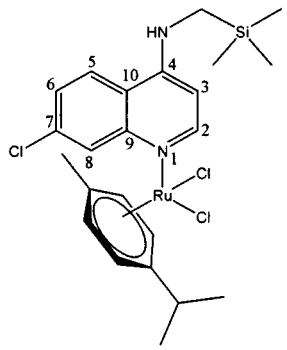

A solution of **2.1** (0.130 g, 0.510 mmol) dissolved in dry DCM (5 mL) was added dropwise to a solution mixture of **2.3** (0.151 g, 0.250 mmol) dissolved in dry DCM (5 mL). The yellow solution mixture was then heated to 45 °C, and then refluxed at 45 °C for two hours. The resulting light yellow solution mixture was then cooled to room temperature, and stirred further for additional four hours at ambient conditions. The reaction produced a milky yellow solution mixture that was reduced to less than half of its initial volume. The mud-like, sticky yellow solution mixture was then placed in ice for approximately 30 minutes to aid the precipitation process. A yellow-orange precipitate was formed. This was filtered and washed with a minimum amount of cold DCM (3 x 4 mL), and then dried under vacuum. The reaction yielded **2.8** as a dark yellow solid.

Yield = 0.180 g (60.1%). **M.p.** 238-241 °C. **^{1}H NMR** (399.95 MHz, DMSO-d_6): δ (ppm) = 0.10 (9H, s, 3*C$\underline{H}_3$); 1.19 (6H, m, 2*C$\underline{H}_3$ *p*-cym); 2.09 (3H, m, C$\underline{H}_3$ *p*-cym); 2.83 (1H, m, C$\underline{H}$ *p*-cym); 2.90 (2H, m, C$\underline{H}_2$); 5.77 (2H, d, $^3J_{HH}$ = 6.3 Hz, 2*C$\underline{H}$ *p*-cym); 5.81 (2H, d, $^3J_{HH}$ = 6.3 Hz, 2*C$\underline{H}$ *p*-cym); 6.56 (1H, d, $^3J_{HH}$ = 6.0 Hz, H_3); 7.51 (1H, dd, $^4J_{HH}$ = 9.1 Hz, $^3J_{HH}$ = 2.1 Hz, H_6); 7.81 (2H, m, H_8 & NH); 8.39 (2H, m, H_5 & H_2). **^{13}C NMR** (100.58 MHz, DMSO-d_6) δ (ppm) = -1.17 (Si$\underline{C}H_3$); 18.04, 21.68, 30.16, ($\underline{C}$ *p*-cym); 33.84 (CH_2); 85.69, 86.54, 98.75, 101.42 (Ar$\underline{C}$ *p*-cym); 108.54, 117.87, 124.42, 124.90, 135.05, 147.21, 148.10, 148.36, 152.27 (ArC). **IR** (KBr, cm^{-1}): ν(NH) 3297; ν(C=N) 1611; ν(C=C aromatic) 1590.

Elemental Analysis (%): Calc. For $C_{23}H_{31}Cl_3N_2RuSi.H_2O$ (589.04): C, 46.90; H, 5.30; N, 4.76; Found: C, 47.06; H, 5.27; N, 4.61. **MS** (ESI^+, *m/z*): 572.0 $[M]^+$, 536.5 $[M\text{-}Cl]^+$.

2.8.2. Synthesis of neutral mononuclear ruthenium complex 2.9

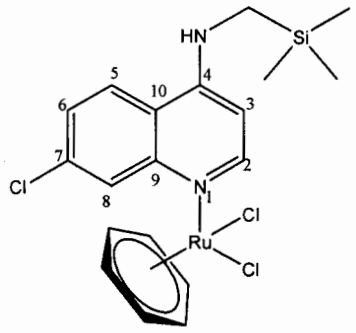

Compound **2.1** (0.220 g, 0.830 mmol) was reacted together with **2.4** (0.210 g, 0.420 mmol). The reaction yielded **2.9** as an orange solid. Yield = 0.24 g (55.5%). **M.p.** 261-265 °C. **^{1}H NMR** (399.95 MHz, DMSO-d_6): δ (ppm) = 0.12 (9H, s, 3*C$\underline{H}_3$); 2.91 (2H, d, $^3J_{HH}$ = 9.6 Hz, C$\underline{H}_2$); 5.97(6H, s, Ar$\underline{H}$ benze); 6.56 (1H, d, $^3J_{HH}$ = 6.1 Hz, H_3); 7.52 (1H, dd, $^4J_{HH}$ = 9.0 Hz, ^3J_H = 2.1 Hz, H_6); 7.82 (1H, d, $^3J_{HH}$ = 2.0 Hz, H_8); 7.90 (1H, s, NH); 8.39-8.43 (2H, m, H_5 & H_2). **^{13}C NMR** (100.58 MHz, DMSO-d_6) δ (ppm) = -1.72 (Si$\underline{C}H_3$); 33.75 (CH_2); 87.84 (Ar$\underline{C}$ benz); 98.76, 117.47, 124.80, 124.81, 135.05, 147.11, 147.10, 148.83, 152.27 (ArC). **IR** (KBr, cm^{-1}): ν(NH) 3287; ν(C=N) 1619; ν(C=C aromatic) 1588. **Elemental Analysis** (%): Calc. For $C_{19}H_{23}Cl_3N_2RuSi.H_2O$ (532.93): C, 42.82; H, 4.35; N, 5.26; Found: C, 42.52; H, 4.24; N, 4.74. **MS** (ESI^+, *m/z*): 479.0 $[M\text{-}Cl]^+$.

2.8.3. Synthesis of neutral mononuclear ruthenium complex 2.10

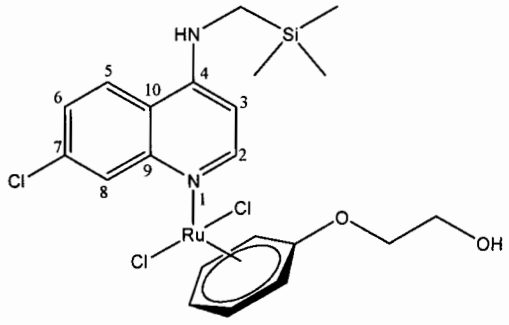

Compound **2.1** (0.171 g, 0.640 mmol) was reacted together with **2.5** (0.202 g, 0.320 mmol). The reaction yielded **2.10** as an orange solid. Yield = 0.201 g (53.9%). **M.p.** 222-225 °C. **^{1}H NMR** (300.066 MHz, DMSO-d_6): δ (ppm) = 0.14 (9H, s, 3*C$\underline{H}_3$); 3.01 (2H, s, C$\underline{H}_2$); 3.74 (2H, t, $^3J_{HH}$ = 5.0 Hz, C$\underline{H}_2$ Glu); 4.23 (2H, t, $^3J_{HH}$ = 5.0 Hz, C$\underline{H}$ Arene); 5.39 (1H, t, $^3J_{HH}$ = 5.4 Hz, C$\underline{H}$ Arene); 5.55 (2H, d, $^3J_{HH}$ = 6.2 Hz, C$\underline{H}$ Arene); 6.15 (2H, dd,

$^3J_{HH}$ = 6.6 Hz, $^3J_{HH}$ = 5.4 Hz, CH Arene); 6.65 (1H, d, $^3J_{HH}$ = 6.5 Hz, H_3); 7.59 (1H, dd, $^4J_{HH}$ = 9.0 Hz, $^3J_{HH}$ = 2.2 Hz, H_6); 7.89 (1H, d, $^3J_{HH}$ = 2.2 Hz, H_8); 8.40 (1H, d, $^3J_{HH}$ = 6.4 Hz, H_2); 8.51 (1H, d, $^3J_{HH}$ = 9.0 Hz, H_5). **^{13}C NMR** (100.58 MHz, DMSO-d_6) δ (ppm) = -1.71 (SiCH$_3$); 34.12 (CH_2); 59.18, 65.79 (CH_2 Arene); 71.71, 74.65, 86.71, 94.21, 98.72 (ArC); 116.23, 122.98, 125.16, 125.38, 136.81, 140.05, 143.57, 146.71, 153.18 (ArC). **IR** (KBr, cm^{-1}): ν(NH) 3417; ν(C=N) 1611; ν(C=C aromatic) 1588. **Elemental Analysis** (%): Calc. For $C_{21}H_{25}Cl_3N_2O_2RuSi.2H_2O$ (608.99): C, 41.42; H, 4.14; N, 4.60; Found: C, 41.90; H, 4.56; N, 4.21. **MS** (ESI$^+$, *m/z*): 538.0 [M-Cl]$^+$.

2.8.4. Synthesis of neutral mononuclear rhodium complex 2.11

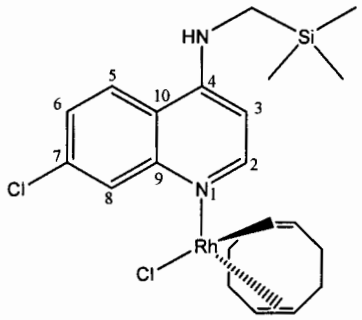

Compound **2.1** (0.171 g, 0.641 mmol) was reacted together with **2.6** (0.170 g, 0.330 mmol). The reaction yielded **2.11** as a light yellow powder. Yield = 0.201 g (61.2%). **M.p.** 268-270 °C. **^{1}H NMR** (399.95 MHz, DMSO-d_6): δ (ppm) = 0.12 (9H, s, 3*CH$_3$); 1.91 (4H, m, 2*CH_2 COD); 2.46 (4H, m, 2*CH_2 COD); 2.81 (4H, m, $^3J_{HH}$ = 5.6 Hz, CH_2); 4.27 (4H, s, 4*CH COD); 6.48 (1H, d, $^3J_{HH}$ = 5.9 Hz, H_3); 7.34 (1H, s, NH); 7.47 (1H, dd, $^4J_{HH}$ = 8.9 Hz, $^3J_{HH}$ = 2.1 Hz, H_6); 8.32 (1H, d, $^3J_{HH}$ = 9.1 Hz, H_5); 8.42 (2H, m, H_8 & H_2). **^{13}C NMR** (100.58 MHz, DMSO-d_6) δ (ppm) = 1.3 (SiCH$_3$); 30.8 (CH_2 COD); 32.9 (CH_2); 83.5 (CH COD); 99.8, 119.2, 124.4, 128.1, 133.5, 149.4, 151.1, 153.4 (ArC). **IR** (KBr, cm^{-1}): ν(NH) 3311; ν(C=N) 1610; ν(C=C aromatic) 1590. **Elemental Analysis** (%): Calc. For $C_{21}H_{29}Cl_2N_2RhSi$ (511.38): C, 49.32; H, 5.72; N, 5.48; Found: C, 49.03; H, 5.78; N, 5.26. **MS** (ESI$^+$, *m/z*): 475.1 [M-Cl]$^+$.

2.8.5. Synthesis of neutral mononuclear rhodium complex 2.12

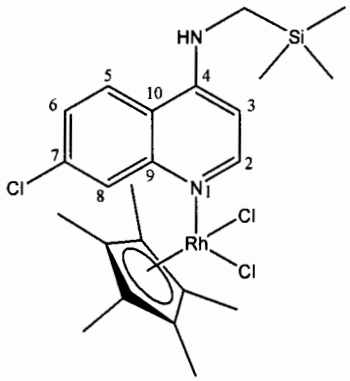

Compound **2.1** (0.171 g, 0.641 mmol) was reacted together with **2.7** (0.212 g, 0.341 mmol). The reaction yielded **2.12** as a bright orange sheet-like solid. Yield = 0.191 g (51.6%). **M.p.** 285-289 °C. **^{1}H NMR** (399.95 MHz, DMSO-d_6): δ (ppm) = 0.13 (9H, s, 3*C$\underline{H}_3$); 1.63 (15H, s, 5*C$\underline{H}_3$ Cp*); 2.78 (2H, d, $^3J_{HH}$ = 5.5 Hz, C$\underline{H}_2$); 6.46 (1H, d, $^3J_{HH}$ = 5.4 Hz, H_3); 7.09 (1H, s, NH); 7.41 (1H, m, H_6); 7.76 (1H, s, H_8); 8.31-8.33 (2H, m, H_5 & H_2). **^{13}C NMR** (100.58 MHz, DMSO-d_6) δ (ppm) = 1.3 (Si$\underline{C}H_3$); 9.0 ($\underline{C}H_3$ Cp*); 32.9 ($\underline{C}H_2$); 99.8, 119.3, 124.4, 124.4, 128.2, 133.6, 149.3, 151.5, 153.4 (ArC).**IR** (KBr, cm^{-1}): ν(NH) 3268; ν(C=N) 1611; ν(C=C aromatic) 1587. **Elemental Analysis** (%): Calc. For $C_{23}H_{32}Cl_3N_2RhSi$ (573.87): C, 48.09; H, 5.58; N, 4.88; Found: C, 47.82; H, 5.61; N, 4.81. **MS** (ESI$^+$, *m/z*): 539.1 $[M\text{-}Cl]^+$, 572.0 $[M\text{-}H]^+$.

2.8.6. Synthesis of neutral mononuclear ruthenium complex 2.13

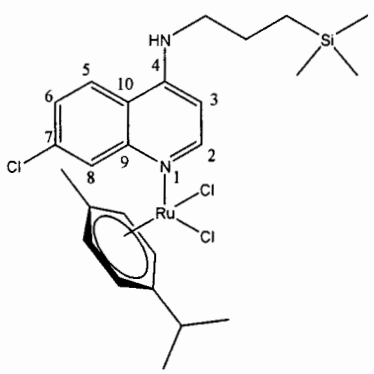

Compound **2.2** (0.150 g, 0.491 mmol) was reacted together with **2.3** (0.150 g, 0.251 mmol). The reaction yielded **2.13** as a light yellow-orange solid. Yield = 0.241 g (62.1%). **M.p.** 171-172 °C. **^{1}H NMR** (399.95 MHz, DMSO-d_6): δ (ppm) = 0.00 (9H, s, 3*C$\underline{H}_3$); 0.58 (2H, m, C$\underline{H}_2$); 1.20 (6H, m, 2*C$\underline{H}_3$ *p*-cym); 1.65 (2H, m, C$\underline{H}_2$); 2.09 (3H, m, C$\underline{H}_3$ *p*-cym); 2.84 (1H, m, C$\underline{H}$ *p*-cym); 3.36 (2H, m, C$\underline{H}_2$); 5.77 (2H, d, $^3J_{HH}$ = 6.2 Hz, 2*C$\underline{H}$ *p*-cym), 5.81 (2H, d, $^3J_{HH}$ = 6.2 Hz, 2*C$\underline{H}$ *p*-cym); 6.46 (1H, d, $^3J_{HH}$ = 5.5 Hz, H_3);

7.36 (1H, s, NH); 7.44 (1H, dd, $^4J_{HH}$ = 9.0 Hz, $^3J_{HH}$ = 2.1 Hz, H_6); 7.77 (1H, d, $^4J_{HH}$ = 2.1 Hz, H_8); 8.28 (1H, d, $^3J_{HH}$ = 9.0 Hz, H_5); 8.39 (1H, d, $^3J_{HH}$ = 5.4 Hz, H_2). **^{13}C NMR** (100.58 MHz, DMSO-d_6) δ (ppm) = -3.5 (Si$\underline{C}H_3$); 13.0 ($\underline{C}H_2$); 18.1 ($\underline{C}H_3$ *p*-cym); 20.8 ($\underline{C}H_3$ *p*-cym); 22.2 ($\underline{C}H_2$); 31.0 ($\underline{C}$H *p*-cym); 46.3 ($\underline{C}H_2$); 76.0, 77.1, 78.0, 92.1, 96.6 (Ar$\underline{C}$ *p*-cym); 98.0 (C_3); 115.6 (C_4); 118.8 (C_8); 124.2 (C_5); 126.9 (C_6); 139.4 (C_9); 139.7 (C_{10}); 142.2 (C_2); 156.4 (C_7). **IR** (KBr, cm^{-1}): ν(NH) 3303; ν(C=N) 1611; ν(C=C aromatic) 1591. **Elemental Analysis** (%): Calc. For $C_{25}H_{35}Cl_3N_2RuSi$ (599.71): C, 50.25; H, 5.86; N, 4.09; Found: C, 50.00; H, 5.49; N, 3.90. **MS** (ESI$^+$, *m/z*): 601.1 $[M+H]^+$.

2.8.7. Synthesis of neutral mononuclear ruthenium complex 2.14

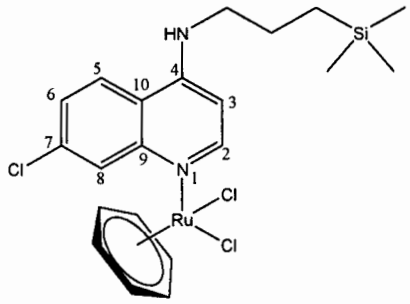

Compound **2.2** (0.25 g, 0.84 mmol) was reacted together with **2.4** (0.210 g, 0.421 mmol). The reaction yielded **2.14** as a yellow-orange solid. Yield = 0.280 g (61.8%). **M.p.** 282-285 °C. **^{1}H NMR** (399.95 MHz, DMSO-d_6): δ (ppm) = -0.02 (9H, s, 3*C$\underline{H}_3$); 0.56 (2H, m, C$\underline{H}_2$); 1.63 (2H, m, C$\underline{H}_2$); 3.23 (2H, m, C$\underline{H}_2$); 5.94 (6H, s, Ar$\underline{H}$ benz); 6.45 (1H, d, $^4J_{HH}$ = 11.9 Hz, H_3); 7.33 (1H, s, NH); 7.43 (1H, dd, $^4J_{HH}$ = 9.7 Hz, $^3J_{HH}$ = 3.8 Hz, H_6); 7.75 (1H, d, $^3J_{HH}$ = 2.2 Hz, H_8); 8.25 (1H, d, $^3J_{HH}$ = 9.1 Hz, H_5); 8.36 (1H, d, $^3J_{HH}$ = 5.5 Hz, H_2). **^{13}C NMR** (100.58 MHz, DMSO-d_6) δ (ppm) = -3.5 (Si$\underline{C}H_3$); 13.1 ($\underline{C}H_2$); 22.3 ($\underline{C}H_2$); 46.7 ($\underline{C}H_2$); 76.1, 78.2, 79.5, 81.5 (Ar$\underline{C}$ benz); 98.8, 115.8, 118.6, 124.2, 127.0, 139.5, 139.7, 142.4, 156.1 (ArC). **IR** (KBr, cm^{-1}): ν(NH) 3305; ν(C=N) 1611; ν(C=C aromatic) 1592. **Elemental Analysis** (%): Calc. For $C_{21}H_{25}Cl_3N_2RuSi$ (541.59): C, 46.75; H, 4.64; N, 5.19; Found: C, 46.20; H, 5.12; N, 4.90. **MS** (ESI$^+$, *m/z*): 541.8 $[M]^+$, 542.8 $[M+H]^+$.

2.8.8. Synthesis of neutral mononuclear ruthenium complex 2.15

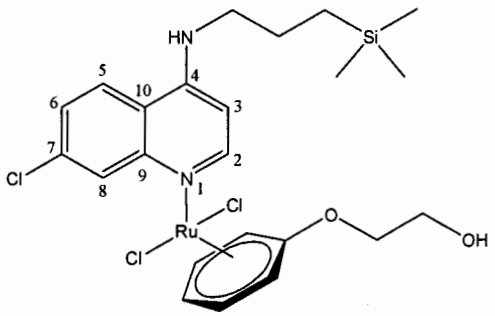

Compound **2.2** (0.19 g, 0.65 mmol) was reacted together with **2.5** (0.210 g, 0.321 mmol). The reaction yielded **2.15** as a yellow solid. Yield = 0.240 g (61.4%). **M.p.** 237-240 °C. **^{1}H NMR** (399.95 MHz, DMSO-d_6): δ (ppm) = 0.00 (9H, s, 3*C$\underline{H}_3$); 0.58 (2H, m, C$\underline{H}_2$); 1.64 (2H, m, C$\underline{H}_2$); 3.25 (2H, m, C$\underline{H}_2$); 3.73 (2H, dd, $^4J_{HH}$ = 7.20 Hz, $^3J_{HH}$ = 12.81 Hz, C$\underline{H}_2$OH Arene); 4.22 (2H, t, $^3J_{HH}$ = 4.99 Hz, OCH_2 Arene); 5.37 (1H, m, C$\underline{H}$ Arene); 5.54 (2H, d, $^3J_{HH}$ = 6.33 Hz, 2*C$\underline{H}$ Arene); 6.14 (2H, m, 2*C$\underline{H}$ Arene); 6.46 (1H, d, $^3J_{HH}$ = 5.55 Hz, H_3); 7.38 (1H, s, NH); 7.44 (1H, dd, $^4J_{HH}$ = 2.25 Hz, ^3J_H = 8.99 Hz, H_6); 7.77 (1H, d, ^4J_H = 2.21 Hz, H_8); 8.28 (1H, d, $^3J_{HH}$ = 9.04 Hz, H_5; 8.38 (1H, d, $^3J_{HH}$ = 5.47 Hz, H_2). **^{13}C NMR** (100.58 MHz, DMSO-d_6) δ (ppm) = -3.5 (Si$\underline{C}H_3$); 13.0 ($\underline{C}H_2$); 22.3 ($\underline{C}H_2$); 46.4 ($\underline{C}H_2$); 58.6 ($\underline{C}H_2$ Arene); 60.1 ($\underline{C}H_2$ Arene); 76.1, 78.2, 79.5, 81.1 (Ar$\underline{C}$ Arene); 98.8, 115.8, 118.6, 124.2, 127.0, 139.5, 139.7, 142.4, 156.1 (ArC). **IR** (KBr, cm^{-1}): ν(NH) 3310; ν(C=N) 1609; ν(C=C aromatic) 1591. **Elemental Analysis** (%): Calc. For $C_{23}H_{29}Cl_3N_2O_2RuSi.H_2O$ (619.02): C, 44.63; H, 4.72; N, 4.53; Found: C, 44.86; H, 5.13; N, 4.11. **MS** (ESI$^+$, *m/z*): 566.1 [M-Cl]$^+$.

2.8.9. Synthesis of neutral mononuclear rhodium complex 2.16

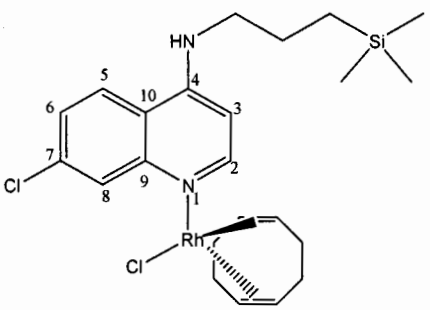

Compound **2.2** (0.171 g, 0.601 mmol) was reacted together with **2.6** (0.150 g, 0.301 mmol). The reaction yielded **2.16** as a bright yellow solid. Yield = 0.19 g (59.4%). **M.p.** 270-272 °C. **^{1}H NMR** (399.95 MHz, DMSO-d_6): δ (ppm) = -0.02 (9H, s, 3*C$\underline{H}_3$); 0.56 (2H, m, C$\underline{H}_2$); 1.62 (2H, m, C$\underline{H}_2$); 1.86 (4H, q, $^3J_{HH}$ = 7.4 Hz, 2*C$\underline{H}_2$ COD);

2.44 (4H, d, $^3J_{HH}$ = 7.6 Hz, 2*C$\underline{H}_2$ COD); 3.25 (2H, m, C$\underline{H}_2$); 4.25 (4H, s, 4*C$\underline{H}$ COD); 6.46 (1H, d, $^3J_{HH}$ = 5.86 Hz, H_3); 7.46 (1H, dd, $^4J_{HH}$ = 2.22 Hz, $^3J_{HH}$ = 9.00 Hz, H_6); 7.52 (1H, s, NH); 8.25 (1H, d, $^3J_{HH}$ = 9.04 Hz, H_5); 8.41 (1H, m, H_8); 8.61 (1H, m, H_2). **^{13}C NMR** (100.58 MHz, DMSO-d_6) δ (ppm) = -1.5 (Si$\underline{C}H_3$); 13.7 ($\underline{C}H_2$); 22.6 ($\underline{C}H_2$); 45.9 ($\underline{C}H_2$); 30.6, 46.1 ($\underline{C}H$ COD); 83.8, 99.8, 119.1, 124.1, 128.0, 132.5, 149.7, 151.1, 153.1 (ArC). **IR** (KBr, cm^{-1}): ν(NH) 3337; ν(C=N) 1613; ν(C=C aromatic) 1591. **Elemental Analysis** (%): Calc. For $C_{23}H_{33}Cl_2N_2RhSi$ (539.43): C, 51.30; H, 6.13; N, 5.20; Found: C, 51.21; H, 6.33; N, 4.88. **MS** (ESI$^+$, *m/z*): 503.1 $[M\text{-}Cl]^+$.

2.8.10. Synthesis of neutral mononuclear rhodium complex 2.17

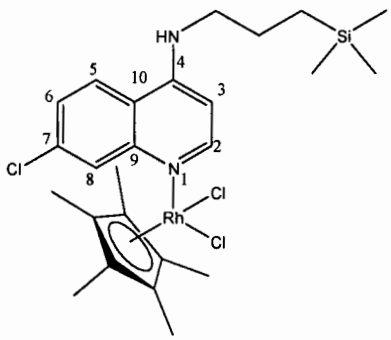

Compound **2.2** (0.190 g, 0.651 mmol) was reacted together with **2.7** (0.201 g, 0.320 mmol). The reaction yielded **2.17** as a bright orange solid. Yield = 0.211 g (53.7%). **M.p.** 263-266 °C. **^{1}H NMR** (399.95 MHz, DMSO-d_6): δ (ppm) = 0.01 (9H, s, 3*C$\underline{H}_3$); 0.59 (2H, m, C$\underline{H}_2$); 1.63 (17H, m, 5*C$\underline{H}_3$ Cp*& C$\underline{H}_2$); 3.23 (2H, m, C$\underline{H}_2$); 6.45 (1H, d, $^3J_{HH}$ = 4.9 Hz, H_3); 7.33 (1H, s, NH); 7.44 (1H, d, $^4J_{HH}$ = 8.6 Hz, H_6); 7.77 (1H, s, H_8); 8.27 (1H, d, $^3J_{HH}$ = 8.9 Hz, H_5); 8.39 (1H, d, $^3J_{HH}$ = 4.7 Hz, H_2). **^{13}C NMR** (100.58 MHz, DMSO-d_6) δ (ppm) = -1.15 (Si$\underline{C}H_3$); 9.03 ($\underline{C}H_3$ Cp*); 14.08 ($\underline{C}H_2$); 23.03 ($\underline{C}H_2$); 40.90 ($\underline{C}$ Cp*); 46.18 ($\underline{C}H_2$); 99.11, 119.10, 124.42, 124.54, 127.87, 133.5, 149.7, 151.1, 152.27 (ArC). **IR** (KBr, cm^{-1}): ν(NH) 3310; ν(C=N) 1612; ν(C=N) 1586. **Elemental Analysis** (%): Calc. For $C_{25}H_{36}Cl_3N_2RhSi$ (601.93): C, 49.88; H, 5.99; N, 4.66; Found: C, 49.58; H, 6.10; N, 4.43. **MS** (ESI$^+$, *m/z*): 601.1 $[M]^+$.

2.9. Single X-ray crystallography studies

In addition to the spectroscopic and analytical data, the incorporation of an organosilane moiety and coordination of rhodium to the silicon-containing aminoquinoline was further established by single-crystal X-ray diffraction analysis of compounds **2.2** and **2.11**. Selected bond angles and lengths are presented in Table 2.2-2.3, 2.6-2.7. X-ray single crystal intensity data were collected on a Nonius Kappa-CCD diffractometer using graphite monochromated

MoKα radiation (λ = 0.71073 Å). Temperature was controlled by an Oxford Cryostream cooling system (Oxford Cryostat).[46] The strategy for the data collections was evaluated using the Bruker Nonius "Collect" program. Data were scaled and reduced using DENZO-SMN software.[47] Absorption correction was performed using SADABS.[48] The structure was refined to R factor of 0.0319. The structure was solved by direct methods and refined employing full-matrix least-squares with the program SHELXL-97 refining on F^2.[49] Diagram was produced using the program PovRay and graphic interface X-seed.[46]

2.10. References

(1) (a) Chavain, N.; Biot, C. *Curr. Med. Chem.* **2010**, *17(25)*, 2729. (b) Guo, Z.; Sadler, P. J. *Angew. Chem., Int. Ed. Engl.* **1999**, *38*, 1512. (c) Gavette, J. V.; Lara, J.; Reling, L. L.; Haley, M. M.; Johnson, D. W. *Chem. Sci.* **2013**, *4*, 585.

(2) Ronconi, L.; Sadler, P. J. *Coord. Chem. Rev.* **2007**, *251*, 1633.

(3) (a) Gasser, G.; Metzler-Nolte N. *Curr. Opin. Chem. Biol.* **2012**, *16*, 84. (b) Patra M.; Gasser G. *ChemBioChem.* **2012**, *13*, 1232.

(4) (a) Jakupec, M. A.; Galanski, M.; Arion, V. B.; Hartinger, C. G.; Keppler, B. K. *Dalton Trans.* **2008**, 183. (b) Jaouen, G.(Ed.): *Bioorganometallics; biomolecules, labeling, medicine.* Wiley-VCH, Weinheim, **2006**. (c) Dyson, P. J.; Sava, G. *Dalton Trans.* **2011**, *40*, 9069.

(5) (a) Peacock, A. F. A.; Sadler, P. J. *Chem. Asian J.* **2008**, *3(11)*, 1890. (b) Süss-Fink, G. *Dalton Trans.* **2010**, *39*(7), 1673. (c) Gasser, G.; Ott, I.; Metzler-Nolte, N. *J. Med. Chem.* **2011**, *54*, 3.

(6) (a) Smith, G. S.; Therrien, B. *Dalton Trans.* **2011**, *40*, 10793. (b) Schatzschneider, U.; Metzler-Nolte, N. *Angew. Chem. Int. Ed.* **2006**, *45*, 1504.

(7) (a) Raja, M. U.; Sindhuja, E.; Ramesh, R. *Inorg. Chem. Commun.* **2010**, *13*, 1321. (b) Biot, C.; Pradines, B.; Sergeant, M. H.; Gut, J.; Rosenthal, P. J.; Chibale, K. *Bioorg. Med. Chem. Lett.* **2007**, *17 (23)*, 6434. (c) Mahajan, A.; Kremer, L.; Louw, S.;

(8) (a) Guéradel, Y.; Chibale, K.; Biot, C. *Bioorg. Med. Chem. Lett.* **2011**, *21 (10)*, 2866. (b) Fujita, M.; Oka, H.; Ogura, K. *Tet. Lett.* **1995**, *36*, 5247. (c) Kumar, K.; Singh, P.; Kremer, L.; Guérardel, Y.; Biot, C.; Kumar, V. *Dalton Trans.* **2012**, *41 (19)*, 5778.

(9) (a) Salas, P. F.; Herrmann, C.; Orvig, C. *Chem. Rev.* **2013**, *113*, 3450. (b) Ikeue, T.; Handa, M.; Chamberlin, A.; Ghosh, A.; Ongayi, O.; Vicente, M. G.; Ikezaki, A.; Nakamura, M. *Inorg. Chem.* **2011**, *50*, 3567.

(10) (a) Murray, C. J. L.; Rosenfeld, L. C.; Lim, S. S.; Andrews, K. G.; Foreman, K. J.; Haring, D.; Fullman, N.; Naghavi, M.; Lozano, R.; Lopez, A. D. *Lancet.* **2012**, *379*, 413. (b) Dyson, P. J.; Sava, G. *Dalton Trans.* **2006**, 1929. (b) Hartinger, C. G.; Dyson, P. J. *Chem. Soc. Rev.* **2009**, *38*, 391.

(11) Burrows, J.; Chibale, K.; Wells, T.N.C. *Curr. Top. Med. Chem.* **2011**, *11*(10), 1226.

(12) (a) Arancibia, R.; Dubar, F.; Pradines, B.; Forfar, I.; Dive, D.; Klahn, A. H.; Biot, C. *Bioorg. Med. Chem.* **2010**, *18*, 8085. (b) Navarro, M.; Pekerar, S.; Pérez, H. A. *Polyhedron.* **2007**, *26*, 2420. (c) Tacke, R.; Handmann, V. I.; Kreutzmann, K.; Keim, C.; Mutschler, E.; Lambrecht, G. *Organometallics.* **2002**, *21*, 3727.

(13) Bellotti de Souza, N.; Carmo, A. M. L.; Lagatta, D. C.; Alves, M. J. M.; Fontes, A. P. S.; Coimbra, E. S.; da Silva, A. D.; Abramo, C. *Biomed. Pharmacother.* **2011**, *65*, 313.

(14) (a) Beagley, P.; Blackie, M. A. L.; Chibale, K.; Clarkson, C.; Moss, J. R.; Smith, P. J. *Dalton Trans.* **2002**, 4426. (b) Beagley, P.; Blackie, M. A. L.; Chibale, K.; Clarkson, C.; Meijboom, R.; Moss, J. R.; Smith, P. J.; Su, H. *Dalton Trans.* **2003**, 3046.

(15) (a) Sánchez-Delgado, R. A.; Navarro, M.; Pérez, H. A.; Urbina, J. A. *J. Med. Chem.* **1996**, *39*, 1095. (b) Navarro, M.; Pérez, H. A.; Sánchez-Delgado, R. A. *J. Med. Chem.* **1997**, *40*, 1937.

(16) Alfonso, M.; Espinosa, A.; Tarraga, A.; Molina, P. *Chem. Commun.* **2012**, *48*, 6848.

(17) Chailap, B.; Tuntulani, T. *Org. Biomol. Chem.* **2012**, *10*, 3617.

(18) Appelt, C.; Slootweg, J. C.; Lammertsma, K.; Uhl, W. *Angew. Chem., Int. Ed.* **2012**, *51*, 5911.

(19) Valderrey, V.; Escudero-Adán, E. C.; Ballester, P. *J. Am. Chem. Soc.* **2012**, *134*, 10733.

(20) Ciardi, M.; Tancini, F.; Gil-Ramirez, G. N.; Escudero-Adán, E. C.; Massera, C.; Dalcanale, E.; Ballester, P. *J. Am. Chem. Soc.* **2012**, *134*, 13121.

(21) Puchnin, K.; Zaikin, P.; Cheshkov, D.; Vatsouro, I.; Kovalev, V. *Chem. Eur. J.* **2012**, *18*, 10954.

(22) Wendji, A. S.; Lutter, M.; Dietz, C.; Jouikov, V.; Jurkschat, K. *Organometallics.* dx.doi.org/10.1021/om400219r | .

(23) (a) Tacke, R.; Linoh, H.; Bioorganosilicon chemistry, in *The Chemistry of Organic Silicon Compounds* (Patai S and Rappoport Z eds), John Wiley & Sons Ltd., Chichester, **1989**.

(24) (a) Tagne Kuate, A. C.; Iovkova, L.; Hiller, W.; Schürmann, M.; Jurkschat, K. *Organometallics*, **2010**, *29*, 5456. (b) Otón, F.; Ratera, I.; Espinosa, A.; Wurtz, K.; Parella, T.; Tárraga, A.; Veciana, J.; Molina, P. *Chem. Eur. J.* **2010**, *16*, 1532. (c) Tacke, R.; Merget, M.; Bertermann, R.; Bernd, M.; Beckers, T.; Reissmann, T. *Organometallics*. 2000, **19**, 3486. (d) Merget, M.; Gunther, K.; Bernd, M.; Gunther, E.; Tacke, R. *J. Organomet. Chem.* 2001, **628**, 183. (e) Tacke, R.; Kornek, T.; Heinrich, T.; Burschka, C.; Penka, M.; Pulm, M.; Mutschler, C.; Lambrecht, G. *J. Organomet. Chem.* 2001, **640**, 140. (f) Tacke, R.; Handmann, V. I.; Kreutzmann, K.; Keim, C.; Mutschler, E.; Lambrecht, G. *Organometallics*. 2002, **21**, 3727. (g) Tacke, R.; Linoh H. in The Chemistry of Organic Silicon Compounds, Part 2 (Eds.: S. patai, Z. Rappoport), Wiley, Chichester, 1989, 1143. (h) Tacke, R.; Wagner S. A. in The Chemistry of Organic Silicon Compounds, Part 3, Vol. 2 (Eds.: Z. Rappoport, Y. Apeloig), Wiley, Chichester, 1998, 2363.

(25) (a) Showell, G. A.; Mills, J. S. *Drug Discovery Today.* **2003,** *8,* 551. (b) Johansson, T.; Weidolf, L.; Popp, F.; Tacke, R.; Jurva, U. *JOHANSSON ET AL.* **2010**, *38 (1)*, 73. (c) Sarauli, D.; Popova, V.; Zahl, A.; Puchta, R.; Ivanovic-Burmazovic, I. *Inorg. Chem.* **2007**, *46*, 7848. (d) Mahoney, J. M.; Beatty, A. M.; Smith, B. D. *Inorg. Chem.* **2004**, *43*, 7617.

(26) (a) Mills, J. S.; Showell, G. A. *Expert Opin Investig Drugs.* **2004**, *13*, 1149. (b) Chenthamarakshan, C. R.; Eldo, J.; Ajayaghosh, A. *Macromolecules.* **1999**, *32*, 5846. (c) Chenthamarakshan, C. R.; Ajayaghosh, A. *Tetrahedron Lett.* **1998**, *39*, 1795.

(27) (a) Pooni, P. K.; Showell, G. A. *Mini Rev Med Chem.* **2006**, *6*, 1169. (b) Reetz, M. T.; Johnson, B. M.; Harms, K. *Tetrahedron Lett.* **1994**, *35*, 2525. (c) Song, M.-K.; Park, S.; Alamgir, F. M.; Cho, J.; Liu, M. *Mater. Sci. Eng. R.* **2011**, *72*, 203.

(28) (a) Gately, S.; West, R. *Drug Dev Res.* **2007**, *68*, 156. (b) Citterio, D.; Takeda, J.; Kosugi, M.; Hisamoto, H.; Sasaki, S.-i.; Komatsu, H.; Suzuki, K. *Anal. Chem.* **2006**, *79*, 1237. (c) Balkhi, S. E.; Megarbane, B.; Poupon, J. l.; Baud, F. d. r. J.; Galliot-Guilley, M. *Clin. Toxicol.* **2009**, *47*, 8.

(29) (a) Tosteson, D. *Sci. Am.* **1981**, *244*, 164. (b) Lazarus, J. H.; Collard, K. J. Endocrine and Metabolic Effects of Lithium; Plenum: New York, **1986**.

(30) Bach, R. O. *Med. Hypotheses.* **1987**, *23*, 157.

(31) Fujimoto, M.; Nogami, T.; Mikawa, H. *Chem. Lett.* **1982**, *11*, 547.

(32) Danil de Namor, A. F.; Tanco, M. A. L.; Joe, C. Y. N.; Salomon, M. *Pure Appl. Chem.* **1995**, *67*, 1095.

(33) Arancibia, R.; Dubar, F.; Pradines, B.; Forfar, I.; Dive, D.; Klahn, A. H.; Biot, C. *Bioorg. Med. Chem.* **2010**, *18*, 8085.

(34) Biot, C.; Dive, D. *Top. Organomet. Chem.* **2010**, *32*, 155.

(35) (a) Biot, C.; Castro, W.; Botté, C. Y.; Navarro, M. *Dalton Trans.* **2012**, *41*, 6335. (b) Navarro, M.; Castro, W.; Biot, C. *Organometallics.* **2012**, *31*, 5715.

(36) Tacke, R.; Kornek, T.; Heinrich, T.; Burschka, C.;nPenka, M.; Pülm, M.; Keim, C.; Mutschler, E.; Lambrecht, G. *J. Organomet. Chem.* **2001**, *640*, 140.

(37) Rajapakse, C. S. K.; Martínez, A.; Naoulou, B.; Jarzecki, A. A.; Suárez, L.; Deregnaucourt, C.; Sinou, V.; Schrével, J.; Musi, E.; Ambrosini, G.; Schwartz, G. K.; Sánchez-Delgado, R. A. *Inorg Chem.* **2009**, *48 (3)*, 1122.

(38) Herrero, M.; Sevilla, R.; Casado, C. M.; Losada, J.; Garcıa-Armada, P.; Rodrıguez-Dieguez, A.; Briones, D.; Alonso, B.; *Organometallics.* dx.doi.org/10.1021/om 400387c |

(39) Bennett, M. A.; Smith, A. K. *J. Chem. Soc. Dalton Trans.* **1974**, *2*, 233.

(40) Zelonka, R. A.; Baird, M. C. *Can. J. Chem.* **1972**, *50*, 3063.

(41) Soleimannejad, J.; White, C. *Organometallics.* **2005**, *24*, 2538.

(42) Gioldano, G.; Crabtree, I. *Inorg. Synth.* **1979**, *19*, 218.

(43) Paz-Michel, B. A.; Felipe, J.; alez-Bravo, G.; Lindsay, S.; andez-Mu~noz, H.; Paz-Sandoval, M. A. *Organometallics.* **2010**, *29*, 3709.

(44) Burger, S.; Therrien, B.; Süss-Fink, G. *Helvetica Chimica Acta.* **2005**, *88*, 468.

(45) Bénech, J.M.; Piguet, C.; Bernardinelli, G.; Bünzli, J.G.; Hopfgartner, G. *J. Chem. Soc., Dalton Trans.* **2001**, 684.

(46) Barbour, L. J. *J. Supramol. Chem.* **2001**, *1*, 189.

(47) Otwinowski, Z.; Minor, W. In *Methods in Enzymology, Macromolecular Crystallography*, Carter Jr, C. W. & Sweet, R. M., Eds.; Academic Press: New York, **1997**; Vol. 276, Part A.

(48) Sheldrick, G. M. *SADABS*; University of Göttingen, Göttingen, Germany, **1997**.

(49) Sheldrick, G. M. *SHELXL-97 and SHELXS-97, Programs for Crystal Structure Refinement;* University of Göttingen, Göttingen, Germany, **1997**.

Chapter 3:
SYNTHESIS AND CHARACTERISATION OF A SILICON-CONTAINING FERROQUINE-DERIVED LIGAND AND ITS RESPECTIVE HETERONUCLEAR METAL COMPLEXES

3.1. Introduction

Introducing chemical diversity into the side chain of chloroquine has paved the way to the discovery of many promising therapeutic agents for the treatment of malaria.[1-5] The discovery of ferrocene in 1951 laid the foundation for the development of many organometallic complexes and became an essential building block for many heteronuclear compounds.[6,7] The structure of ferrocene revealed that iron(II) is sandwiched between two η^5-cyclopentadienyl rings, the π-bonding generating extra electron density, which supplies greater stability to its structure.[7,8] Furthermore, from a biological perspective, studies have shown that ferrocene type compounds will reach the site of action intact, making ferrocenyl compounds ideal candidates for metallo-drugs.[8-10] Thus, investigating the effects of contriving a ferrocene motif in the side chain of the silicon-containing chloroquine analogues synthesised in Chapter 2 was worthwhile endeavor.

It is envisaged that a new series of silicon-containing ferroquine-type ligands and their transition metal complexes will be created. Through this idea, we hope to improve physicochemical properties such as better lipophilicity, to overcome resistant parasitic strains of malaria. By exploiting different chemistry methods and contemplating new design strategies, we wish to further contribute and establish a better understanding towards organometallic and bio-organosilicon chemistry.

3.2. Synthesis of ferroquine (3.5) and silicon-containing ferroquine-derived precursor (3.6)

2-[(*N,N*-dimethylamino)methyl]ferrocene-carboxaldehyde **3.2** was obtained by *ortho*-lithiation of [(dimethylamino)methyl]ferrocene under argon. The dimethylamino group on the reactant has a strong *ortho*-directing effect which is important in the metalation step. The reaction was carried out at room temperature 25 °C in the presence of *n*-butyllithium (*n*-BuLi). Over time, a bright orange precipitate formed yielding the 1,2-disubstituted ferrocene product **3.1**. The *ortho*-lithiated product was reacted with *N,N*-dimethylformamide (DMF), forming the desired aldehyde product **3.2**.

The aldehyde product **3.2** was then converted to the 2-[(*N,N*-dimethylamino)methyl] ferrocenecarboxaldehyde oxime compound **3.3** through a one-pot synthesis in the presence of hydroxylamine hydrochloride. Subsequently, the reduction of the oxime group in

compound **3.3** using $LiAlH_4$ gave rise to 2-[(*N,N*-dimethylamino)methyl]ferrocenyl-methylamine compound **3.4**.

The coupling of the ferrocenyl amine compound **3.4** with 4,7-dichloroquinoline afforded the precursor ferroquine **3.5** in a moderate yield of 45 %. The ammonion salt obtained via quaternerisation of the tertiary amine of ferroquine with methyliodide, was then further reacted with aminomethyl-trimethylsilane to yield the silicon-containing ferroquine-derived analogue **3.6**.

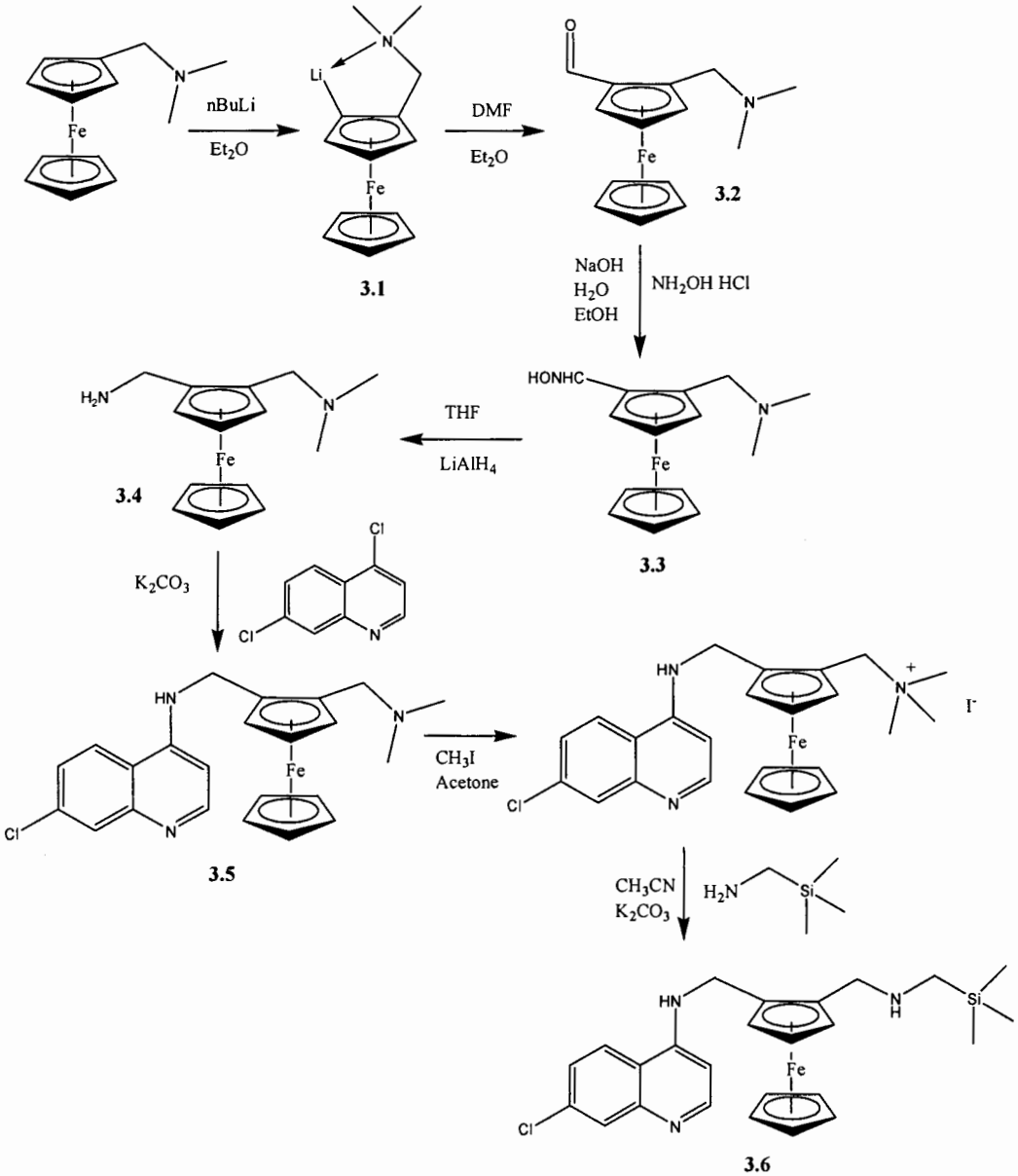

Scheme 3.1: Synthetic route of compounds **3.1-3.6**.

Physical properties

Compounds **3.2-3.6** were isolated in moderate to low yields of approximately 32-74%. Compounds **3.2-3.4** were obtained as orange, or orange-brown oils, while compounds **3.5** and **3.6** were obtained as orange or yellow-orange solids, exhibiting melting points ranging between 171-173 and 151-152 °C respectively (Table 3.1).

Compounds **3.5** and **3.6** are insoluble in hexane and petroleum ether. They are soluble in chlorinated solvents such as DCM, $CHCl_3$, and selected organic solvents such as diethyl ether, toluene and ethyl acetate after slight heating. Compounds **3.5** and **3.6** also display good solubility in acetone, DCM and DMSO.

Table 3.1: Physical appearance, yields and melting points for the compounds **3.2-3.6**.

Compound number	Yield (%)	Physical Appearance	M.p. (°C)
		Brown oil	
3.2	73.5		-
		Orange oil	
3.3	73.7	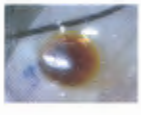	-
		Orange oil	
3.4	71.9		-
		Yellow solid	
3.5	45.7	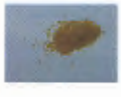	171-173
		Yellow solid	
3.6	31.8		151-152

3.2.1. Spectroscopic and analytical characterisation

Compounds **3.2-3.5** were characterised using ^{1}H NMR spectroscopy and EI^+-mass spectrometry. In addition, the structure of compounds **3.2-3.5** were compared and verified against the reported literature.[11] The newly synthesised compound **3.6** was fully characterised using various analytical and spectroscopic techniques. The molecular structure of compound **3.6** was also elucidated by single-crystal X-ray diffraction analysis. Furthermore, the

assignment of all NMR spectra data was supported by supplementary 2D-NMR spectroscopy, namely COSY and HSQC.

^{1}H NMR spectroscopy

The ^{1}H NMR spectra of compounds **3.2-3.6** displays distinctive peaks associated with the proposed structures. Modifying the ferrocene moiety through the introduction of a substituent *ortho* to the dimethylamino, creates a new chiral plane along the C_5 axis of the ferrocene ring. As a direct result of this planar chirality, and attendant spin-spin coupling effects, the two protons on the CH_2 groups adjacent to the disubstituted ferrocenyl ring appear as two separate doublets. They are diastereotopic, hence couple to each other at around 3.0-4.1 ppm. A singlet observed around 4.2-4.5 ppm corresponds to the five protons on the second unsubstituted ferrocenyl ring. Due to electronic effects, multiplets are observed around 4.2-4.7 ppm integrating for three protons corresponding to the remaining protons on the disubstituted ferrocenyl ring.

For compounds **3.5** and **3.6**, the presence of the six quinoline protons is observed in the aromatic region at around 6.7-8.4 ppm. Again, the protons on the modified side chain, the terminated methyl [$Si(C\underline{H}_3)_3$], are observed close to 0 ppm while $C\underline{H}_2$ groups are observed at around 1.9 and 3.7 ppm respectively. A proton NMR spectrum of compound **3.6** is shown in Figure 3.1 as a representative example. Additional 2D-NMR experiments such as COSY were carried out to offer further validation for the proton assignments.

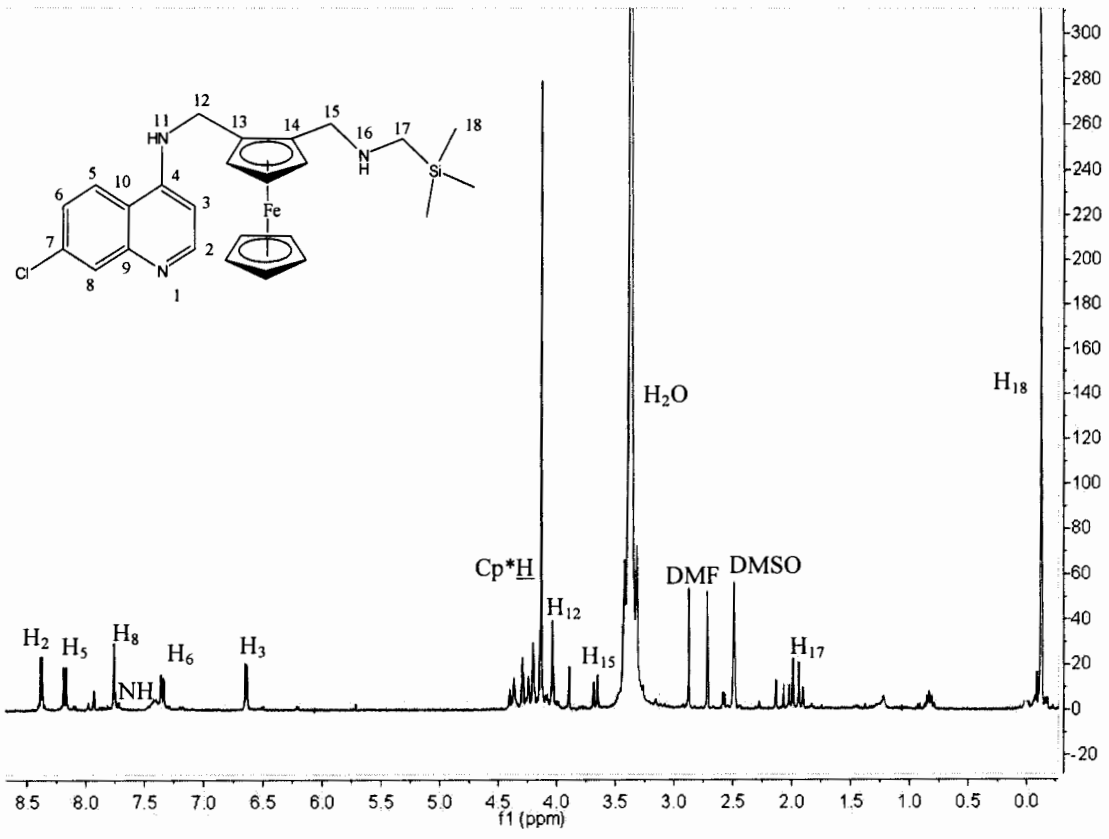

Figure 3.1: ^{1}H NMR spectrum of compound **3.6** recorded in DMSO-d_6.

On inspection of the COSY spectrum for compound **3.6** (Figure 3.2), it was confirmed that the most deshielded proton, H_2 observed as a doublet (J = 5.39 Hz), couples to its adjacent proton H_3 at around 6.6 ppm. Likewise, H_6 appears at around 7.4 ppm as a multiplet, coupling with its adjacent proton H_5. Furthermore, H_6 appears to slightly overlap with the NH proton signal also appearing at around 7.4 ppm. This was confirmed by a D_2O shake experiment. The exchangeable proton will exchange with the deuterium in the D_2O and disappear from the spectrum, in this case the NH proton.

Due to electronic effects H_{17}, found between the terminal silane and the secondary amine, is observed as a multiplet at around 1.9 ppm. Likewise, due to the chirality of the disubstituted ferrocene, two doublets observed at 3.6 and 3.4 ppm corresponds to H_{15} with coupling constant of 12.89 Hz. H_{12} located between the ferrocene and the quinoline moiety appears in the range of 4.0-4.4 ppm. This overlaps with peaks for the ferrocene fragments also appearing in the range of 4.0-4.5 ppm. A sharp singlet observed at around 4.2 ppm corresponds to the five protons on the unsubstituted ferrocenyl ring. The remaining proton signals integrating for five protons all together is associated with the two protons on the CH_2 group and three protons on the disubstituted η^5-cyclopentadienyl ring.

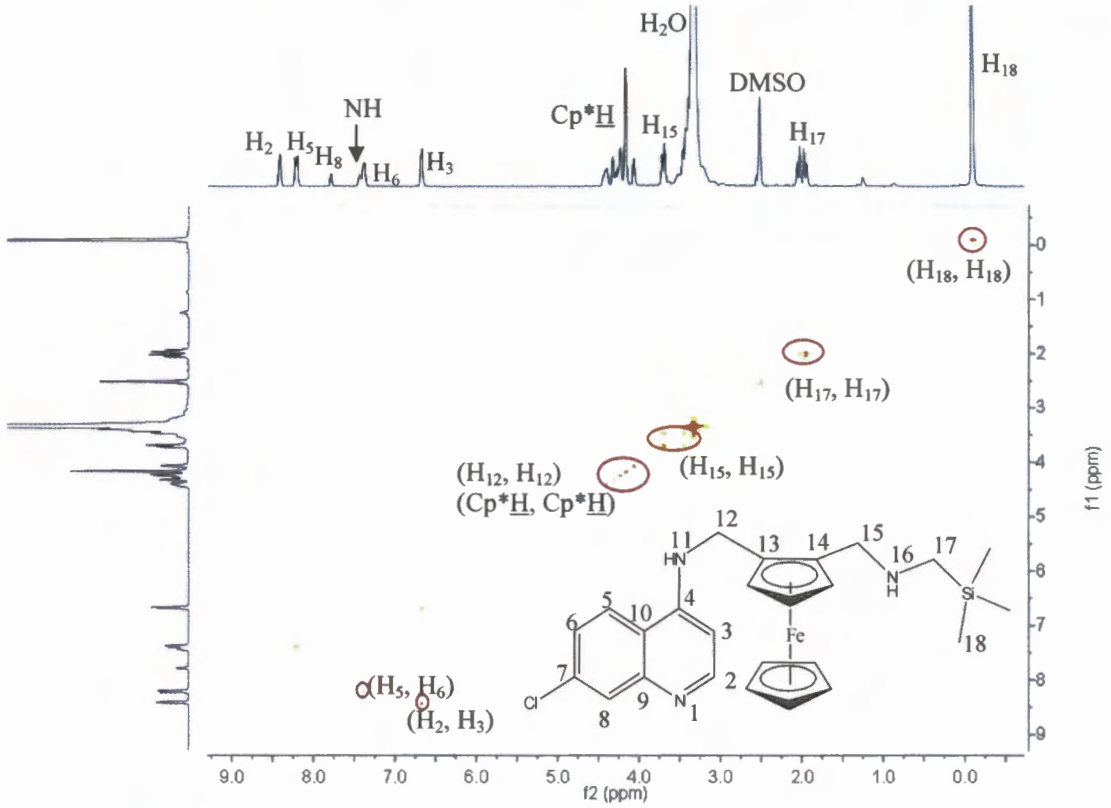

Figure 3.2: 2D-NMR COSY spectrum of compound **3.6** recorded in DMSO-d_6.

^{13}C NMR spectroscopy

The ^{13}C NMR spectra of compound **3.6** correspond with the proposed structure. Due to the electronic effect of the π-system, the quinoline ring carbon atoms were observed in the range of 99.7-152.3 ppm with C_2 being the most deshielded since it is adjacent to the electron withdrawing quinoline nitrogen. C_5 and C_6 being adjacent to each other appear in similar environments; thus, accounting for the two peaks observed in close proximity at 124.4 and 124.6 ppm respectively. Due to the shielding effects of the silicon atom, a singlet observed at -1.96 ppm corresponds to the three terminal $\underline{C}H_3$ groups. Similarly peaks at 40.2, 41.4, and 69.9 ppm are associated with the three $\underline{C}H_2$ groups.

As a consequence of the ferrocenyl group, five peaks at 66.2, 64.4, 69.4, 83.9 and 86.5 ppm were detected, and assigned to the ferrocene moiety. It appears that the carbon chemical shifts are less susceptible to shielding and deshielding with respect to the introduction of the ferrocenyl spacer compared to compounds **2.1** and **2.2** in Chapter 2. Furthermore, additional 2D-NMR (HSQC) experiments were carried out to provide additional supporting evidence for the carbon assignments.

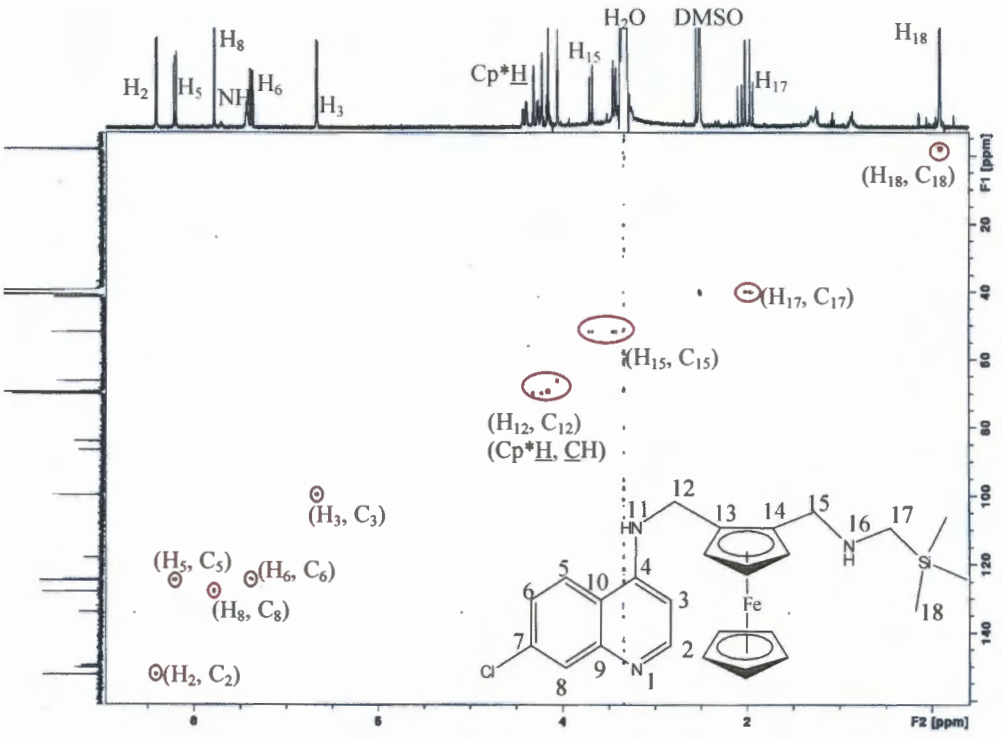

Figure 3.3: 2D-NMR HSQC spectrum of compound **3.6** recorded in DMSO-d_6.

Examination of the HSQC spectrum (Figure 3.3) for compound **3.6** revealed that the most deshielded proton H_2, which is adjacent to the electron-withdrawing quinoline nitrogen, correlates to the most deshielded carbon C_2 at around 150 ppm. The remaining four protons on the quinoline moiety; namely H_3, H_5, H_6, and H_8, couple to four carbon atoms in the region 95-130 ppm; and H_3 being the most shielded appear at around 95 ppm. H_{17} being adjacent to the terminal silane appears to be the most shielded of the three CH_2 groups, observed around 40 ppm. Two separate doublets appearing at around 3.6 and 3.9 ppm in the ^{1}H NMR spectrum couple to one carbon peak in the ^{13}C NMR spectrum at around 53 ppm, and corresponds to (H_{15}, C_{15}). Peaks associated with H_{12}, between the ferrocenyl motif and the quinoline moiety appears to overlap with peaks on the ferrocene moiety in the ^{1}H NMR spectrum. This is evident in the HSQC as two proton peaks in the ^{1}H NMR couple to one carbon signal at around 70 ppm in the ^{13}C NMR spectrum.

The remaining peaks between 4.0-4.5 ppm in the ^{1}H NMR spectrum correlate to carbon signals in the range of 65-75 ppm, and corresponds to CH on the ferrocenyl moiety. Two carbon signals at around 83 and 86 ppm in the ^{13}C NMR spectrum do not couple to any protons suggesting these to be the quaternary carbons C_{13} and C_{14} on the η^5-cyclopentadienyl ring. The most shielded protons $Si(C\underline{H}_3)_3$ couple to a peak at around 1 ppm in the ^{13}C NMR spectrum. The remaining carbon signals at around 90-150 ppm in the HSQC do not couple with any peaks in the ^{1}H NMR spectrum, as expected for the quaternary carbon atoms of the quinoline motif.

Infrared spectroscopy

On close examination of the IR data, all recorded using KBr pellets, the main functional groups present in the molecules exhibited very distinct characteristic absorption patterns. A strong sharp absorption band observed at around 1613 cm^{-1} was assigned to the C=N for compound **3.6**. Furthermore, the primary amine absorption band appearing at 3431 cm^{-1} and a strong sharp band at 1582 cm^{-1} are assigned to the C=C present on the quinoline scaffold. These are comparable to analogous compounds reported in Chapter 2.

Elemental analysis

Elemental analysis of compounds **3.5** and **3.6** attests to the chemical composition for the proposed structures. The percentages of carbon, hydrogen, and nitrogen were found to correlate with the calculated values, all within an error range of 0.4%.

Electron impact mass spectrometry

Mass spectrometry was used to offer alternative confirmation of each compound. Compounds **3.2-3.5** were compared with literature. A base peak at m/z 490.80 in the EI^{+}-MS for **3.6** corresponds to the molecular ion, while the peak observed at 491.80 corresponds to the $[M+H]^{+}$ ion of compound **3.6**.

Molecular structure of compound 3.6

Single crystals of compound **3.6** were obtained by diffusion of hexane into a DCM solution of compound **3.6**. Table 3.2 illustrates the data collection and processing parameters for compound **3.6**, and Table 3.3 lists selected bond angles and lengths. The molecular structure of compound **3.6** (Figure 3.4) crystallises in the triclinic space group $P\bar{1}$, displaying the planar aromatic aminoquinoline moiety and free rotation around the ferrocenyl group.

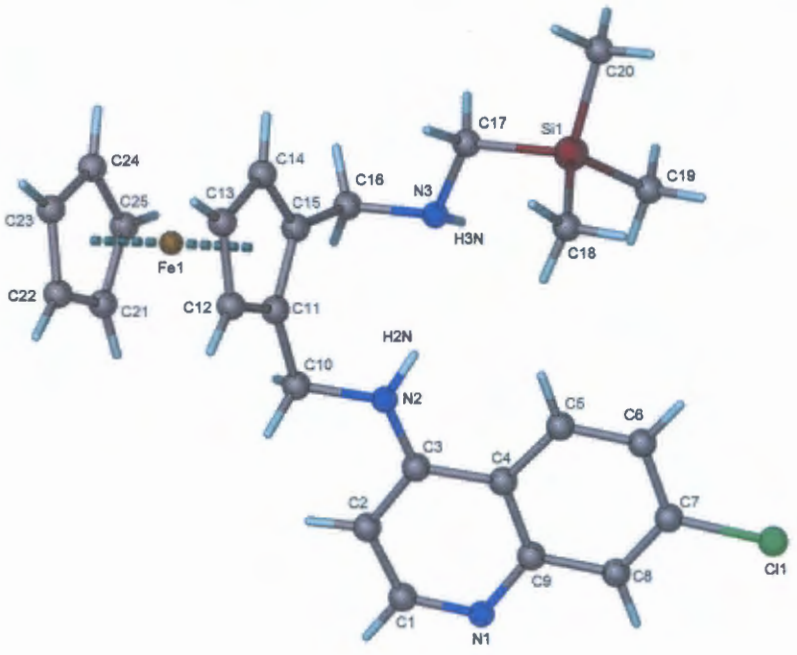

Figure 3.4: Molecular structure of compound **3.6** showing the atomic numbering scheme.

For compound **3.6**, all non-hydrogen atoms were refined anisotropically. All hydrogen atoms, except amine hydrogen atoms on N_2 and N_3, were placed in idealised positions and refined in riding models with U_{iso} assigned the values to be 1.2 or 1.5 times those of their parent atoms and the constraint distances of C-H ranging from 0.95 Å to 0.99 Å.

The hydrogen atoms on N_2 and N_3 were located in the difference electron density maps and refined independently with simple bond length constraint [d(N-H) = 0.88(1) Å]. The structure was refined to R factor of 0.0389.

Table 3.2: Crystal data for compound **3.6**.

	3.6
Chemical formula	$C_{25}H_{30}ClFeN_3Si$
Formula weight	491.91
Crystal system	Triclinic
Space group	*P*-1
Crystal color and shape	Yellow crystalline
Crystal size	0.05 x 0.10 x 0.18
a / Å	8.598 (2)
b / Å	11.434 (3)
c / Å	13.384 (4)
α/ °	84.800 (9)
β/ °	77.444 (7)
γ/ °	73.074 (8)
V /Å^3	1228.2 (6)
Z	2
T / K	173
D_c / g·cm^{-3}	1.330
μ / mm^{-1}	0.789
Scan range / °	$1.9 < \sigma < 28.0$
Unique reflections	5847
Reflections used [$I > 2$sigma(I)]	4199
R_{int}	0.045
R indices (all data)	R_1 0.0389, wR_2 0.0925, S 1.03
Goodness-of-fit	1.031
Min, Max Δρ/e Å^{-3}	-0.38, 0.48
Radiation [Å]	0.71073

For compound **3.6**, carbon-carbon bond lengths around the quinoline component are approximately equal due to delocalisation of the π-electrons in the ring. Furthermore, as a result of the delocalisation, bond lengths around N_1 appear to be shorter compared to N_2 and N_3. Atoms around the silicon atom have longer bond lengths compared with the rest of the molecule, which is also apparent in compound **2.2**. The carbon atoms on the ferrocene core all contain similar bond lengths around 2.03-2.05 Å to the iron metal center. In addition, the iron(II) metal atom is sandwiched between the two η^5-cyclopentadienyl rings.

Introduction of the ferrocene core provides additional flexibility to the ligand, allowing free rotation between the quinoline moiety and the terminal silane group. This is evident in the arbitrary bonding angles (Table 3.3). Furthermore, the two secondary amine groups seem to distort the carbon chain spacer due to possible intermolecular hydrogen bonding. They appear to be locked in a concave position with regards C_{10}, C_{11} and C_{15}, C_{16} on the ferrocene core.

Table 3.3: Selected Bond Lengths (Å) and Angles (°) for compound **3.6.**

Inter atomic distances (Å)	
Atoms	**3.6**
Fe1-C11	2.032 (19)
Fe1-C21	2.035 (2)
Fe1-C15	2.047 (2)
Si1-C18	1.859 (3)
Si1-C20	1.862 (3)
N1-C1	1.319 (3)
N1-C9	1.370 (3)
N2-C10	1.460 (3)
N3-C17	1.473 (3)
Angles (°)	
C11-Fe1-C22	123.4 (10)
C23-Fe1-C25	67.62 (11)
C24-Fe1-C12	162.6 (11)
C18-Si1-C19	108.9 (13)
C20-Si1-C17	106.6 (12)
C1-N1-C9	115.5 (18)
C3-N2-C10	119.9 (18)
C17-N3-C16	111.7 (16)
C5-C4-C3	123.4 (18)

3.3. Ru(II), Rh(I) and Rh(III) silicon-containing ferroquine-derived complexes (3.7-3.11)

Heterometallic complexes **3.7-3.11** were obtained by reacting precursor **3.6** with the reported metal dimers namely, $[Ru(\eta^6\text{-}C_6H_5OCH_2CH_2OH)\ (\mu\text{-}Cl)Cl]_2$, $[Ru(\eta^6\text{-}C_6H_6)(\mu\text{-}Cl)\ Cl]_2$, $[Ru(\eta^6\text{-}p\text{-}^iPrC_6H_4Me)(\mu\text{-}Cl)Cl]_2$, $Rh(\eta^4\text{-}C_8H_{12})(\mu\text{-}Cl)]_2$ and $[Rh(\eta^5\text{-}C_{10}H_{15})(\mu\text{-}Cl)_2Cl]_2$, compounds **2.3-2.7** in Section 2.3 (Scheme 3.2). These complexation reactions were conducted under similar conditions to those described in Section 2.4.

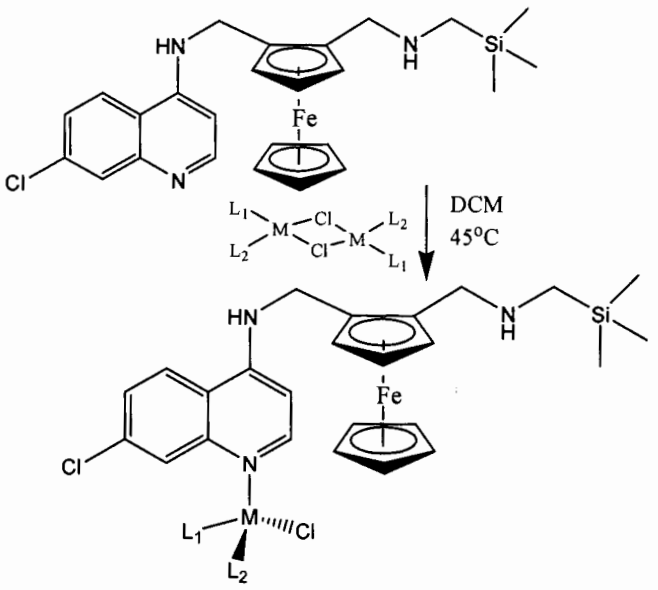

Compound	M	L_1	L_2
3.7	Ru	η^6-benz	Cl
3.8	Ru	η^6-*p*-cymene	Cl
3.9	Ru	η^6-$C_6H_5C_2H_4OH$	Cl
3.10	Rh	COD	-
3.11	Rh	Cp*	Cl

Scheme 3.2: Synthetic route to complexes **3.8-3.11**.

Metallation occurs at the nucleophilic nitrogen of the pyridine ring through coordination to either ruthenium or rhodium in an analogous manner to the compounds discussed in Chapter 2. The ferrocene moiety does not seem to alter the electronic density of the quinoline and thus not affecting its coordination reactivity.

Physical properties

The silicon-containing ferroquine-derived metal complexes **3.7-3.11** were isolated in relatively moderate yields of 53-66%. With the exception of complex **3.7**, which decomposed without melting in the range of 277-279 °C, all other complexes exhibit melting points ranging between 171-176 °C (Table 3.4).

Complexes **3.7-3.11** displayed poor solubility in most organic solvents. They appeared to be slightly soluble in MeOH and EtOH, but displayed good solubility in DCM and DMSO. These newly formed metal complexes were generally obtained as light orange solids, and are all air stable.

Table 3.4: Physical appearance, yields and melting points for the metal complexes **3.7-3.12**.

Compound number	Structures	Yield (%)	Physical Appearance	M.p. (°C)
3.7	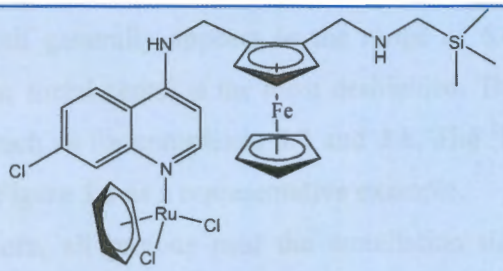	66.4	Brown solid 	Decomp. 277-279
3.8	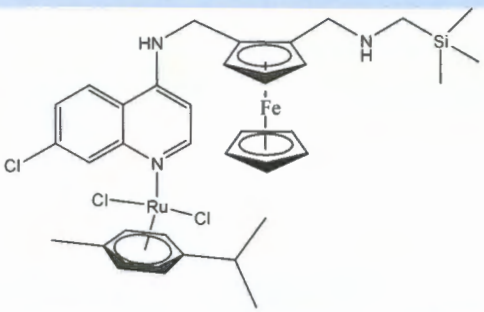	53.1	Orange solid 	171-173
3.9	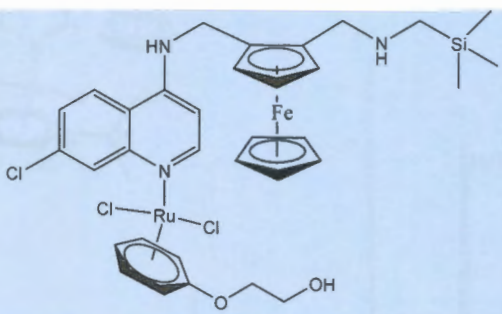	55.5	Bright orange solid 	174-176
3.10	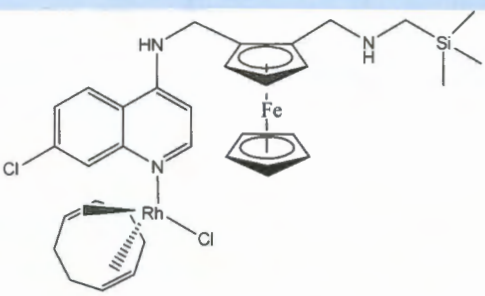	65.5	Orange solid 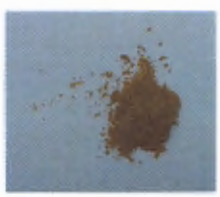	245-247
3.11	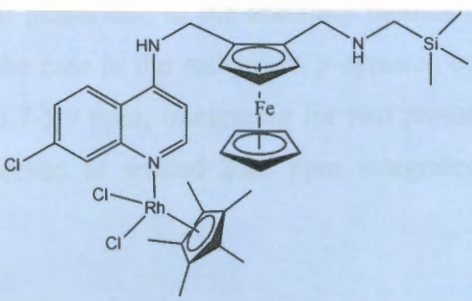	53.8	Bright orange solid 	174-176

3.3.1. Spectroscopic and analytical characterisation

^{1}H NMR spectroscopy

Inspection of the ^{1}H NMR spectra data for complexes **3.7-3.11** supported the proposed structure. The terminal silicon methyl tail appears around 0.0-0.2 ppm for all complexes. These are comparable to those observed in the precursor **3.6**. The proton resonance of the quinoline motif generally appears in the range of 6.6-8.6 ppm. Proton H_2 adjacent to N_1 attached to the metal center is the most deshielded. The NH proton signal is not observed in some cases such as for complexes **3.7** and **3.8**. The ^{1}H NMR spectrum of compound **3.8** is presented in Figure 3.5 as a representative example.

Furthermore, all protons near the metallation site are shifted 1-3 ppm upfield in the metallated complexes compared to the metal free ligand **3.6**. Additional peaks due to the ancillary ligands coordinated to the metal center are also observed. Due to metal co-ordination, proton signals are slightly shifted as a result of shielding and deshielding effects.

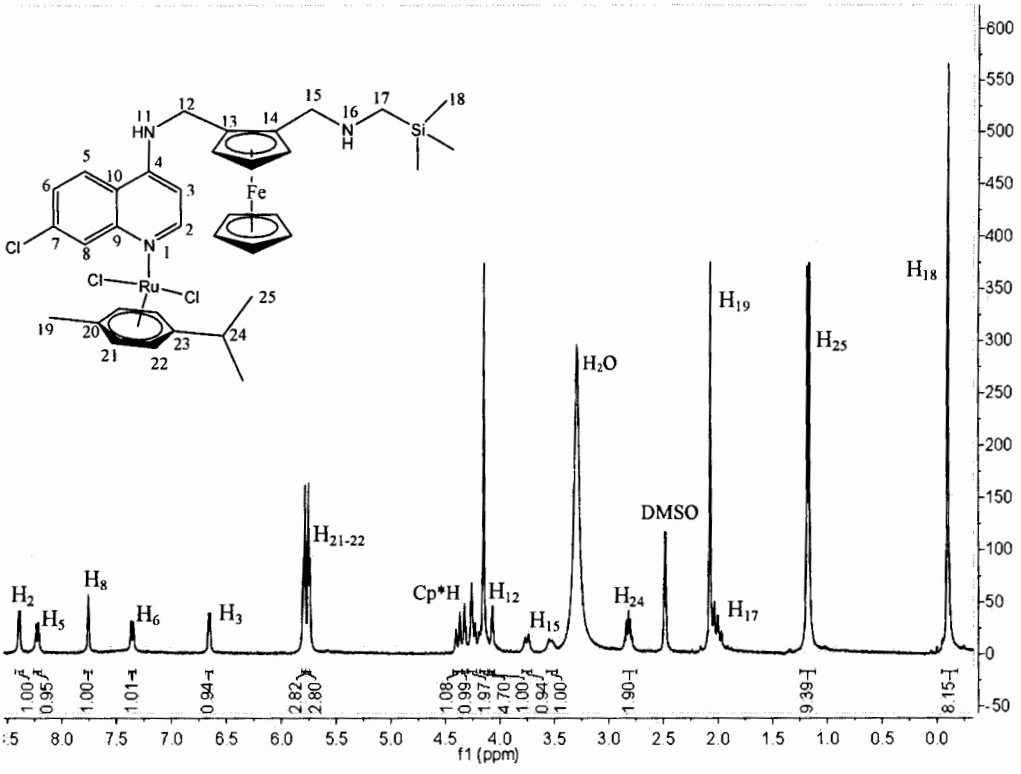

Figure 3.5: ^{1}H NMR spectrum of compound **3.8** recorded in DMSO-d_6.

Additional peaks due to the ancillary ligands coordinated to the metal center are also observed. In the case of the ruthenium *p*-cymene, complex **3.8**, two doublets are observed in the range of 5.7-5.9 ppm, integrating for two protons each corresponding to H_{21} and H_{22}. A multiplet observed at around 2.85 ppm integrates for one proton corresponding to H_{24}.

Likewise, a singlet observed at around 2.09 ppm integrating for three protons corresponds to H_{19}, while a multiplet at around 1.19 ppm integrating for six protons accounts for the remaining two methyl groups H_{25}.

In the case of the ruthenium benzene complex **3.7**, one additional singlet at around 5.94 ppm integrating for six protons is observed in the ^1H NMR of complexes **3.7**. Likewise, in the case of the rhodium Cp* complex, one additional singlet at around 1.61 ppm integrating for 15 protons confirms the presence of the pentamethylcyclopentadienyl ligand on the rhodium in complex **3.11**. Evidence for the remaining ancillary ligands, the ruthenium $C_6H_5C_2H_4OH$ and rhodium COD was gleaned from the ^1H NMR spectra data. Furthermore, additional COSY 2D-NMR experiments provided additional support for the proton assignments. The COSY NMR spectrum of complex **3.8** is represented in Figure 3.6 as an example.

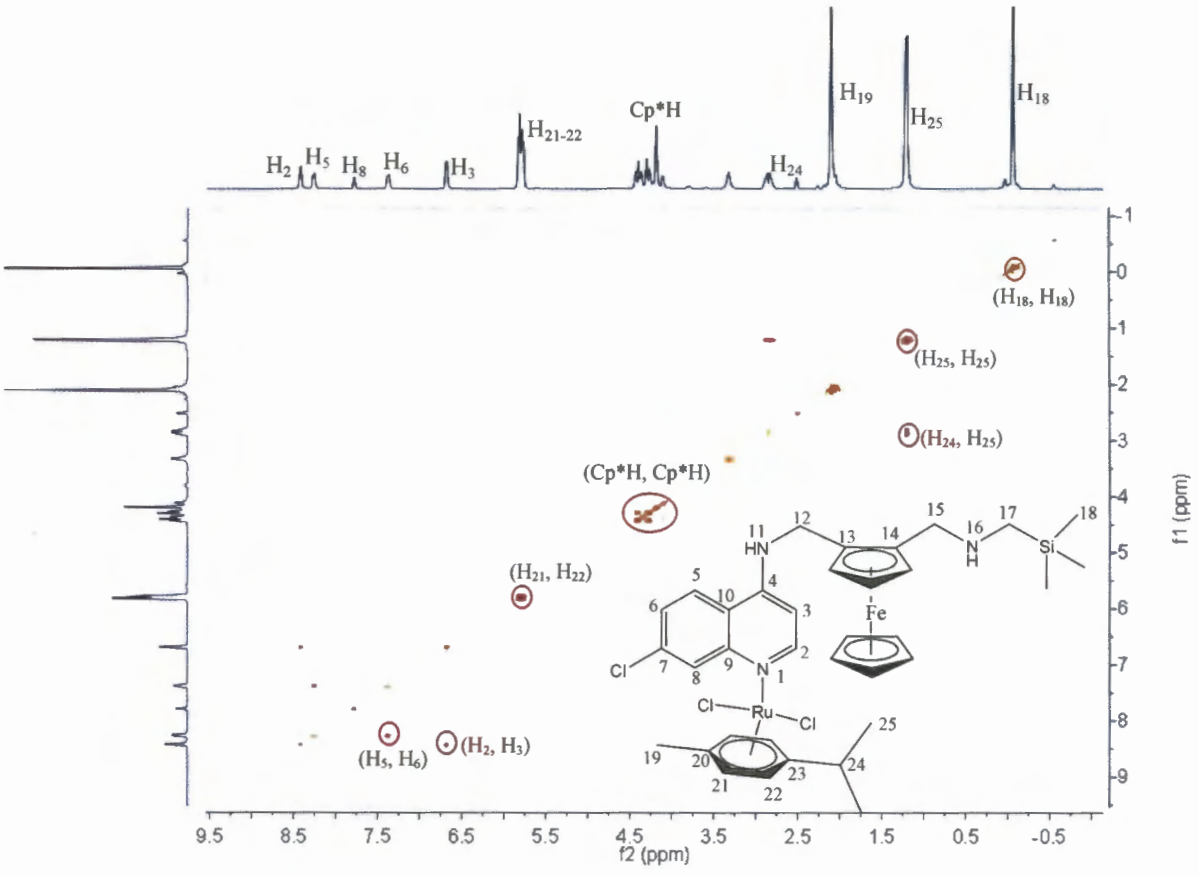

Figure 3.6: COSY 2D-NMR spectrum of compound **3.8** recorded in DMSO-d_6.

Inspection of the COSY spectrum of complex **3.8** shown in Figure 3.6 reveals a similar coupling pattern to that of precursor **3.6**. The most deshielded proton, H_2 observed as a doublet, couples to its adjacent proton H_3 at around 6.6 ppm, and H_6 appearing around 7.5 ppm as a doublet couples to its adjacent proton H_5. In addition, the extended metal moiety

containing the *p*-cymene results in additional coupling interactions. For example H_{21-22} couple to each other around 5.7 ppm, while the methyl protons H_{25} couple to its neighboring H_{24} at around 1.4 ppm. All remaining proton signals and peaks associated with the *p*-cymene ligand are evident in the COSY and ^1H NMR spectra.

^{13}C NMR spectroscopy

Examination of the ^{13}C NMR spectra data for complexes **3.7-3.11** revealed prominent signals for carbon atoms correlating to the proposed structures. The quinoline carbon atoms are generally observed in the range of 99-153 ppm, and the $Si(CH_3)_3$ carbon atoms are relatively shielded being observed close to 0.1 ppm. Furthermore, carbon atoms on the ferrocene moiety are generally observed in the range of 66-72 ppm. The four carbon signals identified are consistent with the proposed structure.

Additional peaks corresponding to the different ancillary metal ligands are also observed. For example in the case of the Rh Cp*, two additional peaks at 9.1 and 41 ppm respectively corresponded to the $R\underline{C}(CH_3)$ and $\underline{C}H_3$ groups on the pentamethylcyclopentadienyl ligand.

Likewise, in the case of the Ru *p*-cymene complex, carbon signals observed around 18.3, 22.0, 30.5, 86.0 (ArC) and 86.8 (ArC) ppm corresponded to $\underline{C}H$ and $\underline{C}H_3$ on the *p*-cymene ligand. Overall, the ^{13}C NMR spectra data of the metal complexes **3.7-3.11** is comparable to the ligand precursor **3.6** with the addition of the ancillary arene on the metal. Furthermore, additional HSQC 2D-NMR experiments were carried out to offer additional support for the carbon assignments.

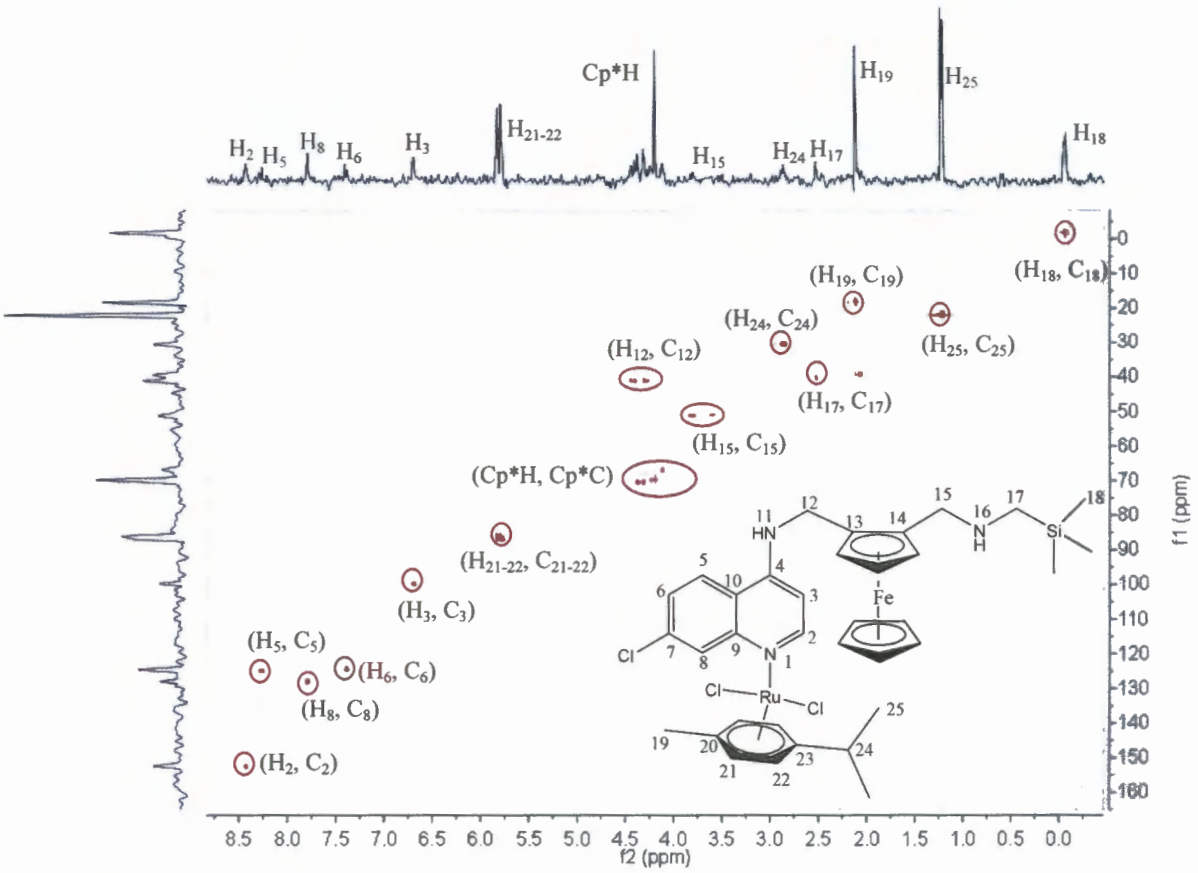

Figure 3.7: HSQC 2D-NMR spectrum of compound **3.8** recorded in DMSO-d_6.

Examination of the HSQC spectrum of complex **3.8** (Figure 3.7) revealed that the most deshielded proton, H_2, corresponds to the most deshielded carbon atom C_2 at around 150 ppm. The remaining protons on the quinoline moiety couple to carbon atoms in the region 90-130 ppm, which is comparable to the precursor **3.6**. The three CH_2 groups correspond to three carbon atoms C_{12}, C_{15} and C_{17} observed in the range of 30-50 ppm. The diastereotopic nature is evident in (C_{12}, H_{12}) and (C_{15}, H_{15}). One carbon signal in the ^{13}C NMR spectrum couples with two split doublets in the ^{1}H NMR spectrum at 40.1 and 50.4 ppm respectively. Lastly, the most shielded protons $Si(C\underline{H}_3)_3$ couple to one peak at around 1 ppm in the ^{13}C NMR spectrum, while the remaining carbon signals around 100-150 ppm correspond to quaternary carbon atoms on the quinoline motif. Overall, all peaks in the ^{1}H and ^{13}C NMR spectra were accoutered for, and further evidence was gleaned from 2D-NMR experiments.

Infrared spectroscopy

Data obtained did not differ much compared to precursor **3.6**. However, one noticeable shift in the IR spectra is the absorption band due to C=N and C=C aromatic vibration of the quinoline ring from 1613 and 1582 cm^{-1} in the metal-free ligand to around 1609 and 1590 cm^{-1} for the metallated compounds respectively.

Elemental analysis

The elemental analysis of complexes **3.7-3.11** offered alternative confirmation data; the percentages of carbon, hydrogen, and nitrogen found to be within an error range of 0.4 % to the calculated values.

Electrospray ionisation mass spectrometry

Mass spectrometry was a tool used to further confirm the molecular ions/fragments with calculated values. Complexes **3.7-3.11** were analyzed using low resolution ESI-MS, and all complexes exhibited peaks in the ESI-MS corresponding to the molecular ions and fragments, either the $[M+H_2O+H]^+$ or the $[M-Cl]^+$ adduct.

Table 3.5: ESI^+-MS for metal complexes **3.7-3.11**.

Compound number	Molecular formula	Molecular weight (g/mol)	m/z
3.7	$C_{31}H_{36}Cl_3FeN_3RuSi$	742.64	761.1 $[M+H_2O+H]^+$
3.8	$C_{35}H_{44}Cl_3FeN_3RuSi$	798.74	763.1 $[M-Cl]^+$
3.9	$C_{33}H_{40}Cl_3FeN_3O_2RuSi$	802.06	822.7 $[M+H_2O+H]^+$
3.10	$C_{33}H_{42}Cl_2FeN_3RhSi$	738.46	738.1 $[M]^+$
3.11	$C_{35}H_{45}Cl_3FeN_3RhSi$	800.96	801.2 $[M]^+$

3.4. Conclusion

A new ferrocene aminoquinoline ligand **3.6** modified in the lateral side chain with an organosilicon moiety, and a corresponding series of neutral mononuclear ruthenium and rhodium metal complexes **3.7-3.11** have been successfully synthesised. Compound **3.6** acts as monodentate donor that coordinates to the transition metals selectively via the quinoline nitrogen of the aminoquinoline scaffold. The ferrocene moiety provides extra flexibility. Furthermore, all the compounds are air-stable, and were characterised using various analytical and spectroscopic techniques. The molecular structure of compound **3.6** was elucidated by single-crystal X-ray diffraction analysis.

3.5. Experimental

3.5.1. *General methods*

All synthetic procedures were performed under inert gas, standard Schlenk and vacuum-line techniques were employed. All reagents were purchased from either Sigma-Aldrich or ABCR Specialty Chemicals and used as received without further purification. Reaction solvents were purchased from the commercial supplier Kimix, distilled and stored over molecular sieves.

Nuclear Magnetic Resonance (NMR) Spectra were recorded on a Varian Unity XR400 MHz (^{1}H at 399.95 MHz, ^{13}C at 100.58 MHz), Varian Mercury XR300 (^{1}H at 300.006 MHz, ^{13}C at 75.46 MHz) or alternatively a Bruker Biospin GmbH (^{1}H at 400.22 MHz, ^{13}C at 100.65 MHz) spectra at ambient temperature. All chemical shifts for ^{1}H and ^{13}C NMR shifts are reported using tetramethylsilane (TMS) as the internal standard. Furthermore, NMR spectra were recorded in deuterated dimethylsufoxide (DMSO-d_6) unless otherwise stated.

Infrared absorptions (IR) were measured on a Perkin-Elmer Spectrum 100, FT-IR Spectrometer as KBr pellets. Melting points were determined using a Büchi melting point B-540 apparatus and corrected. Microanalyses for C, H, N were carried out using a Thermo Flash 1112 Series CHN-O Analyser. Mass Spectrometry determinations were carried out on all new compounds using either electron impact (EI+) on a JEOL GC Matell instrument or alternatively, electrospray ionisation (ESI+) on a Waters API Quattro Micro instrument in the positive-ion mode.

3.5.2. Lithiation of [(Dimethylamino)methyl]ferrocene followed by condensation of 3.1 with *N,N*-Dimethylformamide 3.2[11]

[(Dimethylamino)methyl]ferrocene (2.43 g, 10 mmol) was added to a solution of anhydrous diethyl ether (20 mL) under argon gas and protected from light. The dark solution was placed over liquid nitrogen and acetone slurry. This was than treated with *n*-butyllithium in hexane (6.31 mL, 12.5 mmol). The dark-red solution mixture was then stirred overnight for 24 hrs at ambient conditions.

The red-orange solution mixture **3.1** was reacted with *N,N*-dimethylformamide (0.810 mL, 12.5 mmol) under argon gas and protected from light. After 5 hours of stirring at room temperature, approximately 20 mL of distilled water was added to hydrolyze the reaction. The organic layer was separated and collected, and the remaining aqueous phase was washed with small portions of diethyl ether (2 x 20 mL). The ether extracts were combined and dried over Na_2SO_4, the resulting dark-orange solution was than evaporated to

yield a red oil, which was than further purified through silica gel chromatography. A light-orange solution was eluted with ether/hexane/triethylamine (7:2:1), the solution was dried under vacuum to give the product **3.2** 2-[(*N,N*-dimethylamino) methyl]ferrocene-carboxaldehyde as a dark red oil.

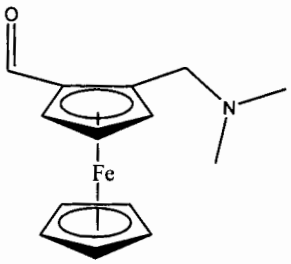

Yield = 2.10 g (73.5%). **^{1}H NMR** (399.95 MHz, $CDCl_3$): δ (ppm) = 10.09 (1H, s, HOCR); 4.77 (1H, m, CH); 4.59 (1H, m, CH); 4.54 (1H, m, CH); 4.21 (5H, s, 5*CH) 3.81 (1H, t, $^4J_{HH}$ = 9.77 Hz, CH); 3.33 (1H, d, $^3J_{HH}$ = 13.03 Hz, CH); 2.25 (6H, s, 2*CH_3). **MS** (EI, *m/z*): 271 $[M]^+$.

3.5.3. Synthesis of 2-[(*N,N*-Dimethylamino)methyl]ferrocenecarboxaldehyde oxime 3.3[11]

A solution of NaOH (0.501 g, 12.5 mmol) in distilled water (4 mL) was added to a stirring solution mixture of **3.2** (0.992 g, 3.70 mmol) and NH_2OH HCl (0.451 g, 6.01 mmol) in absolute EtOH 99.6% (30 mL) at room temperature. The resulting red solution mixture was stirred under reflux for 3 hours. After which the solution mixture was cooled to room temperature and quenched with distilled water (50 mL) to produce an orange solution.

The solution mixture was then neutralised by bubbling CO_2 gas, the treatment of CO_2 gas turns the orange coloured solution into a transparent orange-yellow solution. The resulting solution mixture was extracted with dry DCM (2 x 25 mL), and the combined extracts were dried over Na_2SO_4 and evaporated to give **3.3** as a dark red-brown oil.

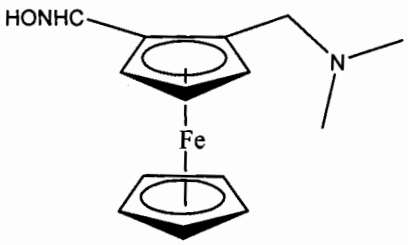

Yield = 0.781 g (73.7%). **^{1}H NMR** (399.95 MHz, $CDCl_3$): δ (ppm) = 7.95 (1H, s, HONR); 4.49 (1H, m, CH); 4.28 (1H, m, CH); 4.21 (1H, m, CH); 4.03 (5H, s, 5*CH) 3.72 (1H, d, $^4J_{HH}$ = 13.00 Hz, CH); 3.33 (1H, d, $^3J_{HH}$ = 13.22 Hz, CH); 2.16 (6H, s, 2*CH_3). **MS** (EI, *m/z*): 286 $[M]^+$.

3.5.4. Reduction of 3.3 to form 2-[(N,N-Dimethylamino)methyl]ferrocenyl-methyl-amine 3.4[11]

$LiAlH_4$ (0.992 g, 26.0 mmol) was add slowly over a 5 minutes interval to a solution of **3.3** (0.671 g, 2.30 mmol) dissolved in dry THF (15 mL) under argon at room temperature. The dark solution was then heated under reflux for 6 hours. The solution was then cooled to room temperature, diluted with dry diethyl ether (20 mL), and washed with brine (5 x 20 mL). The light orange solution was then dried over K_2CO_3 and evaporated to yield **3.4** as a light yellow-orange oil.

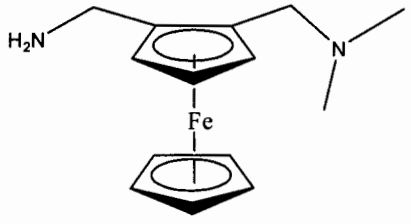

Yield = 0.450 g (71.9%). **^{1}H NMR** (399.95 MHz, $CDCl_3$): δ (ppm) = 4.07 (2H, m, NH_2); 4.02 (5H, m, CH_5); 3.92 (1H, m, CH); 3.59 (1H, m, CH); 3.52 (1H, m, CH); 3.38 (1H, m, CH); 2.79 (1H, m, CH); 2.08 (6H, s, 2*CH_3). **MS** (EI, *m/z*): 272 $[M]^+$.

3.5.5. Condensation of 3.4 with 4,7-Dichloroquinoline to yield ferroquine 3.5[11]

A mixture of **3.4** (0.55 g, 2.0 mmol), 4,7-dichloroquinoline (2.01 g, 10.0 mmol), triethylamine (2.0 mL, 14.0 mmol), and K_2CO_3 (0.4 g, 3.0 mmol) was combined together in 1-methyl-2-pyrrolidinone (7 mL); the dark solution mixture was stirred under argon at 135 °C for 5 hours, after which it was cooled to room temperature. The dark solution was then diluted with dry DCM (50 mL), and then washed with brine (5 x 50 mL). The organic layer was collected and dried over Na_2SO_4. The black solution was then reduced, and the resulting dark-red oil was purified through column silica gel, eluting with ethyl acetate/hexane/triethylamine, (9:10:1). The reaction yielded **3.5** as a yellow-orange solid which was then dried under vacuum.

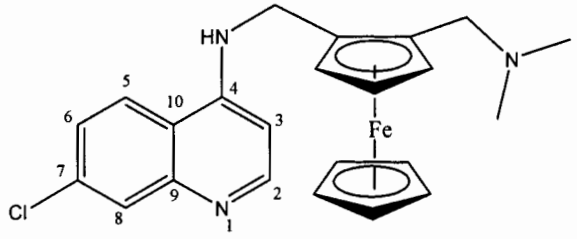

Yield = 0.411 g (45.7%). **^{1}H NMR** (399.95 MHz, $CDCl_3$): δ (ppm) = 8.53 (1H, d, $^3J_{HH}$ = 5.37 Hz, H_2); 7.91 (1H, d, $^4J_{HH}$ = 2.15 Hz, H_8); 7.64 (1H, m, NH); 7.61 (1H, d, $^3J_{HH}$ = 8.99 Hz, H_6); 7.27 (1H, d, $^3J_{HH}$ = 2.18 Hz, H_5); 6.45 (1H, d, $^3J_{HH}$ = 5.43 Hz, H_3); 4.37

(1H, d, $^3J_{HH}$ = 13.04 Hz, CH_2); 4.27 (1H, m, CH_2); 4.17 (1H, m, CH); 4.14 (5H, m, CH_5); 4.09 (2H, m, 2*CH); 3.79 (1H, d, $^3J_{HH}$ = 12.52 Hz, CH_2); 2.88 (1H, d, $^3J_{HH}$ = 12.59 Hz, CH_2); 2.22 (6H, s, 2*CH_3). **IR** (KBr, cm^{-1}): ν(NH) 3422; ν(C=N) 1611; ν(C=C) 1578. **Elemental Analysis** (%): Calc. For $C_{23}H_{24}N_3ClFe$ (433.35): C, 63.74; H, 5.54; N, 9.70; Found: C, 63.61; H, 5.65; N, 9.58. **MS** (EI, *m/z*): 433 $[M]^+$.

3.5.6. Synthesis of silicon-containing ferroquine-derived precursor 3.6

Methyl-iodide (0.160 mL, 2.57 mmol) was reacted with ferroquine **3.5** (0.554 g, 1.28 mmol) in dry acetone (15 mL). The yellow solution mixture was stirred at room temperature under argon gas for 3 hrs. The resulting yellow suspension was reduced, and a solution of K_2CO_3 (0.501 g, 3.60 mmol) in dry acetonitrile : DMF (10 : 10 mL) was combined together with the resulting amine salt, diluted with dry acetonitrile (10 mL). Trimethylamine (3 mL) and catalytic amount of KI was added to the combined solution, which was then refluxed at 89 °C over 4 days.

Dry DCM (20 mL) was added to the reaction mixture, which was then filtered by gravity, and then reduced to approximately 5 ml. The extract was washed with brine (5 x 40 mL). The organic layer was collected and dried over $NaSO_4$. The orange solution was then reduced, drops of hexane was added to the solution mixture. The reaction yielded red-orange precipitate, this was collected by filtering. The red-orange solid was recrystalised in DCM, the reaction yielded a yellow-orange solid which was then dried under vacuum.

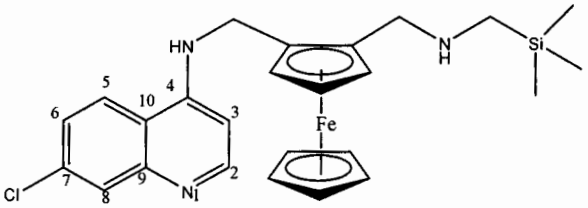

The reaction yielded **3.6** as a yellow-orange solid. Yield = 0.210 g (31.8%). **^{1}H NMR** (399.95 MHz, DMSO-d_6): δ (ppm) = 8.38 (1H, d, $^3J_{HH}$ = 5.43 Hz, H_2); 8.18 (1H, d, $^3J_{HH}$ = 8.97 Hz, H_5); 7.75 (1H, d, $^4J_{HH}$ = 2.18 Hz, H_8); 7.41 (1H, m, NH); 7.35 (1H, dd, $^4J_{HH}$ = 2.18 Hz, $^3J_{HH}$ = 9.03 Hz, H_6); 6.64 (1H, d, $^3J_{HH}$ = 5.54 Hz, H_3); 4.38 - 4.20 (3H, m, 3*CH); 4.13 (5H, m, CH_5); 3.91 (2H, m, 2*CH); 3.68 (1H, d, $^3J_{HH}$ = 12.89 Hz, CH_2); 3.48 (1H, d, $^3J_{HH}$ = 12.01 Hz, CH_2); 2.07 (2H, m, CH_2); -0.10 (9H, s, 3*CH_3). **^{13}C NMR** (75.46 MHz, DMSO-d_6): δ (ppm) = -2.0 ($\underline{C}H_3$); 41.4 ($\underline{C}H_2$); 51.8 ($\underline{C}H_2$); 66.2, 69.4, 70.0, 83.9, 86.5 (Fe$\underline{C}$); 99.7, 117.8, 124.4, 124.6, 127.9, 133.8, 149.6, 150.2, 152.3 (ArC). **IR** (KBr, cm^{-1}): ν(NH) 3431; ν(C=N) 1613; ν(C=C) 1582. **Elemental Analysis** (%):

Calc. For $C_{25}H_{30}N_3ClFeSi$ (491.90): C, 61.04; H, 6.15; N, 8.54; Found: C, 61.22; H, 6.27; N, 8.51. **MS** (EI, *m/z*): 491 $[M]^+$.

3.6. Synthesis of neutral heteronuclear silicon-containing complexes 3.7-3.11

Neutral heteronuclear silicon-containing complexes **3.7-3.11** was synthesised by reacting precursor **3.6** with the appropriate Ru(II)-arene (benzene, *p*-cymene, $C_6H_5C_2H_4OH$), Rh(I) COD or Rh(III) Cp* dimers. The general synthetic procedure is described below.

3.6.1. Synthesis of neutral heteronuclear ruthenium complex 3.7

A solution of precursor **3.6** (0.215 g, 0.436 mmol) dissolved in dry DCM (5 mL) was added dropwise to a solution mixture of the $[Ru(benz)Cl_2]_2$ metal dimer **2.4** (0.159 g, 0.318 mmol) dissolved in dry DCM (5 mL). The red solution was then heated at 45 °C for 2 hrs under argon. Upon cooling to room temperature, the red-orange solution was filtered by gravity and then reduced to less than half of its initial volume by rotary evaporation.

The reduced red-orange solution was then added dropwise to approximately 50 ml of stirring dry diethyl ether, after 5 minutes of stirring at room temperature, an orange precipitate forms. the supernatant was then decanted with minimum solvent remaining, fresh ether (50 ml) was then added to the orange precipitate, decanted again after stirring for approximately 5 minutes. This was repeated until the supernatant appears clear. The resulting solution was filtered, washed with ethyl acetate (3 x 20 ml), and then ether (2 x 20 ml). The orange solid was dried under vacuum. The reaction yielded **3.7** as a yellow-orange solid.

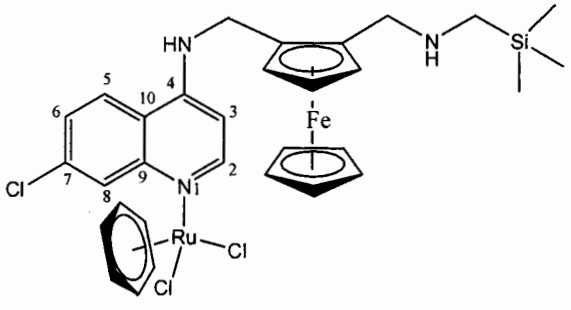

An orange solid, yield = 0.215 g (66.4%). **M.p.** Decomp. 277-279 °C. **^{1}H NMR** (399.95 MHz, DMSO-d_6): δ (ppm) = 0.01 (9H, s, 3*C$\underline{H}_3$); 2.08 (2H, s, C$\underline{H}_2$); 3.64 (1H, m, C$\underline{H}_2$); 3.90 (1H, m, C$\underline{H}_2$); 4.12-4.15 (2H, m, C$\underline{H}_2$); 4.15 (5H, s, 5*C$\underline{H}$); 4.16-4.31 (3H, m, C$\underline{H}$); 5.94 (6H, s, ArH); 6.68 (1H, d, $^3J_{HH}$ = 6.15 Hz, H_3); 7.35 (1H, d, $^4J_{HH}$ = 8.91 Hz, H_6); 7.75 (1H, s, H_8); 8.30 (1H, d, $^3J_{HH}$ = 5.60 Hz, H_5); 8.40 (1H, d, $^3J_{HH}$ = 5.44 Hz, H_2). **^{13}C NMR** (100.58 MHz, DMSO-d_6) δ (ppm) = -1.79 (Si$\underline{C}H_3$); 40.69 ($\underline{C}H_2$); 67.19, 69.68, 70.45 (Fe$\underline{C}$); 88.13 (Ar$\underline{C}$ benz); 99.66, 117.87, 124.41, 124.84, 127.92, 128.79, 133.82, 149.62, 150.19, 152.32 (Ar$\underline{C}$). **IR** (KBr, cm^{-1}): ν(NH) 3430; ν(C=N) 1609; ν(C=C aromatic) 1590.

Elemental Analysis (%): Calc. For $C_{31}H_{36}Cl_3FeN_3RuSi(1/2)DMF$ (778.55): C, 47.82; H, 4.66; N, 5.40; Found: C, 47.71; H, 4.75; N, 5.02. **MS** (ESI^+-MS, *m/z*): 761.1 $[M+H_2O+H]^+$.

3.6.2. Synthesis of neutral heteronuclear ruthenium complex 3.8

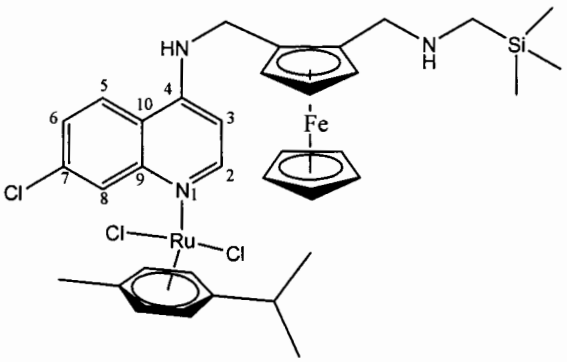

A solution of precursor **3.6** (0.219 g, 0.445 mmol) was reacted together with **2.3** (0.152 g, 0.248 mmol). The reaction yielded **3.8** as an orange solid, yield = 0.189 g (53.1%). **M.p.** 171-173 °C. **^{1}H NMR** (399.95 MHz, DMSO-d_6): δ (ppm) = -0.10 (9H, s, 3*C$\underline{H}_3$); 1.18 (6H, d, $^3J_{HH}$ = 6.9 Hz, 2*C$\underline{H}_3$ *p*-cym); 2.05-2.08 (2H, m, C$\underline{H}_2$); 2.09 (3H, s, C$\underline{H}_3$ *p*-cym); 2.82 (1H, m, C$\underline{H}$ *p*-cym); 3.55 (1H, m, C$\underline{H}_2$); 3.74 (1H, m, C$\underline{H}_2$); 4.15 (5H, s, 5*C$\underline{H}$); 4.07-4.14, 4.16-4.39 (5H, m, C$\underline{H}$ & C$\underline{H}_2$); 5.75 (2H, d, $^3J_{HH}$ = 6.1 Hz, 2*C$\underline{H}$ *p*-cym), 5.80 (2H, d, $^3J_{HH}$ = 6.05 Hz, 2*C$\underline{H}$ *p*-cym); 6.66 (1H, d, $^3J_{HH}$ = 5.3 Hz, H_3); 7.36 (1H, d, $^3J_{HH}$ = 8.73 Hz, H_6); 7.76(1H, s, H_8); 8.23 (1H, d, $^3J_{HH}$ = 8.65 Hz, H_5); 8.39 (1H, d, $^3J_{HH}$ = 5.50 Hz, H_2). **^{13}C NMR** (100.58 MHz, DMSO-d_6) δ (ppm) = -1.88 (Si$\underline{C}H_3$); 18.34 ($\underline{C}H_3$ *p*-cym); 21.98 ($\underline{C}H_3$ *p*-cym); 30.46 ($\underline{C}H$ *p*-cym); 41.10 ($\underline{C}H_2$); 53.31 ($\underline{C}H_2$); 66.76, 69.58, 70.27 (Fe-$\underline{C}$); 86.00, 86.84 (Ar$\underline{C}$ *p*-cym); 99.68, 100.60, 117.86, 124.42, 124.71, 127.93, 133.80, 149.61, 150.17, 152.32 (Ar$\underline{C}$). **IR** (KBr, cm^{-1}): ν(NH) 3307; ν(C=N) 1611; ν(C=C aromatic) 1586. **Elemental Analysis** (%): Calc. For $C_{35}H_{44}Cl_3FeN_3RuSi.DMF$ (871.21): C, 48.25; H, 5.09; N, 4.82; Found: C, 48.34; H, 5.53; N, 4.34. **MS** (ESI^+-MS, *m/z*): 763.1 $[M-Cl]^+$.

3.6.3. Synthesis of neutral heteronuclear ruthenium complex 3.9

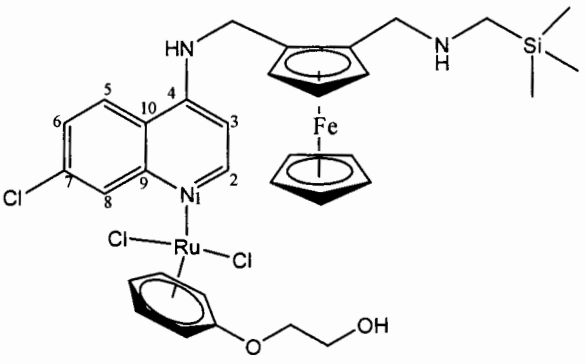

A solution of precursor **3.6** (0.219 g, 0.445 mmol) was reacted together with **2.5** (0.151 g, 0.244 mmol). The reaction yielded **3.9** as an orange solid, yield = 0.247 g (55.5%). **M.p.** 174-176 °C. **^{1}H NMR** (399.95 MHz, DMSO-d_6): δ (ppm) = -0.06 (9H, s, 3*C$\underline{H}_3$); 2.06 (2H, s, C$\underline{H}_2$); 3.71 (2H, t, $^3J_{HH}$ = 4.97 Hz, C$\underline{H}_2$ Arene); 3.89 (2H, m, C$\underline{H}_2$); 4.12-4.19 (2H, m, C$\underline{H}_2$); 4.19 (5H, s, 5*C$\underline{H}$); 4.20-4.23 (5H, m, 3*C$\underline{H}$ & C$\underline{H}_2$ Arene); 5.36 (1H, m, C$\underline{H}$ Arene); 5.52 (2H, d, $^3J_{HH}$ = 6.46 Hz, C$\underline{H}_2$ Arene); 6.13 (2H, m, C$\underline{H}_2$ Arene); 6.66 (1H, d, $^3J_{HH}$ = 5.54 Hz, H_3); 7.36 (1H, dd, $^3J_{HH}$ = 9.00 Hz, $^4J_{HH}$ = 2.25 Hz, H_6); 7.76 (1H, s, H_8); 8.39 (1H, d, $^3J_{HH}$ = 5.41 Hz, H_5); 8.40 (1H, d, $^3J_{HH}$ = 5.49 Hz, H_2). **^{13}C NMR** (100.58 MHz, DMSO-d_6) δ (ppm) = -1.71 (Si$\underline{C}H_3$); 14.1 ($\underline{C}H_2$); 22.4 ($\underline{C}H_2$); 40.7 ($\underline{C}H_2$); 58.6, 60.1 ($\underline{C}H_2$ Arene); 66.8, 69.6, 70.3 (Fe-$\underline{C}$); 83.2, 95.5 100.1, 114.8, 117.8, 119.6, 124.5, 129.1, 130.5, 135.7, 149.6, 150.1, 153.1, 159.1 (ArC). **IR** (KBr, cm^{-1}): ν(NH) 3417; ν(C=N) 1611; ν(C=C aromatic) 1588. **Elemental Analysis** (%): Calc. For $C_{33}H_{40}Cl_3FeN_3O_2RuSi$.DMF (875.15): C, 45.29; H, 4.61; N, 4.80; Found: C, 45.14; H, 4.90; N, 4.42. **MS** (ESI$^+$-MS, *m/z*): 822.7 $[M+H_2O+H]^+$.

3.6.4. Synthesis of neutral heteronuclear rhodium complex 3.10

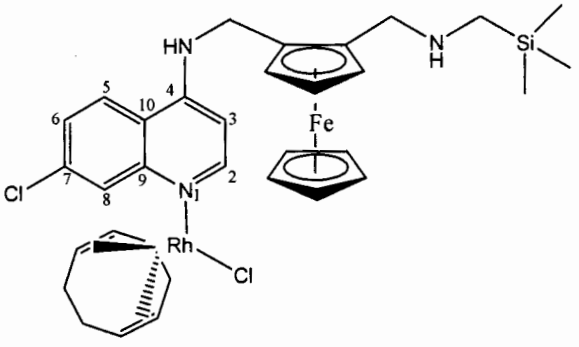

A solution of precursor **3.6** (0.121 g, 0.244 mmol) was reacted together with **2.6** metal dimer (0.0611 g, 0.122 mmol) . The reaction yielded **3.10** as an orange solid, yield = 0.118 g (65.5%). **M.p.** 171-173 °C. **^{1}H NMR** (399.95 MHz, DMSO-d_6): δ (ppm) = 0.02 (9H, s, 3*C$\underline{H}_3$); 1.92-1.95 (6H, m, C$\underline{H}_2$ & 2*C$\underline{H}_2$ COD); 2.41-2.43 (4H, m, 2*C$\underline{H}_2$ COD); 3.42 (1H,

m, C$\underline{H}_2$); 3.72 (1H, m, C$\underline{H}_2$); 4.09-4.13 (2H, m, C$\underline{H}_2$); 4.13 (5H, s, 5*C$\underline{H}$); 4.14-4.39 (7H, m, 3*C$\underline{H}$ & 4*C$\underline{H}$ COD); 6.73 (1H, d, $^3J_{HH}$ = 5.99 Hz, H_3); 7.46 (1H, d, $^3J_{HH}$ = 8.65 Hz, H_6); 7.77 (1H, s, NH); 8.25 (1H, d, $^3J_{HH}$ = 5.20 Hz, H_5); 8.48 (1H, d, $^3J_{HH}$ = 5.72 Hz, H_2); 8.61 (1H, s, H_8). **^{13}C NMR** (100.58 MHz, DMSO-d_6) δ (ppm) = -1.5 (Si$\underline{C}H_3$); 13.7 ($\underline{C}H_2$); 22.6 ($\underline{C}H_2$); 45.9 ($\underline{C}H_2$); 30.6, 46.1 ($\underline{C}$H COD); 66.8, 69.6, 70.3 (Fe-$\underline{C}$); 83.8, 99.8, 119.1, 124.1, 128.0, 132.5, 149.7, 151.1, 153.1 (ArC).**IR** (KBr, cm^{-1}): ν(NH) 3431; ν(C=N) 1611; ν(C=N) 1586. **Elemental Analysis** (%): Calc. For $C_{33}H_{42}Cl_2FeN_3RhSi$.DMF (811.56): C, 48.84; H, 5.22; N, 5.18; Found: C, 49.58; H, 5.20; N, 4.84. **MS** (ESI$^+$-MS, *m/z*): 738.1 $[M]^+$.

3.6.5. Synthesis of neutral heteronuclear rhodium complex 3.11

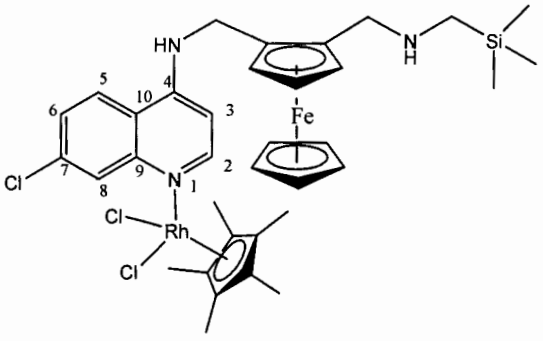

A solution of precursor **3.6** (0.213 g, 0.433 mmol) was reacted together with **2.7** (0.141 g, 0.228 mmol). The reaction yielded **3.11** as an orange solid, yield = 0.187 g (53.8%). **M.p.** 174-176 °C. **^{1}H NMR** (399.95 MHz, DMSO-d_6): δ (ppm) = -0.12 (9H, s, 3*C$\underline{H}_3$); 1.61 (15H, s, 5*C$\underline{H}_3$ Cp*); 1.89-1.94 (2H, m, C$\underline{H}_2$); 3.43 (1H, m, C$\underline{H}_2$); 3.68 (1H, m, C$\underline{H}_2$); 3.90–4.13(2H, m, C$\underline{H}_2$); 4.14 (5H, s, 5*C$\underline{H}$); 4.20-4.37 (3H, m, 3*C$\underline{H}$); 6.64 (1H, d, $^3J_{HH}$ = 5.24 Hz, H_3); 7.34-7.38 (2H, m, NH & H_6); 7.75 (1H, s, H_8); 8.19 (1H, d, $^3J_{HH}$ = 9.36 Hz, H_5); 8.39 (1H, d, $^3J_{HH}$ = 5.64 Hz, H_2). **^{13}C NMR** (100.58 MHz, DMSO-d_6) δ (ppm) = -1.90 (Si$\underline{C}H_3$); 9.06 ($\underline{C}H_3$ Cp*); 40.68 ($\underline{C}$ Cp*); 41.13 ($\underline{C}H_2$); 69.85 ($\underline{C}H_2$); 66.51, 69.58, 70.26 ($\underline{C}$ Fe); 99.31, 99.69, 119.21, 124.44, 124.69, 127.93, 133.82, 150.18, 152.34 (Ar $\underline{C}$). **IR** (KBr, cm^{-1}): ν(NH) 3431; ν(C=N) 1611; ν(C=N) 1586. **Elemental Analysis** (%): Calc. For $C_{35}H_{45}N_3Cl_3SiFeRh$.DMF (874.06): C, 48.10; H, 5.19; N, 4.81; Found: C, 48.25; H, 5.59; N, 4.46. **MS** (ESI$^+$-MS, *m/z*): 801.2 $[M]^+$.

3.7. References

(1) (a) Chavain, N.; Biot, C. *Curr. Med. Chem.* **2010**, *17(25)*, 2729. (b) Guo, Z.; Sadler, P. J. *Angew. Chem., Int. Ed. Engl.* **1999**, *38*, 1512. (c) Gavette, J. V.; Lara, J.; Reling, L. L.; Haley, M. M.; Johnson, D. W. *Chem. Sci.* **2013**, *4*, 585.

(2) (a) Ronconi, L.; Sadler, P. J. *Coord. Chem. Rev.* **2007**, *251*, 1633. (b) Schatzschneider, U.; Metzler-Nolte, N. *Angew. Chem. Int. Ed.* **2006**, *45*, 1504.

(3) (a) Gasser, G.; Metzler-Nolte N. *Curr. Opin. Chem. Biol.* **2012**, *16*, 84. (b) Patra M.; Gasser G. *ChemBioChem.* **2012**, *13*, 1232.

(4) (a) Jakupec, M. A.; Galanski, M.; Arion, V. B.; Hartinger, C. G.; Keppler, B. K. *Dalton Trans.* **2008**, 183. (b) Jaouen, G.(Ed.): *Bioorganometallics; biomolecules, labeling, medicine.* Wiley-VCH, Weinheim, **2006**. (c) Dyson, P. J.; Sava, G. *Dalton Trans.* **2011**, *40*, 9069.

(5) (a) Peacock, A. F. A.; Sadler, P. J. *Chem. Asian J.* **2008**, *3(11)*, 1890. (b) Süss-Fink, G. *Dalton Trans.* **2010**, *39*(7), 1673. (c) Gasser, G.; Ott, I.; Metzler-Nolte, N. *J. Med. Chem.* **2011**, *54*, 3. (c) Smith, G. S.; Therrien, B. *Dalton Trans.* **2011**, *40*, 10793.

(6) (a) Jones, F. N.; Hauser, C. R. *J. Org. Chem.* **1962**, *27*, 701. (b) Wright, M. E. *Organometallics.* **1990**, *9*, 853. (c) Delhaes, L.; Biot, C.; Berry, L.; Maciejewski, L. A.; Camus, D.; Brocard, J. S.; Diver, D. *Bioorg. Med. Chem.* **2000**, *8*, 2739.

(7) Kealy, T. J.; Pauson, P. L.; *Nature.* **1951**, *168*, 1039.

(8) Cotton, F. A. *J. Chem. Soc. Dalton Trans.* **2000**, 1961.

(9) (a) Navarro, M.; Castro, W.; Biot, C. *Organometallics.* **2012**, *31*, 5715. (b) Salas, P. F.; Herrmann, C.; Orvig, C.; *Chemical Reviews*, **2012**, doi.org/10.1021/cr3001252| Chem. Rev. (c) Biot, C.; Castro, W.; Botté, C. Y.; Navarro, M. *Dalton Trans.* **2012**, *41(21)*, 6335. (d) Wilkinson, G.; Rosenblum, M.; Whiting, M. C.; Woodward, R. B. *J. Am. Chem. Soc.* **1952**, *74*, 2125. (e) Pauson, P. L. *J. Organomet. Chem.* **2001**, *637-639*, 3.

(10) (a) Foley, M.; Tilley, L. *Pharmacol. Ther.* **1998**, *79*, 55. (b) Tilley, L.; Loria, P.; Foley, M. *Antimalar. Chemother.* **2001**, *47*, 87. (c) Martinez-Gamboa, L.; Brezinschek, H-P.; Burmester, G. R.; Dörner, T. *Autoimmun. Rev.* **2006**, *5*, 437. (d) Burrows, J.; Chibale, K.; Wells, T.N.C. *Curr. Top. Med. Chem.* **2011**, *11*(10), 1226.

(11) Biot, C.; Glorian, G.; Maciejewski, L. A.; Brocard, J. S.; Domarle, O.; Blampain, G.; Millet, P.; Georges, A. J.; Abessolo, H.; Dive, D.; Lebibi, J. *J. Med. Chem.* **1997**, *40 (23)*, 3717.

Chapter 4:

In Vitro PHARMACOLOGICAL EVALUATION

4.1. Outline

It is essential to note that pharmacological evaluation is a difficult and complicated process. There are several possible variables such as growth of the cells under study, solubility issues of compounds being tested, and the same experiments being repeated on separate occasions. Taking all possible variables into account, all the laboratories running the assays on new compounds use a standard commercially available drug as a control to ensure reliability and reproductively. In addition, the tests are all done in triplicate to reduce random and human errors.

The IC_{50} and MIC_{99} values used in this chapter to represent pharmacological activity are essentially inhibitory concentrations required to kill 50% and 99% of the respective cell population. Thus the lower the value, the more effective the compound is.

Lastly, since all compounds are coloured, they were all screened in the range of 350 to 750 nm to ensure that this does not affect the biological data obtained from reading the microplates generating dose-response curves providing $IC_{50/99}$ values. The results illustrate that absorption of all compounds discontinue at around 370 nm. Absorbance of compound **2.17** is presented in Figure 4.1 as a typical example.

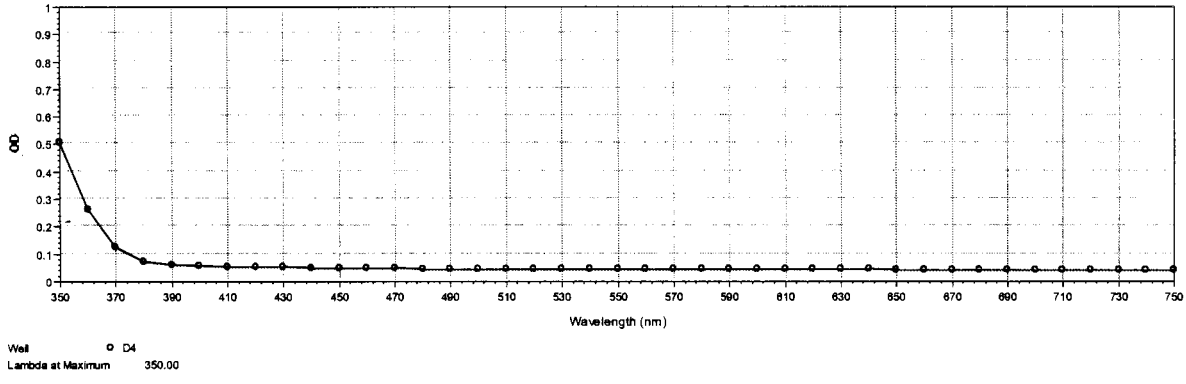

Figure 4.1: Absorbance of compound **2.17** between the range of 350-750 nm.

In this chapter, the *in vitro* pharmacological evaluation of the newly synthesised silicon-containing chloroquine and ferroquine derivatives, which includes ligands, mono- and heteronuclear metal complexes (Figure 4.2) was performed against chloroquine-sensitive (NF54) and chloroquine-resistant (Dd2) strains of the malaria parasite *Plasmodium falciparum*, and against the pathogenic bacterium *Mycobacterium tuberculosis* $H_{37}R_v$ strain, as well as an esophageal (WHCO1) cancer cell line.

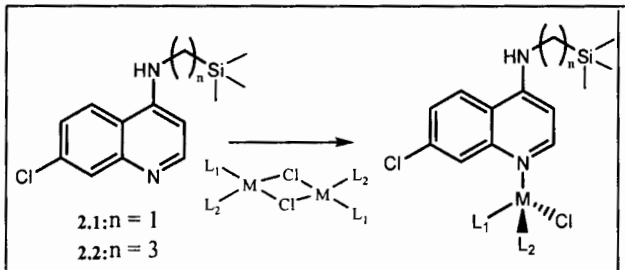

Compound	n	M	L_1	L_2
2.8	1	Ru	η^6-*p*-cymene	Cl
2.9	1	Ru	η^6-benz	Cl
2.10	1	Ru	η^6-$C_6H_5C_2H_4OH$	Cl
2.11	1	Rh	COD	-
2.12	1	Rh	Cp*	Cl
2.13	3	Ru	η^6-*p*-cymene	Cl
2.14	3	Ru	η^6-benz	Cl
2.15	3	Ru	η^6-$C_6H_5C_2H_4OH$	Cl
2.16	3	Rh	COD	-
2.17	3	Rh	Cp*	Cl

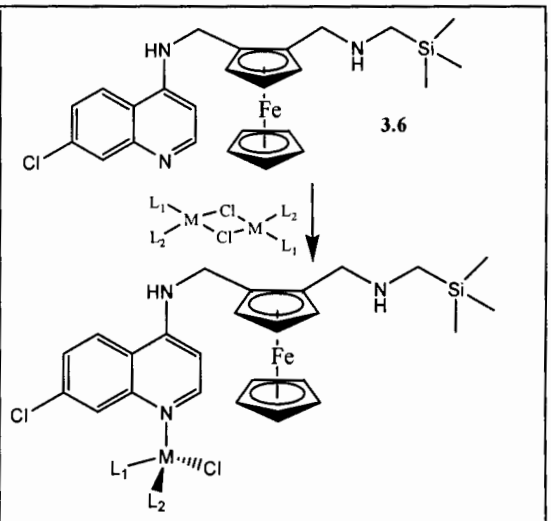

Compound	M	L_1	L_2
3.7	Ru	η^6-benz	Cl
3.8	Ru	η^6-*p*-cymene	Cl
3.9	Ru	η^6-$C_6H_5C_2H_4OH$	Cl
3.10	Rh	COD	-
3.11	Rh	Cp*	Cl

Figure 4.2: Compounds used for *in vitro* pharmacological evaluations.

4.2. *In vitro* analysis against *P. falciparum* strains

As already mentioned, the *in vitro* antiplasmodial activity of all the synthesised compounds were evaluated against the chloroquine-sensitive (NF54) and chloroquine-resistant (Dd2) strains of *P. falciparum*. The chloroquine derivatives synthesised in Chapter 2 are listed in Table 4.1. Likewise, the results obtained for ferroquine derivatives synthesised in Chapter 3 are listed in Table 4.2.

In general, for the chloroquine series, these new silicon-containing chloroquine derivatives displayed moderate to weak inhibitory effects relative to chloroquine. Compound **2.2** with the three carbon methylene spacer displayed better activity compared to compound **2.1** with a one carbon methylene spacer. In the organometallic series, the introduction of a transition metal in some cases (complexes **2.13** and **2.14**), resulted in improved antiplasmodial activity with the ruthenium complexes generally showing superior activity compared to the rhodium complexes. When comparing the ancillary ligands on the metal

center, in general the *p*-cymene ligand exhibited the best overall activities with the ruthenium *p*-cymene metal complex **2.14** displaying the lowest IC_{50} values against the Dd2 strain.

In the chloroquine-sensitive (NF54) strain, the results revealed that the ruthenium complexes **2.2**, **2.13** and **2.14** are the most active with IC_{50} values less than 100 nM. Compounds **2.1**, **2.8**, **2.10-2.12** and **2.15-2.17** displayed moderate activities with IC_{50} values in the range of 100-460 nM. In general, the compounds were less active against the Dd2 strain suggesting that these compounds show some degree of cross resistance to chloroquine albeit all compounds had lower resistance indices than chloroquine.

The resistance index (RI) calculated by (IC_{50} Dd2) / (IC_{50} NF54) was established based on the IC_{50} values obtained for each compound. The lower the RI value suggests that the compound is likely to be active against drug CQ resistant strains.[1,2] With the exception of compounds **2.9**, **2.11**, **2.12** and **2.16**, all other compounds displayed lower RI values in the range of 2-3, comparable to chloroquine (RI = 12.67).

Table 4.1: *In vitro* IC_{50} data for compounds **2.1, 2.2 2.8-2.17** against *P. falciparum* strains.

Compound	*P. falciparum* (IC_{50}, nM)		RI[a]
	NF54	Dd2	
2.1	248	525	2.11
2.2	97.6	270	2.76
2.8	277	527	1.90
2.9	61.4	> 1749	-
2.10	270	835	3.09
2.11	460	> 1955	-
2.12	307	> 1742	-
2.13	81.6	229	2.81
2.14	71.7	212	2.95
2.15	152	386	2.54
2.16	101	721	7.12
2.17	135	370	2.75
CQ	23.3	295	12.7
Artesunate	22.6	-	-

[a] Resistance Index (RI) = (IC_{50} Dd2) / (IC_{50} NF54)

Generally, the newly synthesised silicon-containing ferroquine derivatives displayed comparable inhibitory properties relative to ferroquine. In the organometallic series (**3.7-3.11**), the introduction of a transition metal such as ruthenium or rhodium resulted in improved antiplasmodial activity relative to the precursor **3.6**, exemplified by the ruthenium metal complex **3.9**. Furthermore, with the exception of the rhodium COD metal complex **3.10**, all other metal complexes exhibited better activity in the Dd2 strain compared to the compound **3.6**.

Lastly, all the ferroquine derivatives, demonstrated superior biological activity compared to the chloroquine series in both *P. falciparum* strains.

Table 4.2: *In vitro* IC_{50} data for compounds **3.5-3.11** against *P. falciparum* strains.

Compound	*P. falciparum* (IC_{50}, nM)		RI[a]
	NF54	Dd2	
Ferroquine (3.5)	42.6	27.7	0.65
3.6	7.32	53.9	7.36
3.7	30.7	42.9	1.40
3.8	8.26	42.7	5.17
3.9	4.86	35.9	7.39
3.10	28.0	77.2	2.75
3.11	10.4	34.3	3.31
CQ	23.3	108	4.66
Artesunate	5.20	-	-

[a] Resistance Index (RI) = (IC_{50} Dd2) / (IC_{50} NF54)

In the NF54 strain, the results (Table 4.2) indicate that ligand **3.6**, ruthenium complexes **3.8** and **3.9** as well as rhodium complex **3.11** are the most active with IC_{50} values less than 10 nM. All remaining compounds display comparable activities relative to ferroquine with IC_{50} values in the range 10-30 nM. In general, all compounds were less active in the Dd2 strain with IC_{50} values in the range 34-77 nM. Examination of the RI data indicated that the most active compounds, **3.6**, **3.8** and **3.9** did not display RI values comparable to ferroquine. However, compounds **3.7**, **3.10** and **3.11** with moderate activities displayed relatively low RI values in the range of 1.40-3.31.

4.3. β-Haematin inhibition studies

It has been suggested in the literature that in spite of the resistance to chloroquine in several *P. falciparum* strains, haemozoin formation remains a unique target for most antimalarial drugs.[1,2] A low-cost modified NP-40 assay was utilized in the assessment of compounds for their ability to inhibit formation of synthetic haemozoin. This assay is able to mimic the conditions of the acidic food vacuole in the malaria parasite. The ability of all compounds **2.1, 2.2, 2.8-2.17, 3.6-3.11** to inhibit haemozoin formation was evaluated and the results obtained are presented in Tables 4.3 and 4.4.

Table 4.3: IC_{50} values determined against β-hematin.

Compound	IC_{50} (μM)	95% confidence intervals
2.1	18.1	16.6 – 19.7
2.2	17.7	16.4 – 19.2
2.8	22.4	21.1 – 24.1
2.9	14.4	14.0 – 14.7
2.10	24.2	22.4 – 26.1
2.11	22.5	19.6 – 25.7
2.12	28.5	27.5 – 296
2.13	19.6	18.5 – 20.8
2.14	18.0	16.7 – 19.7
2.15	14.7	13.9 – 15.5
2.16	10.6	10.4 – 10.9
2.17	15.7	15.2 – 16.3
Chloroquine	27.9	-

From the log-based dose-response curves obtained, all of the compounds were shown to inhibit β-haematin formation at the concentration (1000 ng/mL) tested. The chloroquine series generally showed comparable IC_{50} values (10.6-28.5 μM), which are either comparable to, or slightly better than, chloroquine. This is not surprising as compounds **2.1, 2.2, 2.8-2.17** all contain the 4-aminochloroquinoline motif, which has been shown to be important in the inhibition of β-haematin formation by chloroquine.[3]

In the ferroquine series, the IC_{50} values obtained are in the range of 4.84-16.2 μM. The ferroquine-derived compounds are all three or four times more active than those in the chloroquine series. Compound **3.6** is comparable to ferroquine at inhibiting β-haematin formation. All the heteronuclear metal complexes are around 3-fold more potent at inhibiting β-haematin formation compared to ligand **3.6** and ferroquine **3.5**. Generally, the ferroquine series displayed better potency compared to the chloroquine series (Table 4.1 and 4.2), which is consistent with data reported in literature.[3] One explanation could be, the presence of the ferrocene moiety could undergo redox chemistry *in vivo* and generate reactive oxygen species, thus enhancing the biological activities.[3]

Table 4.4: IC_{50} values determined against β-haematin.

Compound	IC_{50} (μM)	Standard deviation
3.6	16.2	0.0923
3.7	4.98	0.140
3.8	4.92	0.139
3.9	5.36	0.123
3.10	4.84	0.231
3.11	6.81	0.128
Ferroquine (3.5)	15.1	0.330
Amodiaquine	6.36	0.120

4.4. *In vitro* testing against WHCO1 oesophageal cancer cell line

The *in vitro* antitumour activities of compounds **2.1**, **2.2**, **2.8-2.17** were evaluated against the WHCO1 oesophageal cancer cell line. Table 4.5 summarises the IC_{50} values obtained. With the exception of complexes **2.11** and **2.17**, all other compounds displayed cytotoxic activities with IC_{50} values below 60 μM. Compound **2.2** and selected metal complexes **2.13-2.15** exhibited the highest antiproliferative effect with IC_{50} values all less than 10 μM. Of these, complex **2.15** containing the 2-hydroxyethoxy moiety tethered to the arene, showed the best cytotoxic activity with an IC_{50} value of 4.41 μM. In addition, compound **2.1** and metal complexes **2.8-2.10**, **2.12** and **2.16** are all moderately active with IC_{50} values ranging between 25 and 52 μM.

The general trend indicates that the ruthenium metal complexes display superior activity relative to the rhodium complexes and the compounds containing a 3-carbon methylene

spacer generally show better activity when compared to those containing a 1-carbon methylene spacer. Lastly, the presence of the metal moiety did not appear to significantly enhance the biological activity in comparison to the free ligands.

Table 4.5: IC_{50} values determined against WHCO1 oesophageal cancer cells.

Compound	WHCO1 cell lines (IC_{50}, μM)	95% Confidence intervals.
2.1	51.9	45.5 - 59.3
2.2	5.86	4.75 - 7.24
2.8	25.2	18.8 - 33.6
2.9	31.5	25.8 - 38.4
2.10	33.1	28.8 - 37.9
2.11	Inactive	-
2.12	21.9	18.2 - 26.3
2.13	5.70	4.98 - 6.53
2.14	7.03	6.34 - 7.79
2.15	4.41	4.06 - 4.79
2.16	31.6	26.4 - 37.8
2.17	Inactive	-

4.5. *In vitro* testing against *M. tuberculosis* $H_{37}R_v$

All compounds were screened for their *in vitro* antimycobacterial activity against *M. tuberculosis* $H_{37}R_v$. The MIC_{99} ranges are summarised in Table 4.6. In general, these compounds displayed weak to moderate antimycobacterial activities. Compounds **2.2**, **2.8**, **2.16**, **3.6**, **3.8**, **3.10** and **3.11** are the most active with MIC_{99} values of 20 μM. These results are not too dissimilar from other compounds containing a quinoline moiety and that were shown to confer antimycobacterial activity.[4]

Table 4.6: IC_{99} values determined against *M. tuberculosis* $H_{37}R_v$ cells.

Compound	MIC_{99} at Day 7 (μM)	MIC_{99} at Day 14 (μM)
2.1	40	40
2.2	20	20
2.8	20	20
2.9	40	40
2.10	40	40
2.11	40	40
2.12	40	40
2.13	80	80
2.14	40	40
2.15	40	80
2.16	20	20
2.17	40	40
3.5	40	40
3.6	20	40
3.7	40	40
3.8	20	40
3.9	40	80
3.10	20	80
3.11	20	20
Rifampicin	-	0.0121
Kanamycin	-	6.45

4.6. Turbidimetric solubility studies

The turbidimetric solubility assay was used to investigate the kinetic solubility of the compounds through a series of dilutions of the tested compound in DMSO into an aqueous buffer. The solubility of a compound is an important factor in determining its absorption from the gastrointestinal tract and ultimately its bioavailability.[5,6] Compounds with poor solubility can often pose a development challenge.[6] The quality of the data generated from the *in vitro* assays can also be affected by poor solubility.

For most turbidimetric solubility assays utilised in drug discovery programs, generally compounds with solubility less than 1 μM are considered to be highly insoluble, while a compound with solubility value between 1 and 100 μM is considered to be moderately soluble, and a compound with a solubility value above 100 μM is considered to be highly

soluble.[5-7] Although poor solubility is obviously an undesirable situation, it shoud not necessarily preclude the development of an otherwise promising compound.[7] If the compound has high permeability and is highly potent *in vivo*, then solubility may become less limiting.

All compounds were first dissolved in pure DMSO, and then serially diluted with aqueous PBS buffer providing a range of concentrations and allowed to equilibrate. The solubility range of the tested compounds was then determined from the concentration at which the compounds began to precipitate out of solution causing turbidity. This turbidity was detected using UV-vis spectroscopy generating the data obtained in Table 4.7. All compounds showed moderate solubility with compounds **2.10**, **2.15**, **3.9** and **3.10** displaying the poorest solubility while compounds **2.9** and **2.12** had the best solubility properties as determined at physiological pH in a PBS buffer and at room temperature.

Overall, the data established suggests that these newly synthesised silicon-containing chloroquine and ferroquine derivatives are good candidates for *in vitro* pharmacological testing. Turbidity of these compounds from various biological assays would be highly unlikely enforcing that the $IC_{50/99}$ values obtained from biological studies is a true reflection of their *in vitro* activity.

Table 4.7: Turbidimetric solubility values determined against PBS buffer at pH 7.4.

Compound	Turbidimetric Solubility (μM)
2.1	20 - 40
2.2	20 - 40
2.8	60 - 80
2.9	80 - 100
2.10	4 - 5
2.11	10 - 20
2.12	80 - 100
2.13	5 - 10
2.14	20 - 40
2.15	1 - 2
2.16	5 - 10
2.17	10 - 20
3.5	5 - 10
3.6	5 - 10
3.7	10 - 20
3.8	20 - 40
3.9	1 - 5
3.10	1 - 5
3.11	5 - 10
Niclosamide	20 - 40

4.7. Summary

Two series of compounds, a chloroquine- and ferroquine-based series, both containing organosilicon motifs integrated into the lateral side chain have been evaluated for *in vitro* antiplasmodial, antitumour and antimycobacterial activities. All of the complexes and their ligands were found to exhibit moderate to high antiplasmodial activity against the NF54 and Dd2 *P. falciparum* strains. Selected compounds inhibited the growth of the malaria parasite in the nanomolar range with the ferroquine series being the most active. Complex **3.9** was the

most active in the NF54 and the Dd2 strains with IC_{50} values of 4.86 and 35.9 nM respectively.

All the metal complexes and ligands inhibited β-haematin formation with the ferroquine series being superior. It appears that with the incorporation of the ferrocene scaffold, introducing multinuclear characteristics with respect to the mononuclear ruthenium or rhodium compounds could lead to more favourable solubility profile as observed in Table 4.7, better modulation of the stability, and improved lipophilicity of the organometallic complexes, which many lead to more potent antiplasmodial agents.

From the combined pharmacological data, the lack of correlation suggests that this new class of silicon-containing 4-aminoquinoline compounds exert their biological effects through selective mechanisms. This may also point to physicochemical and/or transport properties as the drugs have to cross the membrane of the infected host red blood cells and the parasite in order to reach the site of action, the food vacuole.

In general, further studies are necessary to validate the mechanisms of biological action of this new series of silicon-containing mono- and heteronuclear metal complexes. The initial results support the idea of incorporating organosilicon, tweaking the physical and chemical properties; in addition, introducing a ferrocene moiety, creating heteronuclear metal complexes can enhance biological properties as well as ensuring superior physical properties.

4.8. Experimental

4.8.1. *P. falciparum in vitro* assay

The test samples were tested in triplicate on one occasion against chloroquine-sensitive (CQS) NF54 strain and chloroquine-resistant (CQR) Dd2 strain of *Plasmodium falciparum*. Continuous *in vitro* cultures of asexual erythrocyte stages of *P. falciparum* were maintained using a modified method.[8] Quantitative assessment of antiplasmodial activity *in vitro* was determined via the parasite lactate dehydrogenase assay using a modified method.[9] The test samples were prepared to a 20 mg/ml stock solution in 100% DMSO and sonicated to enhance solubility. Samples were tested as a suspension if not completely dissolved. Stock solutions were stored at -20 °C. Further dilutions were prepared on the day of the experiment. Chloroquine was used as the reference drug in all experiments.

A full dose-response was performed for all compounds to determine the concentration inhibiting 50% of parasite growth (IC_5-value). Test samples were tested at a starting concentration of 100 μg/ml, which was then serially diluted 2-fold in complete medium to give 10 concentrations; with the lowest concentration being 0.2 μg/ml. The same dilution

technique was used for all samples. Chloroquine was tested at a starting concentration of 100 ng/ml against the CQR strain and 1000 ng/ml against the CQS strain. The highest concentration of solvent to which the parasites were exposed to had no measurable effect on the parasite viability. The IC_{50}-values were obtained using a non-linear dose-response curve fitting analysis via Graph Pad Prism v.4.0 software.

4.8.2. Detergent mediated assay for β-hematin inhibitors

The β-hematin formation assay method described by Carter *et al.*[10] was modified for manual liquid delivery. Stock solutions of the test compounds were prepared at 10 mM, 2 mM and 0.4 mM by dissolving each sample in DMSO with sonication. Test compounds were delivered to a 96 well plate (Figure 4.3) in triplicate from 0-500 μM (final concentration) with a total DMSO volume of 10 μL in each well. Deionized H_2O (70 μL) and NP-40 (20 μL; 30.55 μM) were then added. A 25 mM haematin stock solution was prepared by sonicating hemin in DMSO, for complete dissolution, and then suspending 177.76 μL of this in a 2M acetate buffer (pH 4.8). The homogenous suspension (100 μL) was then added to the wells to give final buffer and haematin concentrations of 1 M and 100 μM respectively. The plate was covered and incubated at 37 °C for 5-6 hours in a water bath. Analysis of the assay was carried out using the pyridine-ferrichrome method developed by Ncokazi and Egan.[11]

A solution of 50% (v/v) pyridine, 30% (v/v) H_2O, 20% (v/v) acetone and 0.2 M HEPES buffer (pH 7.4) was prepared and 32 μL added to each well to give a final pyridine concentration of ± 5% (v/v). Acetone (60 μL) was then added to assist with hematin dispersion. The UV-vis absorbance of the plate wells was read on a SpectaMax plate reader. Sigmoidal dose-response curves were fitted to the absorbance data using GraphPad Prism v3.02.

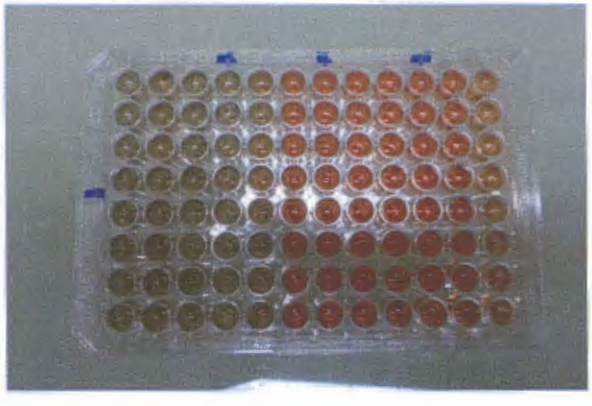

Figure 4.3: β-hematin NP-40 assay after 5 hrs of incubation at 37°C followed by addition of pyridine solution. The orange colour indicates β-hematin inhibition of the compound at the tested concentrations.

4.8.3. MTT assay for cancer cells

The oesophageal cancer cell line, WHCO1, derived from a primary oesophageal squamous cell carcinoma was kindly provided by Professor Rob Veale (University of the Witwatersrand, Johannesburg, South Africa). IC_{50} determinations were carried out using the MTT [3-(4,5-dimethylthiazol-2-yl)-2,5-diphenyltetrazolium bromide] assay. Briefly, 3000 cells were seeded per well in 96-well plates. Cells were incubated at 37 °C under 5% CO_2 (24 h), after which aqueous DMSO solutions of each compound (10 μL, with a constant final concentration of DMSO: 0.2%) were plated at various concentrations. After 48 h incubation, observations were made, and MTT (10 μL) solution added to each well.

After a further 4 h incubation, solubilisation solution (100 μL) was added to each well, and plates were incubated overnight. Plates were read at 595 nm on a BioTek microplate reader generating dose-response curves (Figure 4.4).

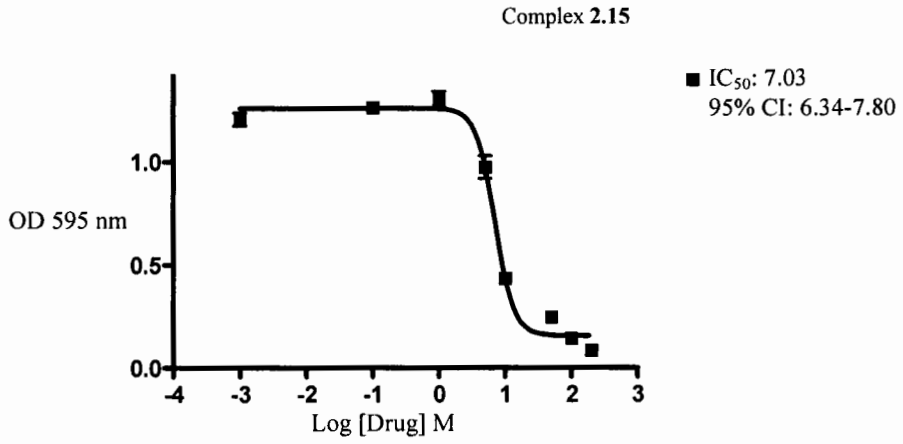

Figure 4.4: dose-response curves of complex **2.15**.

4.8.4. *M. tuberculosis* microdilution method

The broth microdilution method[12] allows a range of antibiotic concentrations to be tested on a single 96-well microtitre plate in order to determine the minimum inhibitory concentration (MIC). Briefly, a 10 ml culture of Mycobacterium tuberculosis H37Rv MA[13] is grown to an OD600 of 0.6 - 0.7. The culture is then diluted 1:500 in liquid 7H9 medium supplemented with ADC (bovine albumin fraction V [5mg/ml], D-Glucose [2mg/ml], sodium chloride [0.81mg/ml]). In a 96-well microtitre plate, 50 μl of 7H9 medium is added to all wells from Rows 2-12.

The compounds to be tested are added to Row 1 in duplicate, at a final concentration of 640 μM (stocks are made up to a concentration of 12.8 mM in DMSO, and diluted to 640 μM in 7H9 medium). A two-fold serial dilution is prepared, using a multichannel pipette, by transferring 50 μl of the liquid in Row 1 to Row 2 and aspirating to mix. A 50 μl aliquot of the liquid in Row 2 is then transferred to Row 3 and aspirated, and so on.

This procedure is repeated until Row 12 is reached, from which 50 μl of the liquid is discarded so as to bring the final volume in all wells to 50 μl. Controls include media only, 5% DMSO, rifampicin and kanamycin. Finally, 50 μl of the 1:500 diluted *M. tuberculosis* culture is added to all wells in Rows 2-12. Cells are not added to Row 1, as this serves as a contamination control. The microtitre plate is sealed in a ziplock bag and incubated at 37°C with humidifier to prevent evaporation of liquid. The lowest concentration of drug that inhibits growth of more than 99% of the bacterial population is considered to be the MIC_{99}. MIC99 values are scored visually at 7-days and 14-days post inoculation, and digital images captured and stored.

4.8.5. Turbidimetric solubility studies

The test samples were prepared to a 1% stock solution in 100% DMSO and sonicated to enhance solubility. All test samples were done in triplicates, paracetamol and ncls was used as the reference drug in all experiments, paracetamol being the positive control and ncls being the negative control. Test samples were then serially diluted in DMSO medium to give concentrations: 0.0, 0.1, 0.5, 1.0, 2.0, 4.0, 8.0, and 10.0 μM in a 96 well plate. After the predilution, the samples were further diluted in DMSO and a 0.01 M phosphate buffered saline pH 7.4 (PBS), final concentrations being 0.0, 1.0, 5.0, 10.0, 20.0, 40.0, 80.0, 100.0 μM in a second 96 well plate. After two hours of incubation at room temperature, turbidimetry is then used as the end-point by measuring absorbance at 620 nm. The plate curve fitting analysis via Microsoft Excel 2010, Graph Computation Data were used to analysis the results.

4.9. References

(1) (a) Chavain, N.; Biot, C. *Curr. Med. Chem.* **2010**, *17(25)*, 2729. (b) Guo, Z.; Sadler, P. J. *Angew. Chem., Int. Ed. Engl.* **1999**, *38*, 1512. (c) Gavette, J. V.; Lara, J.; Reling, L. L.; Haley, M. M.; Johnson, D. W. *Chem. Sci.* **2013**, *4*, 585. (c) Dive, D.; Biot, C. *ChemMedChem.* **2008**, *3*, 383.

(2) Salas, P. F.; Herrmann, C.; Cawthray, J. F.; Nimphius, C.; Kenkel, A.; Chen, J.; de Kock, C.; Smith, P. J.; Patrick, B. O.; Adam, M. J.; Orvig, C. *J. Med. Chem.* **2013**, *56 (4)*, 1596.

(3) (a) Martinez-Gamboa, L.; Brezinschek, H.-P.; Burmester, G. R.; Dörner, T. Autoimmun. *Rev.* **2006**, *5*, 437. (b) Hillard, E. A.; Vessières, A.; Thouin, L.; Jaouen, G.; Amatore, C. *Angew. Chem., Int. Ed.* **2006**, *45*, 285. (c) Hamels, D.; Dansette, P.; Hillard, E. A.; Top, S.; Pigeon, P.; Jaouen, G.; Mansuy, D. *Angew. Chem., Int. Ed.* **2009**, *48*, 9124. (d) Biot, Ch.; Daher, W.; Chavain, N.; Fandeur, T.; Khalife, J.; Dive, D.; De Clerq, E. *J. Med. Chem.* **2006**, *49*, 2845. (e) Delhaes, L.; Biot, Ch.; Berry, L.; Delcourt, P.; Maciejewski, L.; Camus, D.; Brocard, J. S.; Dive, D. *ChemBioChem.* **2002**, *3*, 418.

(4) Bénech, J. M.; Piguet, C.; Bernardinelli, G.; Bünzli, J. G.; Hopfgartner, G. J. Chem. Soc., *Dalton Trans.* **2001**, 684.

(5) Bendrat, K.; Berger, B. J.; Cerami, A. *Nature*. **1995**, *378*, 138.

(6) Egan, T. J.; Mavuso, W. W.; Ncokazi., K. K. *Biochemistry*. **2001**, *40*, 204.

(7) Egan, T. J.; Hunter, R.; Kaschula, C. H.; Marques, H. M.; Misplon, A.; Walden, J. *J. Med. Chem.* **2000**, *43*, 283.

(8) Trager, W.; Jensen, J. B. *Science* **1976**, *193 (4254)*, 673.

(9) Carter, M. D.; Phelan, V. V.; Sandlin, R. D.; Bachmann, B. O.; Wright, D. W. *Comb. Chem. High Throughput Screening.* **2010**, *13*, 285.

(10) Sandlin, R. D.; Carter, M. D.; Lee, P. J.; Auschwitz, J. M.; Leed, S. E.; Johnson, J. D.; Wright, D. W. *Antimicrob. Agents Chemother.* **2011**, *55 (7)*, 3363.

(11) Ncokazi, K. K.; Egan, T. J. *Anal. Biochem.* **2005**, *338 (2)*, 306.

(12) (a) Collins, L.; Franzblau, S. G. *Antimicrob. Agents Chemother.* **1997**, *41*, 1004. (b) Collins, L. A.; Torrero, M. N.; Franzblau, S. G. *Antimicrob. Agents Chemother.* **1998**, *42*, 344.

(13) Ioerger, T. R.; Feng, Y.; Ganesula, K.; Chen, X.; Dobos, K. M.; Fortune, S.; Jacobs, W. R., Jr.; Mizrahi, V.; Parish, T.; Rubin, E.; Sassetti, C.; Sacchettini, J. C. *J. Bacteriol.* **2010**, *192*, 3645.

Chapter 5: OVERALL CONCLUSIONS AND FUTURE OUTLOOK

5.1. Overall Conclusions

A new class of silicon-containing chloroquine and ferroquine-derived compounds, and their respective ruthenium and rhodium metal-containing complexes were synthesised and characterised fully using a range of analytical and spectroscopic techniques.

Three different types of a new class of silicon-containing aminoquinoline ligands were prepared. Compounds **2.1** and **2.2** were derived from chloroquine (Chapter 2), prepared via nucleophilic substitution type reactions with the appropriate amine-terminated silane. Similarly, the ferroquine-derived compound **3.7** (Chapter 3), were prepared via quaternerisation of ferroquine, followed by a nucleophilic substitution reaction with (aminomethyl)trimethylsilane. The molecular structure of compound **2.2** illustrated a planar quinoline moiety, joined to a flexible propyl chain. Likewise, the molecular structure of compound **3.6** is comparable to compound **2.2**, with an extended three-dimensional geometry introduced by integration of the ferrocenyl moiety.

Three ligands obtained in moderate yields were reacted with two different types of rhodium, and three different types of ruthenium metal dimers. The metallation reaction resulted in selective coordination of the metal (either Ru or Rh) to the nucleophilic nitrogen on the quinoline scaffold. 10 mononuclear complexes **2.8-2.17** (Section 2.4) obtained in moderate yields, and 5 heterobinuclear complexes **3.7-3.11** (Section 3.3) obtained in moderate yields were characterised fully utilising a range of analytical and spectroscopic techniques to confirm their structural integrity. Furthermore, the molecular structure of complex **2.16** (Chapter 2) displays a typical square-planar geometry around the rhodium atom.

The *in vitro* antiplasmodial activity of all the synthesised compounds was evaluated against the choloroquine-sensitive (NF54) and chloroquine-resistant (Dd2) strains of *P. falciparum*. They were found to exhibit moderate antiplasmodial activities, in the nanomolar range with the ferroquine-derivatives being the most active. This could be attributed to the presence of the ferrocenyl moiety, altering/enhancing physical properties by increasing the lipophilic nature of the compound; which result in better penetration of the acidic food vacuole in the malaria parasite. The heteronuclear ruthenium metal complex **3.9** (Figure 5.1) is the most active in both of the NF54 and the Dd2 strain.

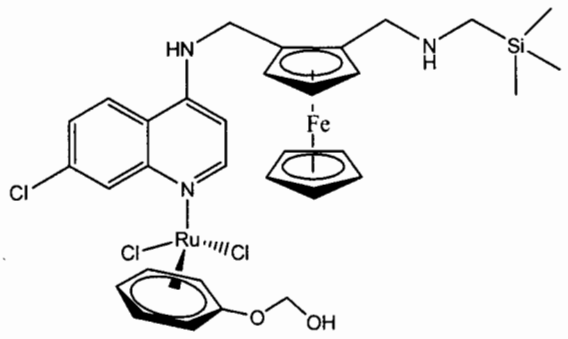

Figure 5.1: Structure of heteronuclear ruthenium metal complex **3.9**.

All compounds were assayed for inhibition of β-haematin formation. It was found that this new class of compounds target β-haematin formation. Evaluation of the preliminary results obtained suggests that the ferroquine derivatives are superior, which correlates with the *in vitro* antiplasmodial data. Compounds with better mechanism of inhibiting β-haematin formation, are better at killing the malaria parasite. Furthermore, these data solidified the idea of using heterobimetallic compounds as potential chemotherapeutic agents.

The *in vitro* antitumour activities of compounds **2.1**, **2.2**, and **2.8-2.17** were evaluated against the WHCO1 oesophageal cancer cell line, these compounds display weak to moderate antitumour activities. The studies also showed that the ruthenium metal complexes generally display better activity in comparison with the rhodium complexes, and the compounds containing a 3-carbon chain spacer generally show better activity when compared to those containing a 1-carbon spacer. Furthermore, the presence of the metal moiety did not appear to significantly enhance the biological activity in comparison with the free ligands. Complex **2.15**, containing the 2-hydroxyethoxy moiety tethered to the arene, showed the best cytotoxic activity with an IC_{50} value of 4.41 μM.

All compounds were evaluated for their *in vitro* antimycobacterial activity against *M. tuberculosis* $H_{37}R_v$ strain. In general, these compounds display weak to moderate antimycobacterial activities. Overall, the turbidimetric solubility assay data suggests that these newly synthesised silicon-containing chloroquine and ferroquine derivatives are relatively good drug candidates for *in vitro* pharmacological testing. All compounds showed moderate solubility in the aqueous PBS buffer.

5.2. Future Outlook

In vitro pharmacological evolution of this new class of silicon-containing aminoquinoline compounds displayed moderate biological activities comparable with commercially available drugs against three different diseases. With the promising preliminary pharmacological data obtained, improvement could be made through structural modifications/enhancements (Figure 5.2).

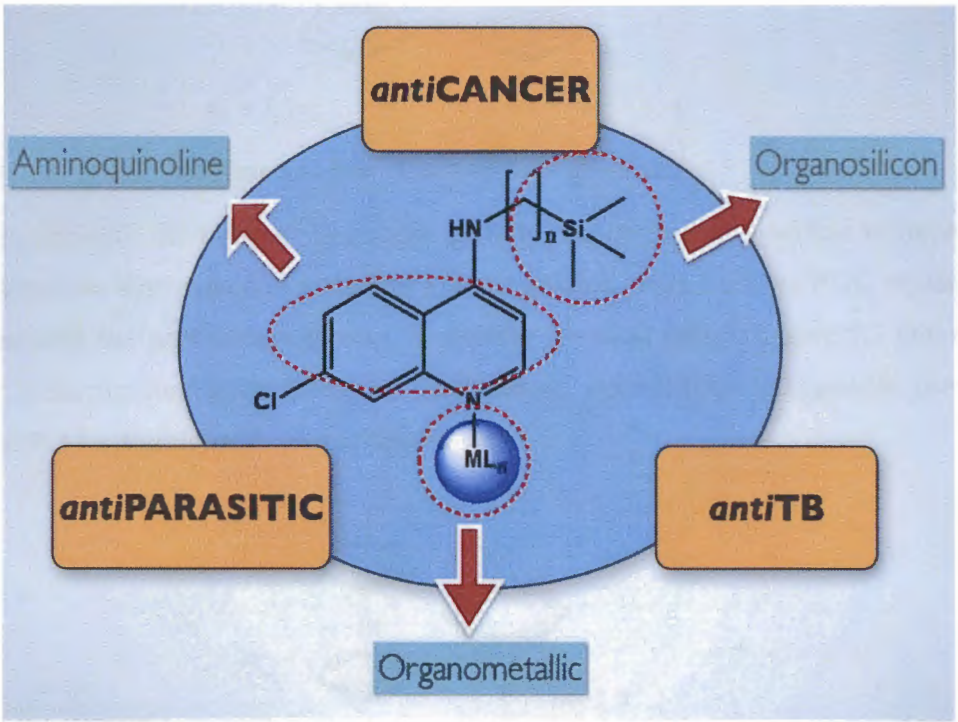

Figure 5.2: Silicon-containing compounds

For example, introducing replacement of the chlorido ligands, using phosphane type moieties could increase hydrophilicity. Linking additional metals to the NH groups, such as platinum salts/precursors, not only increases the number of coordination sites, it could also further stabilise the molecule. Furthermore, it has been suggested in literature that Pt(IV) type complexes are thought to act as pro-drugs, from which the active Pt(II) species is generated in the cancer cells.

In addition, the synthesis of new silicon-containing type ligands show in scheme 5.1, introducing various well-designed moieties which could help enhance biological activities, and improve the physical properties even further.

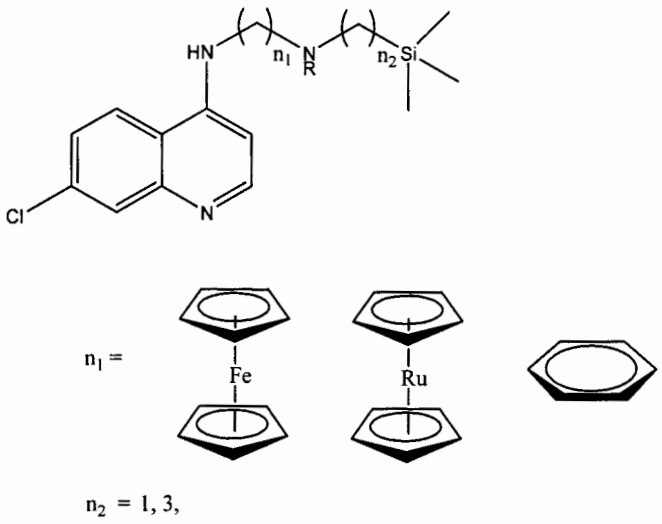

Scheme 5.1: New silicon-containing ligands.

Complex **3.9** with the best antiplasmodial activity can be further modified to improve biological activities. For example, including a water-soluble group such as PTA, replacing the ferrocene with the ruthenocene moiety, or altering the alkyl spacer. Figure 5.3 provides preliminary ideas for further modification. Furthermore, synthesisable compounds can be evaluated further for additional *in vivo* testing/studies.

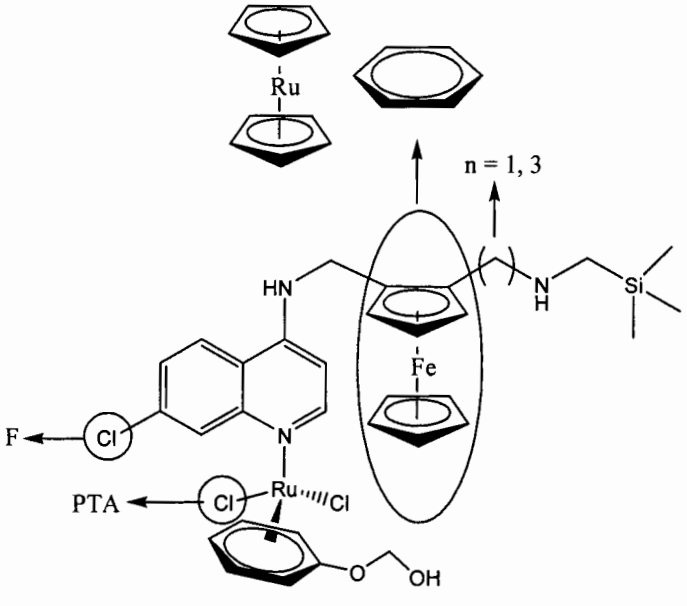

Figure 5.3: Possible structural modifications